

Review

Eco-Friendly and Complex Processing of Vanadium-Bearing Waste for Effective Extraction of Valuable Metals and Other By-Products: A Critical Review

Ahmed H. Ibrahim ^{1,*}, Xianjun Lyu ^{2,*}, Hani E. Sharafeldin ¹ and Amr B. ElDeeb ¹

¹ Mining and Petroleum Department, Faculty of Engineering, Al-Azhar University, Cairo 11884, Egypt; hanisharafeldin@azhar.edu.eg (H.E.S.); engbasuony87@yahoo.com (A.B.E.)

² College of Chemical and Biological Engineering, Shandong University of Science and Technology, Qingdao 266590, China

* Correspondence: ahmedkraiz@azhar.edu.eg (A.H.I.); lyuxianjun@163.com (X.L.); Tel.: +20-100-8519628 (A.H.I.); +86-532-86057101 (X.L.)

Abstract: Achieving the New World Sustainability Vision 2030 leads to enacting environmental restrictions, which aim to partially or totally reduce the negative impacts of different forms of waste and develop alternative technologies for eco-friendly and cost-effective utilization. Solid waste is a hazardous waste with many environmental and economic problems resulting from its storage and disposal. However, at the same time, these wastes contain many valuable elements. One of these solid wastes is heavy oil fly ash “HOFA” generated in power stations using heavy oil as fuel. HOFA is produced annually in massive amounts worldwide, the storage of which leads to the contamination of water resources by the contained heavy metals, resulting in many cancerogenic diseases. At the same time, these ashes contain many valuable metals in significant amounts, such as vanadium “V” and nickel “Ni” that can be extracted effectively compared to their low content and difficulty processing in their main ores. Hence, recycling these types of wastes reduces the environmental adverse effects of their storage and the harmful elements in their composition. This paper critically reviews the world resources of vanadium-bearing waste and various approaches described in the literature for recovering V, Ni, as well as other valuable metals from (HOFA) and other wastes, including pyro- and hydro-metallurgical processes or a combination. Hydro-metallurgical processes include alkaline or acidic leaching using different reagents followed by chemical precipitation, solvent extraction, and ion exchange to extract individual elements. The pyro-metallurgical processes involve the non-salt or salt roasting processes followed by acidic or alkaline leaching processes. The operational parameters and their impact on the efficiency of recovery are also discussed. The digestion mixtures of strong mineral acids used to dissolve metal ions in HOFA are also investigated. Bioleaching is a promising eco-friendly technology for recovering V and Ni through appropriate bacteria and fungi. Oxidation leaching is also a promising environmentally friendly approach and more effective. Among all these processes, the salt roasting treatment showed promising results concerning the cost, technological, and environmental effectiveness. The possibility of complex processing of HOFA has also been investigated, proposing innovative technology for completely utilizing this waste without any remaining residue. Effective zeolite for wastewater treatment has been formulated as a good alternative for conserving the available water resources.

Keywords: sustainability; solid wastes; heavy oil fly ash “HOFA”; vanadium; nickel; hydrometallurgy; pyrometallurgy; wastewater treatment; zeolite



Academic Editor: Ana Paula Paiva

Received: 16 November 2024

Revised: 23 December 2024

Accepted: 2 January 2025

Published: 5 January 2025

Citation: H. Ibrahim, A.; Lyu, X.; E. Sharafeldin, H.; ElDeeb, A.B. Eco-Friendly and Complex Processing of Vanadium-Bearing Waste for Effective Extraction of Valuable Metals and Other By-Products: A Critical Review. *Recycling* **2025**, *10*, 6. <https://doi.org/10.3390/recycling10010006>

Copyright: © 2025 by the authors. Licensee MDPI, Basel, Switzerland. This article is an open access article distributed under the terms and conditions of the Creative Commons Attribution (CC BY) license (<https://creativecommons.org/licenses/by/4.0/>).

1. Introduction

Vanadium is regarded as a rare metal, and its swift and consistently growing demand is challenged by its low concentrations in natural minerals. Vanadium extraction depends on the type of feed materials, efficiency, and technologies applied in processing raw materials. Therefore, recovering V and other valuable metals from secondary industrial resources like steel slag and ash containing these metal ions is highly intriguing regarding ecological and financial aspects. The increased industrial applications of vanadium contribute to the rising demand for vanadium, which has driven up the price of this metal. Currently, the value of vanadium ranges between \$20,000 and \$40,000 per metric ton [1,2]. These industrial uses encompass vanadium redox flow batteries, viewed as a promising solution to the global issue of large-scale energy storage production. They also include applications in the automotive and construction sectors, corrosion inhibitors, fertilizers, petrochemicals, catalysts for gas processing and sulfuric acid production, ferrovanadium alloys, thermistors, and more [3–5].

Unlike copper, nickel, or zinc, vanadium does not form concentrated deposits. Vanadium is found in many minerals, replacing Fe^{3+} or Al^{3+} in the octahedral positions of crystal lattices. This is possible because the ionic radii of V^{3+} and Fe^{3+} are almost the same, which means that vanadium can be found all over the Earth's crust, accounting for approximately 0.014% [6]. Vanadium is found in nature in the form of oxides, sulfides, and phosphates, and it is often associated with other metals such as iron, titanium, aluminum, zinc, lead, and uranium. These compounds include vanadinite, titanomagnetite, descloizite, patronite, and carnotite. The concentrations generally have a V_2O_5 grade between 0.2 and 1%, while higher-grade deposits may have V_2O_5 levels exceeding 2% [7–9].

It is estimated that there are 26 million tons of vanadium reserves worldwide. The only vanadium mine-operating countries with the largest reserves are China with 9.5 million tons, Russia with 5 million tons, Australia with 6 million tons, and South Africa with 3.5 million tons. In contrast, the world's resources total over 63 million tons [10]. Nearly all of the world's vanadium production in 2022 came from China (68%), Russia (17%), South Africa (9%), and Brazil (6%). The total global production of vanadium this year was approximately 120 kilotons/year [8,10]. Over 88% of the total vanadium is primarily produced as co-products from slag during the smelting of titanomagnetite ores or steel refining, representing over 69% of the starting raw material and making them an essential source of vanadium. In contrast, approximately 19% of the vanadium was produced from primary vanadium ores and 12% from secondary sources (Figure 1) [1,8].

The world's vanadium consumption reached 102.1 kilotons, representing an increase of nearly 45% over 2011. By the end of 2023, consumption is predicted to increase by up to 120–125 kilotons at a 5% annual growth rate, with increased demand for high-strength steel serving as the primary driver of this growth [8].

Coulsonite, a mineral of FeV_2O_4 , is commonly found alongside magnetite and forms a series with FeCr_2O_4 , also known as chromite [11]. The mineral ilmenite can also host vanadium, possessing a minor quantity [12]. Likewise, clay containing vanadium in weathered mineral deposits is commonly found, with V^{3+} taking the place of Al^{3+} in phyllosilicates and Fe^{3+} in goethite, FeOOH . A variety of vanadium oxides have been discovered in weathered zones of vanadium titanomagnetite deposits, including chlorite, $(\text{Fe, Mg, Al})_6(\text{Si, Al})_4\text{O}_{10}(\text{OH})_8$, and goethite. It is worth noting that a lot of uranium deposits also contain vanadium in the form of minerals like carnotite ($\text{K}_2(\text{UO}_2)_2\text{V}_2\text{O}_8 \cdot 3\text{H}_2\text{O}$) and tyuyamunite ($\text{Ca}(\text{UO}_2)_2\text{V}_2\text{O}_8 \cdot 5\text{--}8\text{H}_2\text{O}$) that have uranyl vanadate [13].

From ores rich in minerals like carnotite ($\text{K}_2(\text{UO}_2)_2\text{V}_2\text{O}_8 \cdot 3\text{H}_2\text{O}$), vanadium has been generated as a by-product of uranium mining at numerous mines in the southwestern regions of the USA [14]. After a moderate leaching process, a significant portion of the

uranium deposits was dissolved. The remaining vanadium in the uranium-leaching residue was then extracted using a more aggressive leaching condition [1]. The processing of South Korean shale-hosted uranium/vanadium ore has been suggested using a similar strategy [15]. Liu [16] has also been found to have comparable deposits in Western Australia. Coal and bituminous shale also contain trace levels of vanadium [17]. In northern Queensland, an abundant oil shale deposit at Julia Creek has been found to include vanadium and trace quantities of molybdenum [18].

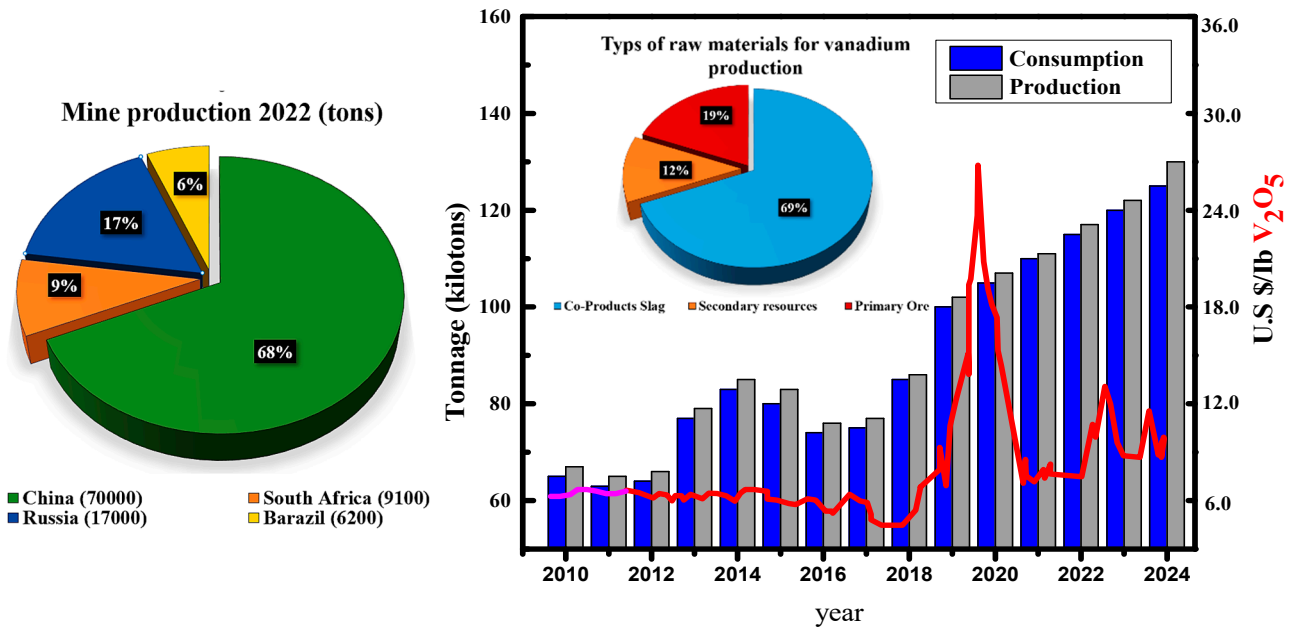


Figure 1. World mine production and global annual vanadium production and consumption [1,8]

Trace amounts of Vanadium have also been found in crude oil [19–22], among other potentially essential sources. Vanadium levels in crude oil are very high, reaching up to 0.05% in certain regions of Venezuelan oil [23,24]. During oil combustion, its vanadium content is transferred to the ash, which contains up to 10~18% of V₂O₅, making it an attractive material for vanadium recovery [25–27].

According to a report by White and Levy [28], the main sources of vanadium released into the environment are steel co-production, which accounts for 75% of the total, crude oil processing, which accounts for 10%, and mining, which accounts for less than 10%. In the Middle East and Africa, fuel oil and crude oil are easily accessible resources for power plants and desalination plants. For instance, it has been approximated that Saudi Arabia, with the world’s largest oil reserves, consumes more than 40 million metric tons of crude oil and heavy fuel oil annually for thermal power plants and seawater desalination [29]. Egypt, Africa’s largest non-OPEC oil producer, produces approximately 11 million metric tons of heavy fuel oil (HFO) annually, of which approximately 9 million metric tons are consumed domestically [30–32]. Petroleum and other liquids contribute 36%, and natural gas 57%; they were considered the most-consumed fuels in Egypt in 2020, according to BP’s Statistical Review of World Energy 2021, in addition to renewable energy and coal, which accounted for 6% and 1% of the country’s total energy consumption [33,34]. The country implemented measures to decrease its natural gas usage in power generation, which typically accounts for up to 90% of its total generation. As part of this effort, the country has significantly increased its use of oil-fired generation, resulting in an average fuel oil burn of over 100 kb/d in the first nine months of 2022, the highest level seen in four years [29].

To date, in many developing countries, most of the generated ashes do not have any industrial application but are only stored in landfills. Compared to other V resources, which are relatively limited and low-grade, these materials have no mining or operating costs. The disposal of ash or steel slag is a major environmental problem facing thermal power plants and iron production industries, and no monitoring is taken to prevent the contamination of groundwater and soil [30,35]. It is recommended to continuously monitor the metals of environmental impact, such as nickel, vanadium, and zinc, in ash samples due to carcinogenic and health hazards. Therefore, it is recommended to consistently monitor and recover valuable metals from industrial waste, as this is highly beneficial for both environmental protection and economic considerations. This review aims to offer a summary of advanced technologies used for vanadium recovery from various types of vanadium-bearing waste, as well as the comprehensive utilization of their solid residue.

2. Chemical and Mineralogical Composition of Vanadium-Bearing Waste

Table 1 shows the chemical composition of vanadium-bearing waste produced from different iron and steel production facilities in different locations worldwide. The chemical structure of vanadium oxides, such as V_2O_3 or V_2O_5 , varies based on the type of feed materials introduced into the furnaces, the efficiency of the processing methods, and the desired final products. Typically, CaO, SiO_2 , MgO, and Al_2O_3 contained in the vanadium-bearing slag are in the ranges 2~45%, 6~25%, 1~16%, and 2~10%, respectively. During reduction smelting, chromium and titanium oxide are also found in the vanadium-bearing slag, so obtaining pure vanadium requires critical separation of those metals after extraction.

Table 1. Chemical composition of vanadium-bearing slag generated from various industrial plants in different locations in the world.

Sources	Technology	Chemical Composition					Ref.
		V_2O_5/V_2O_3	FeO/Fe ₂ O ₃	Cr ₂ O ₃	TiO ₂	MnO/MnO ₂	
Panzhuhua Iron and Steel	BF-BOF	8.5–14.3	32.9–42.1	2.1–4.3	11.1–12.9	5.9–9.1	[36]
Kapok Iron and Steel	BF-BOF	14.2–16.0	31.9–32.3	-	12.0	7.6–8.7	[37]
Chengde Xinxin Vanadium and Titanium Chemical	BF-BOF	8.5	51.1	3.5	10.5	5.2	[38]
Desheng Iron and Steel Group	BF-BOF	15.2–20.8	35.3–64.5	7.7–10.6	6.39–8.5	5.5–7.6	[39]
Chengde Iron and Steel	BF-BOF	10.2–13.4	36.7–49.1	1.7–4.2	6.8–11.1	5.2–7.2	[40]
Esfahan Steel	BF-BOF	1.5–1.9	17.3–17.6	-	1.0–1.5	4.2–4.5	[41]
Sichuan Weiyuan Iron and Steel	BF-BOF	14.3	24.8	4.4	7.4	8.5	[42]
Pan Steel	DR-EAF	8.9	24.3–25.2	2.0–8.7	3.3–14.7	1.6–13.8	[43]
CITIC Jinzhou Ferroalloy	DR-EAF	15.3	30.5	2.3	13.7	10.9	[44]
British Steel	BF-BOF	0.82	32.0	0.2	0.3	4.5	[45]

BF = blast furnace; BOF = basic oxygen furnace; DR = direct reduction; EAF; electric arc furnace.

The chemical structure of HOA reveals that it primarily consists of carbon, along with several metallic elements. Table 2 presents the chemical composition of ash samples generated from burning heavy oil in various power and desalination plants across different global locations. Industrial ashes primarily consist of vanadium (V) and nickel (Ni), along with toxic elements like chromium, arsenic, cadmium, lead, cobalt, and selenium. The maximum content of V and Ni in ash is 5 wt.% and 1.8 wt.%, respectively [35]. Heavy oil ash chemical composition also differs based on the makeup of the heavy fuel oil, parameters of operation, and chemicals used [35,46]. Two types of ash (boiler ash and fly ash) are generated by the combustion of HFO in power plants, which is expected to increase as energy consumption rises in the next few years. Around 3 kg of ash residue is produced when 1000 L of heavy oil is burned [47]. A higher level of V and Ni was found in heavy oil ash (HOA) produced by various power plants worldwide [48]. The ash fraction is too heavy to be introduced into the flue gas and hence deposited outside the boiler tube, which is known as the boiler ash. It is usually classified as high-grade ash which contains

(4.4~19.2%) V, (2.7~8.5%) Ni, and burned C [49,50]. The other type of ash is known as fly ash, which is fine combusted residue usually collected from the stack or electrostatic precipitators (ESPs). It is usually classified as low-grade ash which contains (0.3~1.5%) V, (0.2~0.5%) Ni, and unburned (30~80%) C [51]. The refining of crude oil often entails some kind of thermal cracking to produce a light oil fraction and a heavier residual oil. Most metals and a small amount of sulfur are still linked to the non-volatile elements and end up in a residual oil fraction. Several factors influence the elemental composition of heavy fuel oil, including the source of crude oil, the yield of HFO from crude oil, and the degree of processing [52].

Table 2. Chemical composition of vanadium-bearing waste reported in different studies.

Element (ppm)	Ref. [53], PP	Ref. [53], DP	References								
			Ref. [21]	Ref. [54]	Ref. [55]	Ref. [56]	Ref. [57]	Ref. [58]	Ref. [35]	Ref. [59]	Ref. [25]
Carbon (%)	90.40	56.70	85.56	51.86	-	67.4	-	77.40	-	14.73	18.65
Sulfur (%)	7.77	27.18	-	-	-	8.6	-	7.10	-	5.83	11.23
Vanadium	9072	31,044	2958	34,487	50,000	38,000	7670	12,900	3540	85,000	49,100
Nickel	2382	13,633	1762	11,852	15,400	16,000	18,000	6800	1055	52,500	24,200
Cadmium	1.65	3.7	3.28	1.59	-	-	-	-	60.4	-	920
Arsenic	2.54	1846	2.24	68.29	-	-	-	-	128.5	-	1.61
Cobalt	2.88	12.33	3.28	247.79	2200	-	-	-	60.7	-	2140
Chromium	36.79	113.09	4.06	107.60	8000	-	-	-	70.4	-	-
Selenium	1.00	6.81	11.60	13.20	-	-	-	-	7.25	-	-
Lead	17.09	13.94	11.00	116.10	-	-	-	-	27.85	7200	1900
Zinc	21.92	118	130	592.10	-	-	1110	4000	65.5	38,000	7600
Copper	10.44	50.40	170.4	120.30	-	-	-	17,000	57.12	290	1760
Iron	7210	8771	-	-	220,500	8000	59,800	1400	176.5	97,400	59,600
Magnesium	6971	94,608	-	-	2000	-	3430	14,100	3615	5920	3.6
Manganese	23.9	149.26	-	-	-	-	-	-	12.8	900	2.4
Calcium	582.3	4121.2	-	-	-	-	-	2300	3380	2100	2354
Sodium	1395	7555	-	-	-	19,000	-	-	1310	2045	1524
Aluminum	3541	1041.8	-	-	-	1040	2870	2500	642.4	7123	4252
Barium	7.42	49.68	-	-	-	-	-	-	69.0	-	5214
Others (ppm)	-	-	Hg, 0.25	-	Mo, 3500	Si, 8000	-	Si, 800; O, 93 200	-	Si, 39,000	Si, 36,800

PP = power plant; DP = desalination plant.

Table 3 presents the mineralogical compositions of vanadium-bearing slag produced by different iron and steel-making facilities and ashes. The spinel phases of $[(\text{Fe}, \text{Mn})_2(\text{V}, \text{Ti}) \text{O}_4]$ and $[(\text{Fe}, \text{Mg}, \text{Mn}) (\text{V}, \text{Cr})_2 \text{O}_4]$ contain vanadium, titanium, and chromium. The spinels are distributed throughout the olivine matrix $(\text{Fe}, \text{Mg})_2\text{SiO}_4$, augite $(\text{Ca}(\text{Fe}, \text{Mg})\text{Si}_2\text{O}_6)$, fayalite $(\text{Fe}_2\text{SiO}_4)$, and diopside phases $(\text{Ca}(\text{Fe}, \text{Al})_2\text{SiO}_6)$ [60–62]. Previously reported data indicated that V-Ti and V-Cr spinels are arranged in a layered core configuration. Chromium is primarily located in the central core of the grains, vanadium is prevalent in the outer layer, and titanium is situated along the spinel grain boundary. This distribution reflects the varying crystallization abilities of each spinel, ranked as $\text{Cr} > \text{V} > \text{Ti}$ [43]. Other elements, such as manganese, are evenly dispersed within the spinel grain. Magnesium is concentrated alongside chromium, forming the minor phase of MgCr_2O_4 [60]. The $\text{Ca}_2\text{V}_2\text{O}_7$ phase of vanadium was also documented [41], which resulted from the substantial amount of limestone utilized in the iron and steel production process [63].

Additional oxides, originating from the fluxes added to the furnace charge, have also been identified. Dondi [64] states that X-ray diffraction patterns show that two types of fly ash (ash B from Apulia and ash F from Sardinia) produced from the combustion of orimulsion in Italian thermal power plants have a complex composition. These fly ashes contain high grades of V, Ni, S, and Mg and exhibit increased reflections, several line interferences, and overlaps. This complexity makes it difficult to make certain attributes. The interpretation of these patterns indicates that magnesium sulfate monohydrate $(\text{MgSO}_4 \cdot \text{H}_2\text{O})$ and hydrogen vanadyl sulfate $[(\text{VO})_2\text{H}_2(\text{SO}_4)_3]$ are predominated, along with magnesium monoxide (MgO) , anhydrous, monohydrate, and pentahydrate vanadyl sulfate (a-VOSO_4) ,

$\text{VOSO}_4 \cdot \text{H}_2\text{O}$, $\text{VOSO}_4 \cdot 5\text{H}_2\text{O}$). These phases are associated with minor amounts of calcium sulfate (CaSO_4) and nickel monoxide (NiO), and presumably sodium aluminum silicate ($\text{NaAlSi}_3\text{O}_8$) and traces of magnesium sulfate hexahydrate ($\text{MgSO}_4 \cdot 6\text{H}_2\text{O}$). Other analyses of the insoluble residues indicated that in addition to magnesium, nickel oxides, and anhydrous vanadyl sulfate, other vanadium compounds, i.e., VO_2 , $B\text{-V}_2\text{O}_5$, VOOH , and $\text{VO}(\text{OH})_2$, were present in small amounts of untreated ash, which cannot be detected in the collective sample due to their low concentration. However, identifying these compounds suggests the presence of V^{3+} and V^{5+} , together with the monopolized vanadyl ion valence of V^{4+} . The existence of these vanadyl ions can vary depending on the oxidation conditions during the combustion of heavy oil or the cooling techniques used [65,66].

Table 3. Characterization of the minerals in vanadium-containing waste produced from various industrial plants in different locations in the world.

Source	Mineralogical Phases	Ref.
Panzhuhua Iron and Steel	$(\text{Fe}, \text{Mn})\text{V}_2\text{O}_4, (\text{Fe}, \text{Mn})_2\text{SiO}_4, \text{CaMn}(\text{SiO}_3)_2$	[36]
Kapok Iron and Steel	$(\text{Fe}, \text{Mn})\text{O}, (\text{V}, \text{Ti})_2\text{O}_3, 2(\text{Fe}, \text{Mn})\text{O}, \text{SiO}_2, \text{SiO}_2$	[37]
Chengde Xinxin Vanadium and Titanium Chemical	$(\text{Mn}_{0.84}\text{Fe}_{0.16})(\text{Mn}_{0.16}\text{Fe}_{1.34}\text{Cr}_{0.5})\text{O}_4, \text{Fe}_{2.1}\text{Ti}_{0.74}\text{Mn}_{0.02}\text{V}_{0.01}\text{Ca}_{0.01}\text{Si}_{0.01}\text{Al}_{0.05}\text{Mg}_{0.06}\text{O}_4, \text{Fe}_2\text{SiO}_4, \text{SiO}_2$	[38]
Desheng Iron and Steel Group	$(\text{Mg}, \text{Fe})(\text{V}, \text{Cr})_2\text{O}_4, \text{Fe}_2\text{SiO}_4, \text{Ca}(\text{Fe}, \text{Mg})\text{Si}_2\text{O}_6, \text{Fe}_2\text{TiO}_4$	[39]
Chengde Iron and Steel	$(\text{Mn}, \text{Fe})(\text{V}, \text{Cr})_2\text{O}_4, \text{Fe}_2\text{SiO}_4, \text{SiO}_2$	[40]
Esfahan Steel	$\text{Ca}(\text{OH})_2, \text{Ca}_3\text{SiO}_5, \text{CaFeO}_2, \text{Ca}_2\text{V}_2\text{O}_7$	[41]
Sichuan Weiyuan Iron and Steel	$(\text{Mn}, \text{Fe})(\text{V}, \text{Cr})_2\text{O}_4, \text{Fe}_2\text{SiO}_4, (\text{Fe}, \text{Mg})\text{Si}_2\text{O}_6, \text{Mg}_2\text{TiO}_4$	[42]
Pan Steel	$(\text{Mn}, \text{Fe})(\text{V}, \text{Cr})_2\text{O}_4, \text{Fe}_2\text{TiO}_4, (\text{Fe}, \text{Mn})_2\text{SiO}_4$	[43]
CITIC Jinzhou Ferroalloy	$(\text{Mn}, \text{Fe})(\text{V}, \text{Cr})_2\text{O}_4, \text{CaFeAlSiO}_6, \text{Fe}_{2.5}\text{Ti}_{0.5}\text{O}_4$	[44]
British Steel	$\text{MgO}, \text{Al}_2\text{O}_3, \beta\text{-Ca}_2\text{SiO}_4, \text{Ca}_2(\text{Al}, \text{Fe})_2\text{O}_5, \text{FeO}, \text{Mg}(\text{OH})_2, \text{C}$	[45]
Fiume Santo-Porto Torres	$\text{MgSO}_4 \cdot \text{H}_2\text{O}, (\text{VO}_2)_2\text{H}_2(\text{SO}_4)_3, \text{VOSO}_4 \cdot n\text{H}_2\text{O}, \text{CaSO}_4, \text{NiSO}_4 \cdot n\text{H}_2\text{O}$	[64]
El Kriymat Electric power station	$(\text{VO}_2)_2, \text{FeV}_2\text{O}_4, \text{Mg}_2\text{SiO}_4, \text{Ca}_2\text{V}_2\text{O}_7, (\text{Ca}(\text{Fe}, \text{Al})_2\text{SiO}_6), \text{NiSO}_4 \cdot \text{H}_2\text{O}$	[22,25]

3. Vanadium Processing Technologies

As previously mentioned, steel slag and oil ash are important secondary sources of valuable elements (V, Ni, Cr, and Zn). However, there are two main ways for processing industrial solid waste to extract vanadium and other useful metals. The first method, direct leaching, involves using acid (such as H_2SO_4 , HCl , and HNO_3) or alkaline (such as NaOH and Na_2CO_3) solutions to dissolve the valuable metal from vanadium-bearing waste. The dissolved metals are then recovered from the solution using various techniques such as chemical precipitation, solvent extraction, or ion exchange. The second is the roasting-assisted leaching process, including salt-free, calcium, or salt roasting, in which the solid waste is heated to a high temperature to allow the separation of valuable vanadate materials. Acid, alkaline, and water are frequently employed as leaching agents, as outlined below [67–74]. A comprehensive flowchart for recovering V from solid waste is shown in Figure 2 [35]. After extracting vanadium and nickel as their respective chemical compounds (NH_4VO_3 and NiC_2O_4), calcination is conducted to produce V_2O_5 and NiO .

3.1. Direct Leaching Process

Direct acidic or alkaline leaching is used to dissolve almost all valuable metals into the solution from various types of solid waste and then extract these metals separately using adequate techniques [75–82].

3.1.1. Acid Leaching

H_2SO_4 is a cost-effective option for leaching procedures, which makes it a popular choice due to its economic benefits. The H_2SO_4 acid has the ability to dissolve several metallic cations like V, Ni, Fe, and Mg, among others, creating metal sulfates. The leaching of significant economic and nuclear elements such as uranium, hafnium, and zirconium, as well as vanadium and nickel, with or without oxidant agents (NaClO , MnO_2 , or KClO_3), has

been investigated by Abd El-Hamid [83]. It was noted that vanadium leaching efficiency of 95% at a concentration of 200 g/L H_2SO_4 , 6% (solid/solid) manganese dioxide, 80 °C, 6 h, 1/10 solid/liquid ratio of -200 mesh ore granule size. According to Deng [84], the direct acid leaching technique could increase the vanadium leaching efficiency from 14 to 73% by adding an oxidant. Barik [85] created a technique for extracting vanadium (V) and nickel (Ni) from solid industrial wastes abundant in these metals. The procedure includes leaching with sulfuric acid (H_2SO_4), followed by solvent extraction, precipitation, and crystallization. It was noted that using 1.35 M H_2SO_4 at 40 °C for 90 min, both V and Ni were extracted with a 98% recovery rate. Vanadium is selectively extracted from the pregnant solution using 40% LIX 84-I at pH 0.5, and then by adding an aqueous solution of ammonia NH_3 ; it precipitates as ammonium metavanadate (NH_4VO_3). Ammonium oxalate $(NH_4)_2C_2O_4$ is used to selectively separate Ni that has been converted into Ni oxalate in the raffinate (NiC_2O_4). Finally, NH_4VO_3 can be heated to produce vanadium pentoxide (V_2O_5) [86]. On the other hand, nickel oxide is obtained by heating nickel oxalate at 450 °C for 2 h.

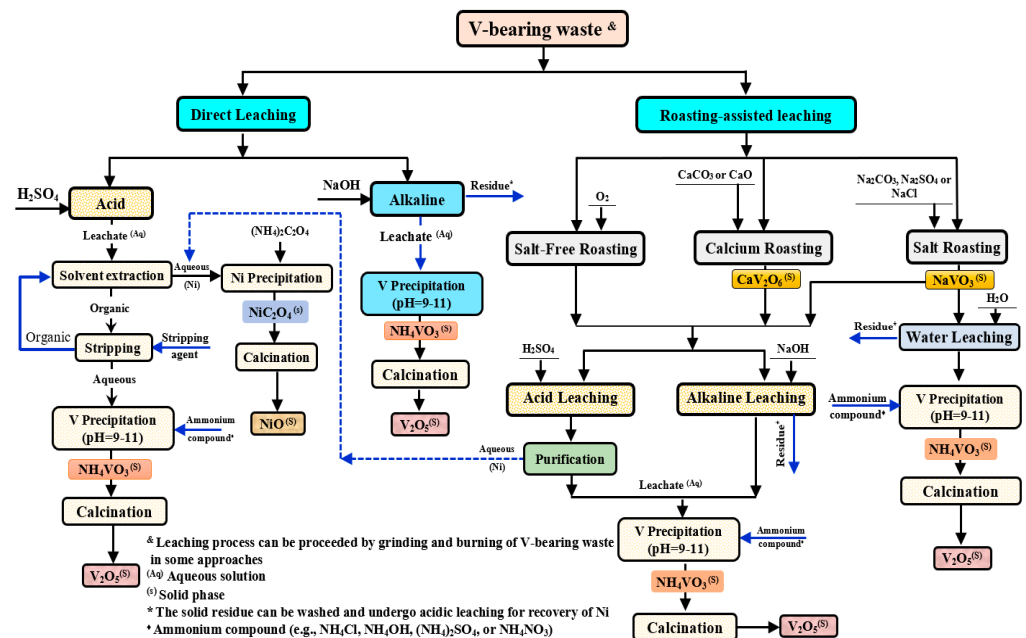


Figure 2. Overall flowchart showing the most common methods for the recovery of vanadium and nickel from industrial solid waste.

Nazari [87] optimized the parameters of the H_2SO_4 leaching process to maximize V and Ni recovery from fly ash samples. The maximum recovery of 94% V and 81% Ni has been achieved at the following optimal conditions: 19.5% H_2SO_4 concentration at 80 °C, 9.15% S/L ratio by weight, and for 2 h. Fly ash was subjected to a three-step procedure, which included leaching with H_2SO_4 , oxidative precipitation, and washing to extract V as V_2O_5 from the fly ash, and about 90% of V was successfully recovered. Boiling 1 M H_2SO_4 for 30 min. at 3 mL/g L/S ratio is considered to be the operational parameter for the leaching process. During the oxidative precipitation process, sodium chlorate ($NaClO_3$) was added as an oxidizing agent of V^{4+} to V^{5+} . The pH dropped because of this oxidation of V, which also released H into the environment; hence, the appropriate pH was maintained by adding Na_2CO_3 . In order to remove Na and other impurities, the V_2O_5 precipitate was then washed with an acidic solution [26]. Leaching experiments on HOA were performed by Navarro [88] in 0.5 M H_2SO_4 solution at 4 mL/g as L/S ratio at 200 rpm agitation speed for 24 h and at room temperature. After the leaching procedure, the material was

washed for 1 h. in water at 4 mL/g L/S ratio. Ni recovery was only about 12% under these conditions, but V reached 98%.

Aburizaiza [89] detailed a multi-step approach for leaching and extracting V, Ni, and Fe from HOA, which involves the following steps: (i) Acidic leaching of fly ash in a solution containing mineral acids like perchloric acid (HClO_4), hydrochloric acid (HCl), and hydrogen peroxide (H_2O_2); (ii) Ammonium pyrrolidine dithiocarbamate ($\text{C}_5\text{H}_9\text{NS}_2\cdot\text{NH}_3$) in chloroform (CHCl_3) is combined and agitated with the leachate during the organic extraction of the metals. Once equilibrium is reached, a layer of organic phase that contains the metal cations is formed. The findings demonstrate that the organic phase successfully extracts the targeted metal ions (V, Ni, and Fe); (iii) the V, Ni, and Fe metal ions are removed from the organic phase by combining them with 1 M HNO_3 that contains Hg^{2+} ions. Therefore, metallic cations (V^{3+} , Ni^{2+} , and Fe^{2+}) are present in the final aqueous nitric acid solution; (iv) The addition of dimethylglyoxime ($\text{C}_4\text{H}_8\text{N}_2\text{O}_2$) in chloroform allows the extraction of the total Ni from the stripped nitric acid solution while leaving the V^{3+} and Fe^{2+} ions dissolved in the aqueous nitric acid solution phase. In order to recover nickel in the form of NiO, the Ni-containing organic phase is separated and evaporated till it is dried; (v) Total Fe is extracted from the aqueous nitric acid solution phase produced in step (iv) by 4-pyridyl treatment. The organic phase that contained Fe was separated, evaporated, and ignited to produce Fe in the form of FeO; (vi) vanadium as V^{3+} and other trace elements can be found in the aqueous solution that was left over. The study does not present an efficient technique for extracting V from the final aqueous solution. Additionally, this approach demands significant amounts of chemicals to handle a small quantity of fly ash.

Tokuyama [58] studied the dissolving of HOA in two steps. In the first step, Ni, Zn, Mg, Al, and Fe are dissolved in water, and in the second stage, V is dissolved in H_2SO_4 , as shown in Figure 3. Moreover, it was found that HCl and H_2SO_4 have similar leaching efficacy. In the same study, leaching with concentrated NaOH might result in the selective leaching of V.

Tsygankova [48] concluded that the HOA leaching process depends on both its phase change and chemical composition. The outcomes of acidic leaching for three distinct types of fly ash, each with different chemical and phase compositions, have been examined. Each type of fly ash requires specific leaching conditions, involving 5 to 9% H_2SO_4 concentration, with temperatures set between 20 and 80 °C, and durations spanning from 30 to 60 min. Vanadium is precipitated as V_2O_5 by oxidizing the leaching solution with H_2O_2 at 20 °C for 30 min. After further heating to 95 °C and at a pH range from 1.8 to 2, precipitation is accomplished.

Khalafalla [90] examined the extraction of V, Ni, and Zn by leaching the heavy oil ash (HOA) in H_2SO_4 solution, as shown in Figure 4. High-tension Magnetic Separation was used to physically concentrate the fly ash, increasing the amounts of V_2O_5 , ZnO, and NiO, to 18.1%, 8.11%, and 11.18%, respectively. Following that, leaching was performed using a 180 g/L H_2SO_4 solution with 4% MnO_2 as an oxidant for 10 h at 80 °C which resulted in the recovery of 96.5% of vanadium, 94.8% of nickel, and 99.1% of zinc. Ultimately, vanadium was extracted from the leach solution using 3% Alamine 336 in kerosene as the solvent, while nickel and zinc remain dissolved in the raffinate. After vanadium was extracted from the organic phase, $\text{V}_2\text{O}_5\cdot\text{H}_2\text{O}$ was precipitated by adding H_2SO_4 . In contrast, when Na_2S was added to the raffinate solution, Ni and Zn co-precipitated, forming a (Zn-Ni) sulfide cake. This cake could be suggested for hydro-metallurgical techniques to recover and separate Zn and Ni [91].

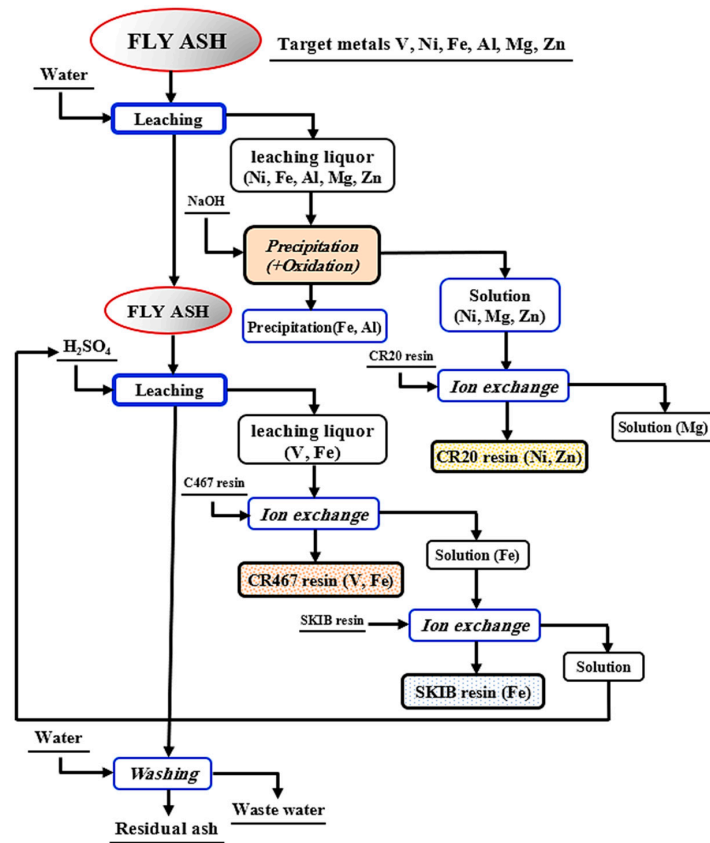


Figure 3. Flowsheet of processing fly ash for recovering metal ions [58].

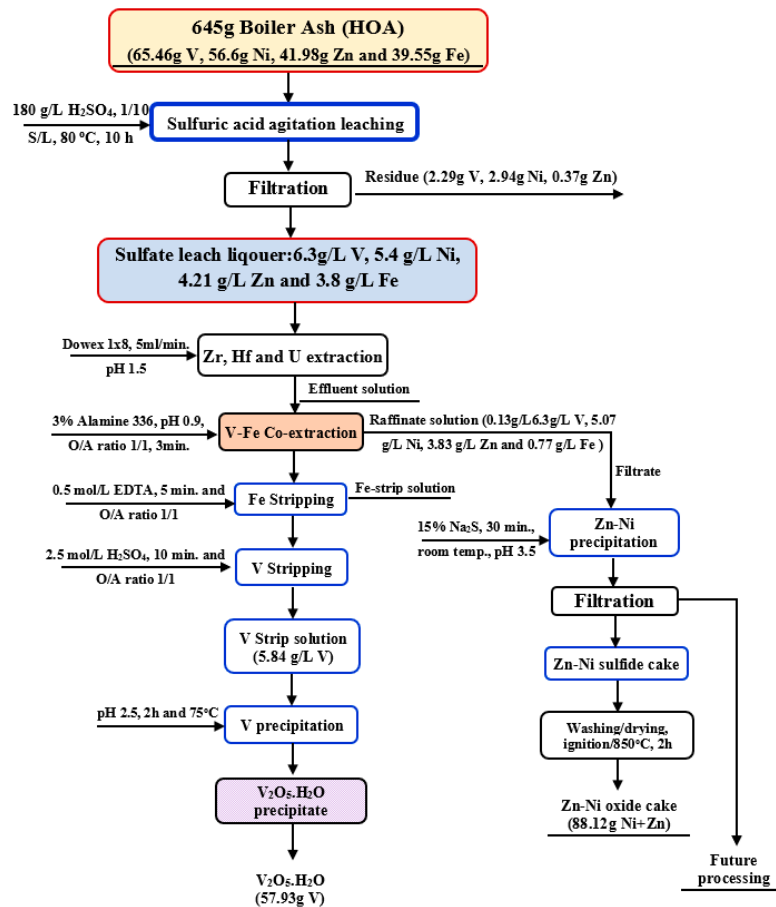


Figure 4. The proposed technical flowsheet for the chemical treatment of El-kuriemat boiler ash [90].

Rahimi [92] developed a distinctive technique for extracting vanadium from HOA utilizing lemon juice and organic acids. The citric acid (90 mg/g), malic acid (0.86 mg/g), and ascorbic acid (1.24 mg/g) are all present in lemon juice. The idea was to obtain organic acids by an ecologically acceptable method as an alternative to bioleaching, which produces such acids through extremely sluggish microbial development. The recommended conditions for the maximum recovery of 88.7% V were 2 h. ultrasonic leaching of HOA in a 27.9% lemon juice solution with 10% hydrogen peroxide at 35 °C and 0.01% S/L ratio. Sodium carbonate (Na_2CO_3) was added to the liquid to raise the pH level to 9 or 10, and the addition of CaCl_2 precipitates Al and Fe. Next, ammonium chloride (NH_4Cl) was added, leading to the precipitation of V as pure NH_4VO_3 , then calcined at 500 °C to obtain vanadium pentoxide (V_2O_5). Eventually, the results revealed that assisting leaching agents, such as H_2O_2 and ultrasonic, is essential in accelerating V dissolution's kinetics.

High-pressure and high-temperature leaching demonstrates significant improvements compared to traditional acid leaching. For instance, according to Mu [93], 97.9% vanadium and 94.5% iron were leached out at a temperature of 140 °C, a concentration of 200 g/L H_2SO_4 , a partial pressure of 0.5 MPa of oxygen, a period of 120 min, and an L/S ratio of 20:1. These are in completely agree with the findings published by Zhang [94–96]. Zhou [97] studied the dissolution kinetics of vanadium trioxide in sulfuric acid-oxygen medium. The highest dissolution rate was obtained with increased stirring speed before 800 rpm, oxygen partial pressure in the range of 0.6–1.4 MPa, and particle size decreased. Still, it was nearly independent of the sulphuric acid concentration from 0.4–2.0 mol/L and stirring speed over 800 rpm. Amer [98] recovered $\text{V}_2(\text{SO}_4)_3$ and NiSO_4 from Egyptian boiler ash by direct leaching using H_2SO_4 under oxygen pressure. The recommended leaching conditions have been determined to be 200 °C, 15 min, 15 bar of oxygen pressure, 60 g/L of H_2SO_4 concentration, and 1 S/L ratio. Adding an aqueous solution of ammonia NH_3 and neutralizing the acidic sulfate solution, V is precipitated as vanadium hydroxide ($\text{V}(\text{OH})_3$). On the other hand, metallic Ni can be electrodeposited from the NiSO_4 electrolyte. The results of comprehensive studies employing acidic leaching methods on various vanadium resources are shown in Table 4.

Table 4. Results of different studies on direct acidic leaching of vanadium from various V-bearing waste.

Ref.	Lixiviant	Acid Leaching Conditions	Temp. °C	Time	S/L Ratio	Leaching Efficiency
[98]	H_2SO_4	–250 μm , 60 g/l H_2SO_4 , 15 bar of O_2 pressure	200 °C	15 min	1:1	• V = 95%
[85]	H_2SO_4	1.35 M H_2SO_4 , 300 rpm stirring	40 °C	90 min	1:5	• V = 98% • Ni = 98%
[87]	H_2SO_4	–75 μm , 19.5% H_2SO_4 Conc.	80 °C	120 min	1:9	• V = 94% • Ni = 90%
[26]	H_2SO_4	1 M H_2SO_4 , 300 rpm stirring	100 °C	30 min	1:3	• V = 90%
[88]	H_2SO_4	–500 μm , 110 °C drying, 0.5 M H_2SO_4	Room Temp.	24 h	1:4	• V = 98% • Ni = 12%
[89]	$\text{H}_2\text{SO}_4 + \text{HCl} + \text{HNO}_3$	1.0 M Conc., 300 rpm stirring	RT	6 h	1:5	• V = 98% • Ni = 95% • Fe = 86%
[48]	H_2SO_4	–75 μm , 5~9% H_2SO_4 Conc.	20~80 °C	30~60 min	1:4	• V = 96%

Table 4. Cont.

Ref.	Lixiviant	Acid Leaching Conditions	Temp. °C	Time	S/L Ratio	Leaching Efficiency
[90]	H ₂ SO ₄	180 g/L H ₂ SO ₄ , 4% MnO ₂ , 500 rpm stirring	80 °C	600 min	1:10	<ul style="list-style-type: none"> • V = 96.5% • Ni = 94.8%
[92]	Ultrasound, H ₂ SO ₄	−75 μm, 27.9% lemon juice, 10% H ₂ O ₂	35 °C	120 min	0.01%	<ul style="list-style-type: none"> • V = 88.7%
[99]	H ₂ SO ₄	−100 μm, 0.5 N H ₂ SO ₄ , 400 rpm stirring	30 °C	120 min	1:5	<ul style="list-style-type: none"> • V = 65% • Ni = 60% • Fe = 42%

3.1.2. Alkaline Leaching

Several investigations on direct alkaline leaching of V-bearing waste have been carried out, indicating that Ni is insoluble in alkali solutions, which are more suitable for selective leaching of V to increase recovery. A two-stage leaching approach for HOA was proposed by Tsai [99]. The fly ash is leached in ammonia water containing ammonium sulfate (NH₄)₂SO₄, and the Ni is extracted from the solution in the first stage. The second step involves recovering V by leaching the ash residue in an alkaline (NaOH) solution. However, the method was not used in more recent research because of the decreased recovery of Ni (60%) in the ammonia/(NH₄)₂SO₄ solution, which also dissolves 8% of V in the first step. Furthermore, the study did not propose or conduct a method to recover V and Ni from the leaching solution. In a power plant, alkaline leaching and sodium hydroxide “NaOH” solution were used by Al-Zuhairi [100] to extract V with a high recovery yield (98%) from red crude oil residues. According to their discussion, 2 M NaOH concentration at 100 °C for 2 h is the ideal extraction environment for V. The effluent is then acidified to lower the pH and treated with aqueous solution of ammonia (NH₃), to precipitate V as NH₄VO₃.

According to Navarro [88], alkaline leaching of HOA by NaOH is favored over acidic leaching because it is more selective for V, which is less efficient than acidic leaching by H₂SO₄. Alkaline leaching with NaOH is carried out using a 2 M NaOH solution at 1/4 g/mL S/L ratio for 24 h at room temperature and stirring at 200 rpm. Leaching is followed by three times for 1 h water rinses. At these conditions, vanadium recovery achieves 90%, but repeated leaching and washing 6 times, each for 1 h, enhances V recovery to 98%. When the contact time approaches 12 h, it is observed that the temperature has a minimal impact on the effectiveness and kinetics of V leaching. In order to improve selectivity for V recovery while preventing Si leaching, sodium carbonate (Na₂CO₃) is used for leaching HOA. However, by employing 0.66 M Na₂CO₃ solution in the leaching procedure under the same conditions as for NaOH leaching, 80% of V is recovered. Leaching with Na₂CO₃ exhibits more excellent vanadium selectivity while having a lower leaching efficiency than leaching with NaOH.

Hakimi [101] established a flowsheet for extracting V with a high percent recovery from V-rich HOA using NaOH solution at 95 °C for 4 h, as shown in Figure 5. Leaching is followed by adding 4.5 M H₂SO₄ solution to neutralize the alkaline leachate. Al and Si are deposited once the pH is raised to 8, leaving V dissolved as sodium vanadate in the filtrate. After being treated with an ammonium compound, the latter precipitates V as NH₄VO₃, which is then heated at 450 °C for 1 h to form V₂O₅.

Akita [102] studied the recovery of nickel and vanadium from fly ash using a two-step leaching process. The first stage involves leaching Ni with NH₄Cl solution, while the second step involves leaching the remaining ash with Na₂CO₃ to dissolve the vanadium. Subsequently, vanadium is extracted using a solvent mixture of TOA and toluene, and then

precipitated as NH_4VO_3 using NH_4Cl . However, nickel can be extracted as NiS from its leach solution by precipitating it with Na_2S , as illustrated in Figure 6.

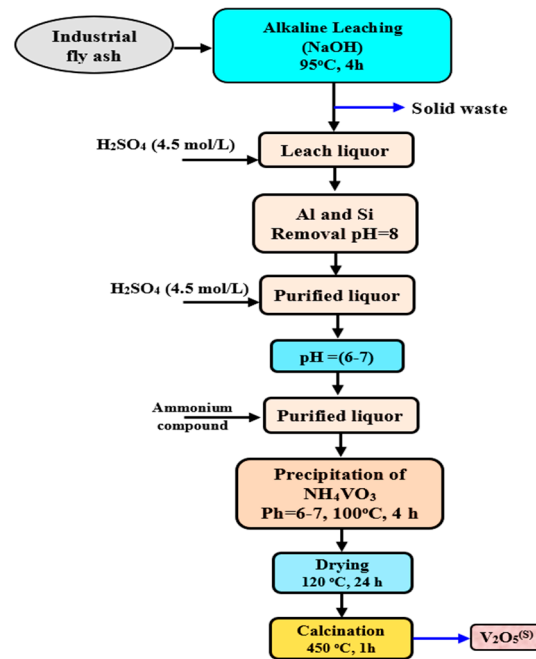


Figure 5. Flowchart of vanadium extraction from fly ash [101]. ^(S) Solid phase.

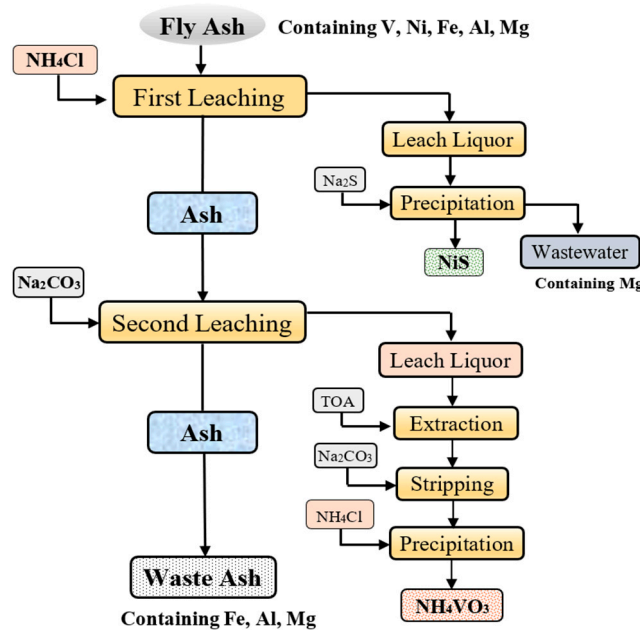


Figure 6. Process flow chart for recovery of vanadium and nickel from fly ash [102].

Vanadium, nickel, and molybdenum recovery from HOA was accomplished by Stas [55], using a two-stage leaching procedure, as shown in Figure 7. The first step is the alkaline leaching using NaOH solution to extract V and Mo . In the subsequent second step, acid leaching using H_2SO_4 leaches the residual fly ash to recover Ni . The maximum V recovery of 90% is obtained at 5 mL/g L/S ratio, at 100 °C, and for 3 h. The alkaline leaching solution containing V and Mo is gently agitated and cooled to 5 °C for one hour, which causes V to precipitate as sodium vanadate. This precipitate is then removed through filtration, leaving behind a filtrate that contains sodium molybdate. The later filtrate is heated to 90 °C and acidified with HNO_3 to precipitate Mo as H_2MoO_4 . Conversely,

sodium vanadate is dissolved again in a 5% HNO_3 solution ($\text{pH} = 8$), and $(\text{NH}_4)_2\text{SO}_4$ is introduced to the solution to precipitate vanadium as N_4HVO_3 . The latter is converted to V_2O_5 after being calcined at 500°C for 24 h. The remaining ash is leached using a 5 M H_2SO_4 solution for 3 h at 100°C and a 4 mL/g L/S ratio, which leads to extraction of 80% in the second acidic leaching stage. The pH is subsequently increased by adding a NaOH solution to the acidic leachate in two stages, which results in the precipitation of Fe and the residual V. Finally, sodium carbonate is introduced to precipitate nickel in the form of nickel carbonate (NiCO_3).

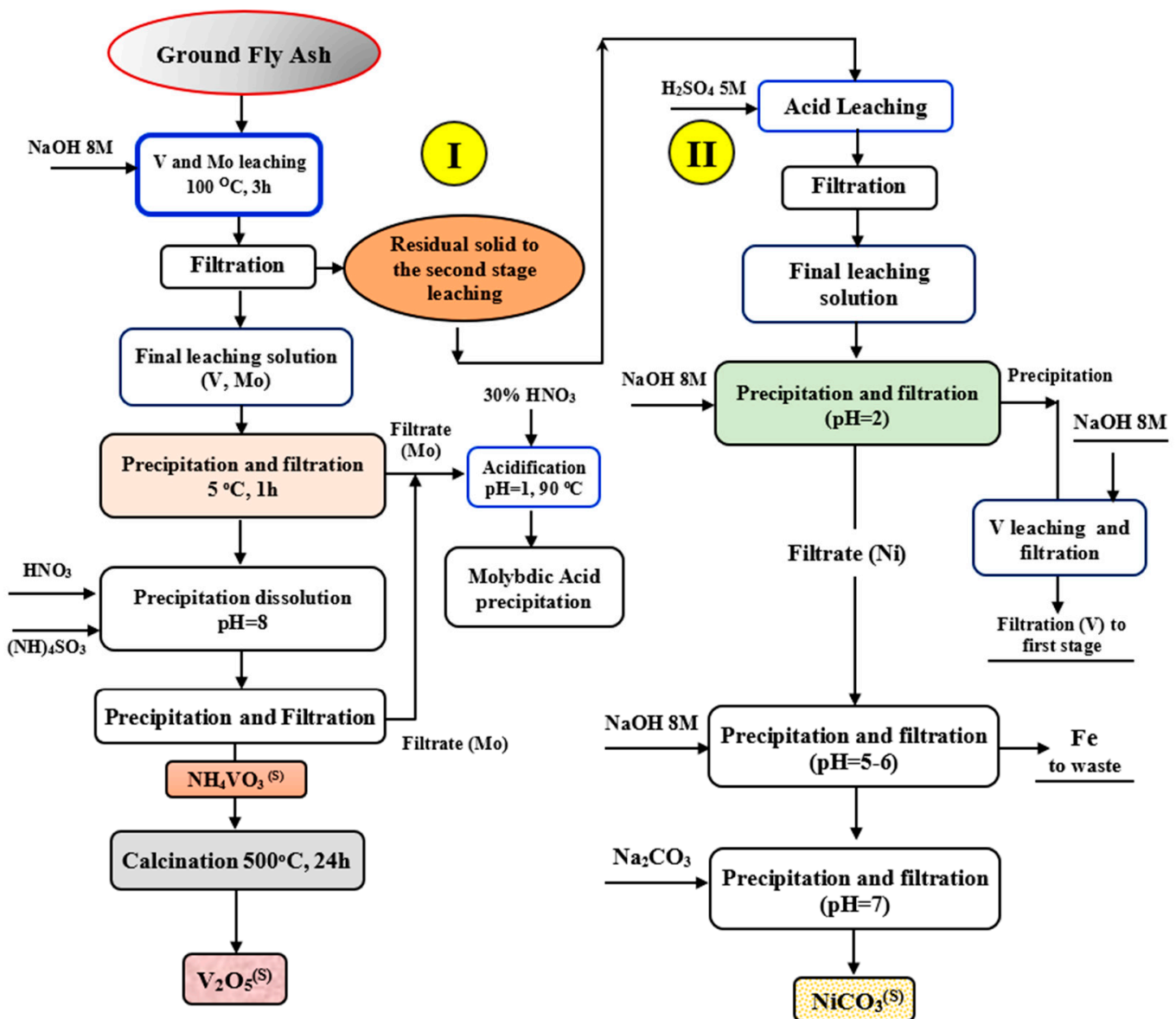


Figure 7. Two-stage leaching procedure to extract V, Mo, and Ni from fly ashes; (I) first stage alkaline leaching; (II) second stage acidic leaching [55]. ^(S) Solid phase.

Al-Ghouthi [103] studied the recovery of vanadium and nickel from HOA by two leaching processes. Using $\text{NH}_4\text{Cl}/\text{NH}_3$ solution made up of 2 M NH_4Cl and 2 M NH_3 at 50°C , at 19 mL/g 1 L/S ratio, and for 6 h, Ni is selectively extracted in the first stage. After treating the leachate with sodium sulfide (Na_2S), nickel is precipitated as NiS with 56% recovery. In the following step, vanadium is extracted from the nickel-free remaining ash using agitation leaching in a 2 M Na_2CO_3 aqueous solution at 70°C and a pH of 5.5 for a duration of 6 h. However, along with V, Fe, Mg, and Ca are also removed by

Na₂CO₃ solution. Triethylamine/toluene solution [0.1 M of (CH₃CH₂)₃N in toluene] is added to the Na₂CO₃ solution to perform selective extraction of V. The organic layer is removed and then blended once again for 3 h with a fresh 2 M Na₂CO₃ solution to extract V from the aqueous layer. Finally, the resultant aqueous layer is mixed with 1.3 M NH₄Cl for 20 h to achieve maximum recovery of 45% by precipitating the extracted V. Alkaline pressure leaching was carried out by Shahnazi [104] with a maximum vanadium leaching of 90% under the concentration of 40 to 50% NaOH and a temperature range of 110 to 160 °C. In the same way, Qiu [105] examined how pure vanadium trioxide dissolves in an oxygen system under alkaline conditions. The findings indicated that higher temperatures (130 °C) and oxygen pressure (700 kPa) resulted in a faster rate of vanadium dissolution. Additionally, stirring speeds above 800 rpm, and sodium hydroxide concentrations at 1.0 M were found to maximize the dissolution rate of vanadium (90%). A novel approach utilizing NaOH-NaNO₃ binary melts has been suggested for treating vanadium slag [106]. This method enables the extraction of both vanadium and chromium during the leaching process. When the reaction conditions are optimized (1:1 NaOH-NaNO₃ solid ratio, 400 °C, 0.5 L/min atmospheric pressure for 2 h), vanadium and chromium recovery rates can reach 93.7% and 88.2%, respectively, within 6 h. The results indicate that the reaction temperature and KOH-to-ore mass ratio are more influential factors for the extraction of vanadium and chromium. Table 5 summarizes the results of in-depth investigations on different vanadium resources using the alkaline leaching technique.

Table 5. Results of different studies on the alkaline leaching of vanadium from various V-bearing wastes.

Ref.	Lixiviant	Alkaline Leaching Condition	Temp. °C	Time	S/L Ratio	Leaching Efficiency
[99]	NaOH	−250 μm, 2 N NaOH, pH 14, 400 rpm agitation speed	30 °C	120 min	1:5	• V = 80%
[99]	NH ₄ OH	−250 μm, 4 N NH ₄ OH, pH 10	30 °C	120 min	1:5	• V = 50% • Ni = 60%
	NH ₄ OH + (NH ₄) ₂ SO ₄ + NaOH	0.25 N NH ₄ OH, 4 N (NH ₄) ₂ SO ₄ , pH 8.5, 2 M NaOH	30 °C	120 min	1:5	• V = 80% • Ni = 60%
[100]	NaOH	2 M H ₂ SO ₄ , 300 rpm stirring	100 °C	120 min	1:3	• V = 98%
[88]	NaOH	2 M NaOH+ H ₂ O, 200 rpm agitation speed	RT	24 h	1:4	• V = 98%
	Na ₂ CO ₃	0.66 M Na ₂ CO ₃ , 200 rpm stirring	RT	24 h	1:4	• V = 80%
[101]	NaOH	−500 μm, 110 °C drying, 0.5 M H ₂ SO ₄	100 °C	240 min	1:2.7	• V = 99.6%
[102]	HN ₄ Cl + NH ₄ OH	2 M HN ₄ Cl + NH ₄ OH	50 °C	300 min	1:5	• Ni = 59%
	Na ₂ CO ₃	2 M Na ₂ CO ₃	70 °C	240 min	1:4	• V = 63%
[103]	NH ₄ Cl + NH ₃	2 M NH ₄ Cl+ 2M NH ₃	50 °C	300 min	1:19	• Ni = 56%
	Na ₂ CO ₃	2 M Na ₂ CO ₃ , 200 rpm stirring	70 °C	300 min	1:20	• V = 45%
[55]	NaOH + H ₂ SO ₄	8 M NaOH 5 M H ₂ SO ₄ ,	100 °C 100 °C	180 min	1:5 1:4	• V = 90% • Ni = 80%

Even though direct acid (H₂SO₄, HCl, and HNO₃) [107–109] and alkaline (NaOH, NH₄OH, NaCO₃, and NH₄Cl) [110–112] leaching methods are the cheapest operational

and energy-efficient ways to extract valuable metal ions from heavy oil ash. They have several drawbacks, including a lack of selectivity in leaching the target metals, requiring large amounts of high acid concentration, using an oxidizing agent, polluting metals in solid ash residue, and producing leachate with hazardous elements that can complicate the precipitation and purification processes [4,113–115]. Due to the lack of an economically feasible alternative for processing vanadium-bearing waste, roasting is utilized to enhance the leaching process.

3.1.3. Bioleaching Process

Choosing the right bioleaching conditions is crucial for the microorganisms to grow ideally. The process has the advantage of being low in production cost and having a minimal environmental impact [116–120]. Bacteria like *Acidithiobacillus*, *A. ferrooxidans*, and *Acidithiobacillus thiooxidans* are well suited for chemolithoautotrophic applications in acidic conditions [121,122]. A study using *A. ferrooxidans* discovered that after 14 days, the roasted slag could leach out 83% of the chromium while only 20% of the vanadium was leached out [117]. Gomes's [123] results align with those obtained from a modified acidophilic culture of *A. thiooxidans* and *A. ferrooxidans*. Under alkaline conditions, high pH-tolerant organisms are being assessed [116,117]. These include *Pseudomonas putida*, a heterotrophic bacterium, and *Aspergillus niger*, a heterotrophic fungus. A study involving *P. putida* revealed that after 15 days, 75% of vanadium was leached from a roasted slag sample. Using the bacterium on the calcine increased dissolution to 90% [107,117].

3.1.4. Electro-Oxidation Leaching

In the leaching reactor, electrodes are inserted, and an electric field is used to convert low-valent vanadium to a higher oxidation state. Outstanding outcomes were obtained, with high recoveries of 95% for vanadium and 90% for chromium. The alkaline leaching system was applied with current densities ranging from 750 to 1000 A/m², NaOH concentration of 40~50 wt.%, and 90~120 °C temperature [124–126]. Both macro and micro perspectives allow for an understanding of the electrooxidation system's assistance in leaching. The schematic of both mechanisms is explained in more detail by Lee et al. [127]. Diffusion of reaction products is the focal point of the micro-viewpoints [124]. During leaching, metallic ions escape from the iron phase more readily in an electrical field, facilitating their directional movement. Macro-perspectives were correlated with direct and indirect oxidation processes [126]. During indirect oxidation, slag particles collide with cathodes and anodes, indirectly oxidizing vanadium and chromium as Fe³⁺ and H₂O₂ are generated.

3.2. Roasting-Leaching Processes

The roasting process of ash aims at the disintegration of the more stable and less soluble spinel phases, like Fe₂VO₄, as shown in Figure 8, and transforms them into more oxidized phases, enhancing the fact that they are more easily attacked by water/acid/alkaline solutions during the subsequent recovering process [128]. The roasting process is conducted with or without additives at temperatures ranging from 400 to 1000 °C, and advanced technologies have been utilized on fly ash to improve vanadium recovery [129,130]. To recover vanadium, the process involves oxidizing V³⁺ into acid-soluble V⁴⁺ and/or water-soluble V⁵⁺ compounds, which can then be dissolved using an appropriate reagent.

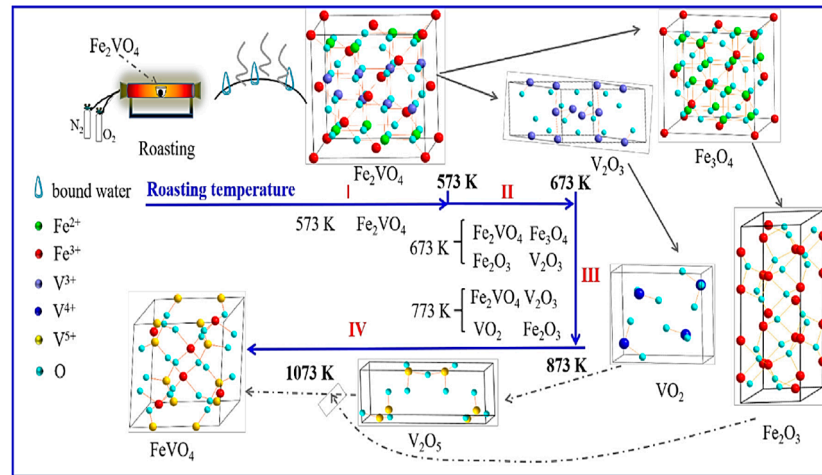


Figure 8. Schematic diagram of selective oxidation roasting of Fe₂VO₄ [131].

3.2.1. Non-Salt Roasting Assisted Leaching

This method results in the breakdown of the iron phases encasing the vanadium and chromium spinels, as explained in Equations (1) and (2) [62,108,132], allowing the formation of highly acidic leachable phases, including CaV₂O₆, Ca₃V₂O₈, MgV₂O₆, and Mg₃V₂O₈. As a result, the procedure involves the treatment of slags that have high levels of CaO/MgO.



The olivine phase breaks down at 500 °C, whereas the spinels decompose at 800 °C, based on the results obtained earlier [36,110]. Wang [110] developed a method for direct extraction of low valence vanadium (LVV) from vanadium slag without producing poisonous waste, as shown in Figure 9. Application of roasting and leaching technique leads to the extraction of LVV from vanadium slag with a recovery rate of 69.37% at 800 °C roasting temperature for 1 h in an atmosphere of N₂/O₂ equals 10. Above this temperature or with longer roasting durations, V⁵⁺ was leached in the leaching solution. Smaller vanadium slag particles resulted in a higher vanadium recovery rate but lowered the amount of LVV.

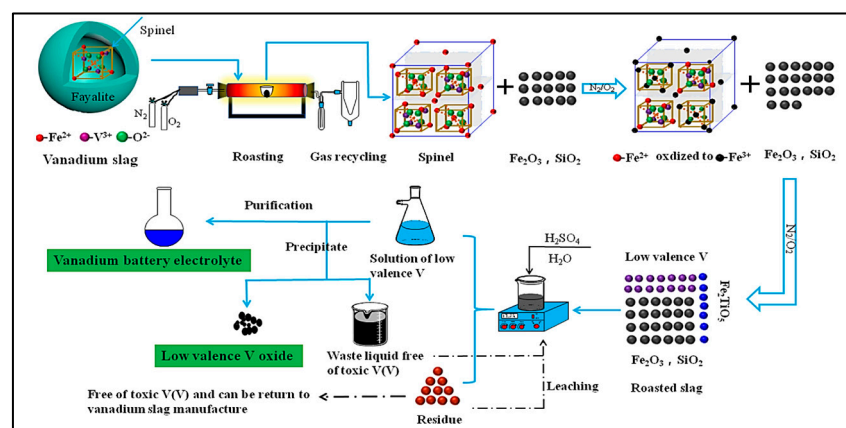


Figure 9. Novel process for extracting low valence vanadium from vanadium slag [110].

In the same context, Vitolo [56] created their three-step technique by first burning the ash under controlled conditions to lower the amount of carbon in the ash (Figure 10). The recovery of vanadium increased to 97% in the subsequent leaching process because of the

reducing the carbon component in the fly ash. The best-recommended temperature for the burning carbon phase was found to be 850 °C and resulted in a higher total recovery of V (83%) as V_2O_5 with fewer impurities. Lower V recovery resulted from higher burning temperatures (over 950 °C), which caused V to fuse and volatilize as well as produce complex V-Ni refractory compounds.

According to Li [109,133,134], the oxidation process of vanadium spinel can be described as follows: (i) conversion of vanadium spinel into a solid solution of $Fe_2O_3.V_2O_3$ at the early stages of roasting, (ii) oxidation of this solid solution to $Fe_2O_3.V_2O_4$, followed by an incomplete reaction of V^{4+} with MgO to produce Mg_2VO_4 , and (iii) extended roasting time leads to the further oxidation of vanadium, resulting in the formation of the highest-valence vanadates. In the non-salt roasting process, the chromium spinel could not convert to carcinogenic chromate salts to avoid the cost and disposal of chromium waste. Also, the vanadium may be directly leached out as NH_4VO_3 , which can be separated after cooling and crystallization (Figure 11). The leaching efficiency of vanadium could be up to 90%.

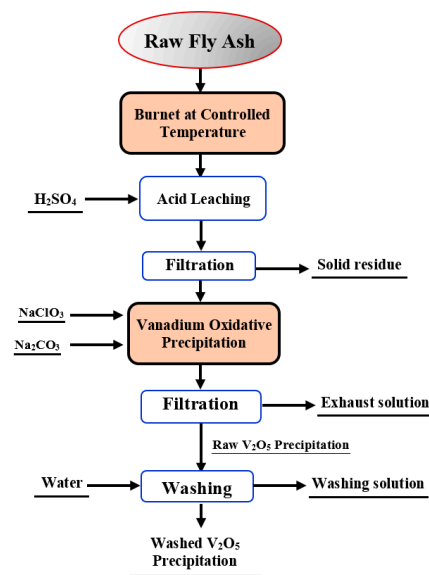


Figure 10. The block diagram for the carbonaceous fly ash combustion followed by acid leaching and oxidative precipitation of vanadium as V_2O_5 [56].

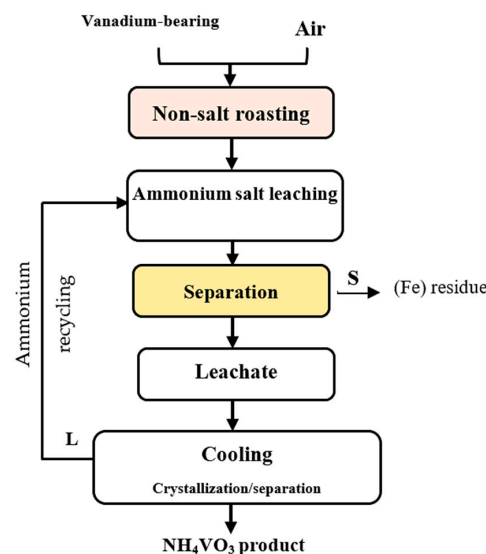


Figure 11. Flowsheet of vanadium extraction from vanadium slag using the non-salt roasting method [109].

To perform the thermodynamic analysis of this process, we attempted to create a diagram, illustrating the relationship between standard Gibbs free energy change and temperature (ΔG^0 -T), and the data required for each reaction were obtained from HSC Chemistry 9.3.0/Fact-Sage software [127]. The ΔG^0 values for all reactions are negative throughout the temperature range of 400 to 1000 °C.

This indicates that direct oxidation of the spinels ($\text{FeV}_2\text{O}_4/\text{FeCr}_2\text{O}_4$) is thermodynamically feasible. The Gibbs free energy change for reaction (1.1) is much more negative than that of reaction (1.2), exhibiting that V-spinels can be preferentially oxidized and hence decomposed before that of Cr-spinels. Zhang [135] compared the different effects of microwave and conventional blank roasting on high-chromium vanadium slag's oxidation conduct, microstructure, and surface structure. The normal spinel was oxidized to inverse spinel at 400 °C which then decomposed at 600 °C. Carrying out the roasting process at high temperatures resulted in the minority of Cr^{3+} ions in the spinel phase being incorporated into VO_2 to form the $\text{Cr}_{0.07}\text{V}_{1.93}\text{O}_4$ or CrVO_4 . Wang [136] found that the roasting process depends on the original state of vanadium in the coal stone. In the case of existing vanadium in amorphous phase form, the non-salt-roasting technology is excellent for leaching out vanadium. While the occurrence of vanadium in the vanadium-bearing waste is in a crystalline phase, the addition of a fluxing agent is necessary to achieve high vanadium leaching efficiency. Table 6 presents a summary of the extensive research conducted on vanadium resources through non-salt roasting and leaching procedures.

Table 6. Various studies on vanadium's non-salt roasting and leaching from various V sources.

Ref.	Non-Salt Roasting Conditions	Lixiviant	Leaching Conditions	Results
[56]	850 °C, $-250 \mu\text{m}$ for 60 min.	H_2SO_4	2.0 M of H_2SO_4 Conc., at 100 °C; for 60 min.	• V = 97%
[36]	850 °C for 60 min.	Na_2CO_3	160.0 (g/L) of Na_2CO_3 Conc., and 10 (mL/g) L/S ratio at 95 °C for 150 min	• V = 90% • Cr remains in the residue
[109]	900 °C for 150 min.	$(\text{NH}_4)_2\text{CO}_3$	25% of Na_2CO_3 Conc., and 4 L/S ratio at 50 °C for 150 min.	• V = 92.8%
[110]	10 N_2/O_2 , at 800 °C for 60 min.	H_2SO_4	2 M of H_2SO_4 Conc., at 90 °C; for 150 min.	• V = 69.37%
[133]	900 °C for 150 min.	$(\text{NH}_4)_2\text{C}_2\text{O}_4$	13% of $(\text{NH}_4)_2\text{C}_2\text{O}_4$ Conc., and 4 L/S ratio at 70 °C for 60 min.	• V = 90%

However, non-salt technology offers several advantages, such as reducing the carbon content of HOA, lowering its volume, and increasing the levels of V and Ni in the ash. There are some limitations, including the release of gas emissions, treating only waste with a high content of CaO or MgO, the chance of V compounds becoming volatile, the possibility of fusion and the creation of V-Ni refractory compounds at temperatures exceeding 900 °C, and alterations in the ash pH that might negatively impact the recovery of V and Ni during the leaching process.

3.2.2. Calcification Roasting Assisted Leaching

As an alternative to non-salt roasting, the clean technique of calcification roasting was used. The calcium roasting process involves combining limestone, lime, or other calcium compounds with vanadium wastes, grinding the mixture to an acceptable size, and then roasting the mixture in a vertical kiln [137,138], as illustrated in Figure 12. According to the chemical reactions listed in Table 7 and the previous studies of thermodynamic assessment, the oxidation processes involving CaO and V-spinels (Equations (3) and (4)) begin around 600 °C, whereas those using Cr-spinels (Equations (5) and (6)) start at 800 °C [139,140]. It

is noted that the vanadium and calcium reaction during the roasting process leads to the formation of calcium vanadates (CaV_2O_6 and $\text{Ca}_3\text{V}_2\text{O}_8$); the compounds mentioned are not soluble in water (Equations (7)–(13)); therefore, they must be leached out through H_2SO_4 acid (Figure 13) [137,141,142] or alkaline leaching with ammonium carbonate solution (Figure 14) [139,143,144].

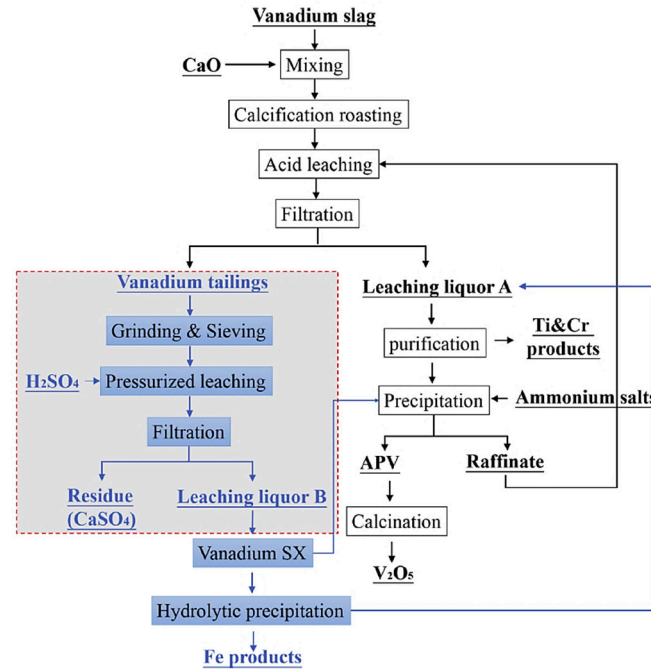


Figure 12. Flowchart of vanadium recovery from slag using calcification roasting-acid leaching technique [137].

Table 7. Reactions during calcium-roasting and leaching of vanadium-bearing waste.

Calcium Oxide (CaO)	ΔG (kJ/mol O_2)	Eqs.
$4/5\text{FeV}_2\text{O}_4 + 4/5\text{CaO} + \text{O}_2 \rightarrow 4/5\text{CaV}_2\text{O}_6 + 2/5\text{Fe}_2\text{O}_3$	$\Delta G(T) = -439.86 + 0.21T$ (kJ/mol O_2)	(3)
$4/5\text{FeV}_2\text{O}_4 + 12/5\text{CaO} + \text{O}_2 \rightarrow 4/5\text{Ca}_3\text{V}_2\text{O}_8 + 2/5\text{Fe}_2\text{O}_3$	$\Delta G(T) = -655.92 + 0.44T$ (kJ/mol O_2)	(4)
$4/7\text{FeCr}_2\text{O}_4 + 8/7\text{CaO} + \text{O}_2 \rightarrow 8/7\text{CaCrO}_4 + 2/7\text{Fe}_2\text{O}_3$	$\Delta G(T) = -255.77 + 0.15T$ (kJ/mol O_2)	(5)
$2/3\text{MgCr}_2\text{O}_4 + 4/3\text{CaO} + \text{O}_2 \rightarrow 4/3\text{CaCrO}_4 + 2/3\text{MgO}$	$\Delta G(T) = -468.37 + 0.32T$ (kJ/mol O_2)	(6)
Acid-leaching of calcified roasted product		
$\text{CaV}_2\text{O}_6 + 2\text{H}_2\text{SO}_4 \rightarrow (\text{VO}_2)_2\text{SO}_4 + \text{CaSO}_4 + 2\text{H}_2\text{O}$		(7)
$\text{Ca}_3\text{V}_2\text{O}_8 + 4\text{H}_2\text{SO}_4 \rightarrow (\text{VO}_2)_2\text{SO}_4 + 3\text{CaSO}_4 + 4\text{H}_2\text{O}$		(8)
$\text{CaCrO}_4 + \text{H}_2\text{SO}_4 \rightarrow \text{H}_2\text{CrO}_4 + \text{CaSO}_4$		(9)
Alkali-leaching of calcified roasted product		
$\text{CaV}_2\text{O}_6 + \text{Na}_2\text{CO}_3 \rightarrow 2\text{NaVO}_3 + \text{CaCO}_3$		(10)
$\text{Ca}_3\text{V}_2\text{O}_8 + 3\text{Na}_2\text{CO}_3 \rightarrow 2\text{Na}_3\text{VO}_4 + 3\text{CaCO}_3$		(11)
$\text{Ca}_3\text{V}_2\text{O}_8 + 3(\text{NH}_4)_2\text{CO}_3 \rightarrow 2(\text{NH}_4)_3\text{VO}_4 + 3\text{CaCO}_3$		(12)
$\text{CaCrO}_4 + (\text{NH}_4)_2\text{CO}_3 \rightarrow (\text{NH}_4)_2\text{CrO}_4 + \text{CaCO}_3$		(13)

Roasting and leaching behaviors of vanadium and chromium using calcification roasting-acid leaching from high-chromium vanadium slag were investigated [145]. The results indicated that more CaO combined with vanadium and reacted to form calcium vanadate ($\text{Ca}_3\text{V}_2\text{O}_8$), resulting in a high leaching efficiency of vanadium, approximately 91.14%, while the chromium remained in the leaching residue, and only 8.48% was leached. Gao [130] studied the roasting process of high chromium vanadium slag using CaO and microwave heating techniques. The effect of CaO dosage on vanadium-roasted products was investigated. At low $m(\text{CaO})/m(\text{V}_2\text{O}_5)$, CaV_2O_6 was formed, which was then converted to $\text{Ca}_2\text{V}_2\text{O}_7$ and CaVO_3 with increasing $m(\text{CaO})/m(\text{V}_2\text{O}_5)$ ratio. Results indicated that microwave radiation can reduce particle size and shorten roasting time, achieving 98.29% vanadium leaching efficiency under optimal conditions. Zhang [42] investigated the use of

lime in roasting vanadium-bearing waste. Vanadium recovery was significantly influenced by the heating rate. Hence, reducing the heating rate resulted in high vanadium recovery. The formation of $\text{Ca}_2\text{V}_2\text{O}_7$ was more favorable for leaching vanadium with sulfuric acid. Xiang [146] applied mechanical activation treatment to enhance the extraction of vanadium from converter slag at a 1:1 mole ratio of vanadium to calcium. Then, the roasted slag was leached in a 15% sulfuric acid solution for 60 min at a temperature of 50 °C, stirring speed of 150 rpm, and S/L ratio of 1:20. The results demonstrated that the mechanical activation significantly decreased the optimum roasting temperature from 900 to 800 °C and increased the leaching efficiency of vanadium from 86.0 to 90.9%, respectively.

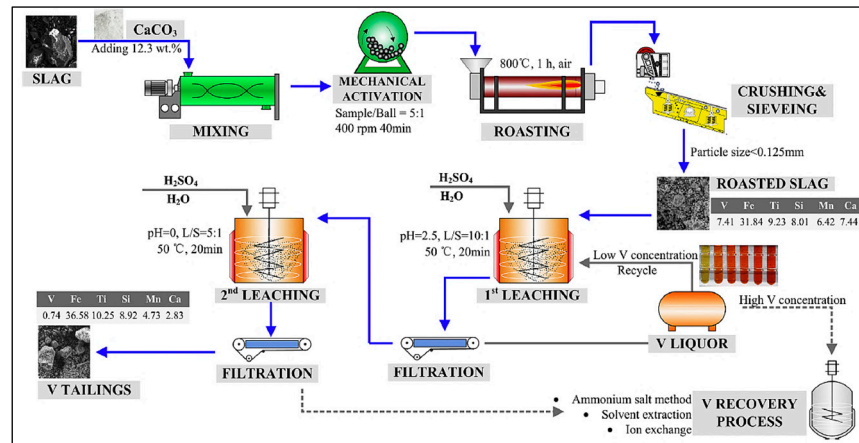


Figure 13. Flowsheet for the recovery of vanadium from vanadium slag by calcification roasting-two step leaching process [142].

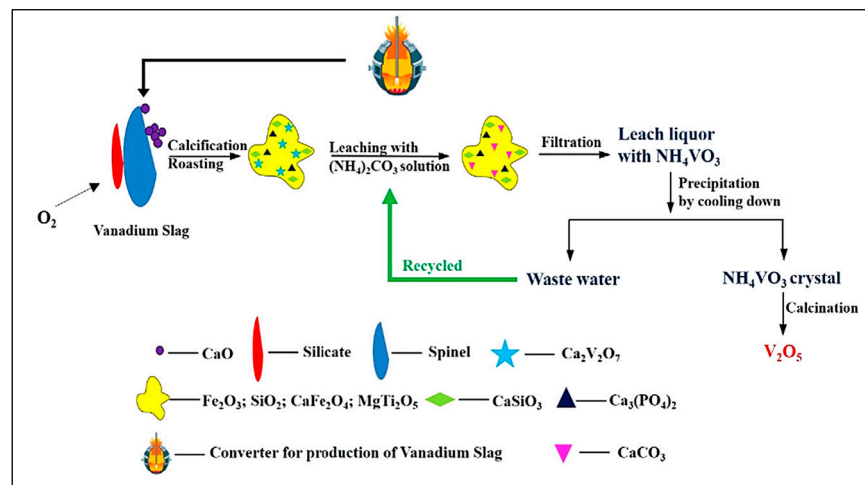


Figure 14. Flowsheet of ammonium carbonate leaching of vanadium slag [143].

Table 8 summarizes extensive research on different vanadium resources utilizing calcium roasting and leaching techniques. Utilizing this technology makes it possible to obtain high-purity vanadium leach solutions with minimal interference from elements such as silicon and phosphorus. The other advantage is that the leaching may proceed at a lower temperature when a particular ammonia salt is used. However, the leaching efficiency is much lower when using ammonia salts compared to the maximum 90% filtration of vanadium with sodium salts due to the precipitation of vanadium as NH_4VO_3 . So, problems linked to ammonia volatilization must also be considered. Additionally, there are several drawbacks associated with this technology, such as the production of a large quantity of leaching residues containing sulfate compounds, equipment corrosion, and the emission of harmful gasses, which can cause environmental contamination.

Table 8. Results of different studies on vanadium's calcium roasting and leaching from various V sources.

Ref.	Salt	Roasting Conditions	Lixiviant	Leaching Conditions	Results
[143]	CaO	1:1.1 V/Ca molar ratio, 900 °C for 120 min.	(NH ₄) ₂ CO ₃	600 g/L of (NH ₄) ₂ CO ₃ Conc., 20 (mL/g) L/S, 80 °C, 70 min.	<ul style="list-style-type: none"> V = 96% P = 9.2%
[144]	CaO	900 °C for 180 min.	NH ₄ HCO ₃	15% NH ₄ HCO ₃ , 75 °C, 180 min.	<ul style="list-style-type: none"> V = 69.2%
[147]	CaO	1:16 CaO/solid ratio, 850 °C for 120 min.	H ₂ SO ₄	15% H ₂ SO ₄ Conc., 10 (mL/g) L/S ratio, 55 °C, 70 min.	<ul style="list-style-type: none"> V = 93%
[42]	CaO	0.42 CaO/solid ratio, 850 °C for 150 min.	H ₂ SO ₄	pH 2.5, 4 L/S ratio, 65 °C, 60 min.	<ul style="list-style-type: none"> V = 91.5%
[148]	CaO	0.5 CaO/V ₂ O ₃ molar ratio, 900 °C for 60 min.	H ₂ SO ₄	20% H ₂ SO ₄ Conc., 5 (mL/g) L/S ratio, 50 °C, 60 min.	<ul style="list-style-type: none"> V = 99.4%
[149]	CaO	1 CaO/V ₂ O ₅ molar ratio, 900 °C for 120 min.	(NH ₄) ₂ SO ₄ + H ₂ SO ₄	250.0 g/L (NH ₄) ₂ SO ₄ Conc., 3.75 M H ₂ SO ₄ conc., 10 (mL/g) L/S ratio, 20 °C, 60 min.	<ul style="list-style-type: none"> V = 93.5% Cr = 0.2%
[139]	CaO	0.5 CaO/V ₂ O ₅ molar ratio, 900 °C for 60 min.	Na ₂ CO ₃	160 (g/L) Na ₂ CO ₃ Conc., 10 L/S, 80 °C, 60 min.	<ul style="list-style-type: none"> V = 93.2% Cr = 0.04%
[150]	CaCO ₃	1 Ca/V molar ratio, 850 °C for 120 min.	H ₂ SO ₄	15% H ₂ SO ₄ Conc., 10 (mL/g) L/S, 10 (mL/g), 50 °C, 60 min.	<ul style="list-style-type: none"> V = 83%
[151]	(1st) CaO (2nd) Na ₂ CO ₃	1st stage: 5 CaO/V ₂ O ₃ molar ratio, 780 °C for 60 min 2nd stage: 3.3 Na ₂ CO ₃ /Cr ₂ O ₃ at 950 °C	1st stage: H ₂ SO ₄ 2nd stage: Water	1st stage: 3.75 M H ₂ SO ₄ Conc., 5 L/S ratio, 70 °C, 60 min. 2nd stage: 3 L/S ratio, 3 (mL/g), 25 °C, 20 min.	1st stage: <ul style="list-style-type: none"> V = 90% Cr = 1% 2nd stage: <ul style="list-style-type: none"> Cr = 87% V = 99%

3.2.3. Sodium Salt Roasting Assisted Leaching Process

Traditional roasting technologies include sodium roasting, which can be traced back to Blecker's first salt-roasting technology in 1912 [128]. Basically, a mixture of sodium salts (Na₂CO₃, Na₂SO₄, NaCl, and NaOH) as a source for alkalis was roasted with vanadium-bearing waste in a furnace at high temperatures, depending on the melting points of the sodium sources as follows: 1200~1250 °C for Na₂SO₄, 750~850 °C for NaCl, 800~1000 °C for Na₂CO₃, and 400~800 °C for NaOH [43,152,153]. A maximum amount of oxygen was used during roasting to oxidize the V³⁺ and convert it into soluble sodium vanadates (NaVO₃, Na₄V₂O₇) through the chemical reactions listed in Table 9 [127]. The vanadium conversion degree in these sodium sources follows the following order: NaOH > Na₂SO₄ > Na₂CO₃ > NaCl [154]. This order can be attributed to several reasons, including the diffusivity of the different sodium sources into the interior layers of the wastes, where they react with the V-spinels [155–157]. Despite all the limitations of this technology, which include the formation of harmful gaseous products, such as SO₂, Cl₂, or CO₂, fusion of NaCl at high temperatures, and high energy consumption while using sodium salts as the alkali source, it remains the best method in terms of selective vanadium extraction with low operating cost. The above serious environmental pollution greatly hinders the sustainable development of V extraction from V-bearing materials [158,159]. Consequently, efforts are still needed to develop an eco-friendly and effective method for extracting V from V-bearing materials. Attention has also been paid to recycling the Na⁺ from the leach solution, using a membrane-assisted electrochemical cell to separate the cation from vanadium ions [160].

Table 9. Reactions during salt roasting and leaching of vanadium-bearing waste.

Sodium Sulfate (Na ₂ SO ₄)	ΔG (kJ/mol O ₂)	Eqs.
4/3FeV ₂ O ₄ + 4/3Na ₂ SO ₄ + O ₂ → 8/3NaVO ₃ + 2/3Fe ₂ O ₃ + 4/3SO ₂	ΔG(T) = −155.62 − 0.08T	(14)
4FeV ₂ O ₄ + 8Na ₂ SO ₄ + O ₂ → 4Na ₄ V ₂ O ₇ + 2Fe ₂ O ₃ + 8SO ₂	ΔG(T) = 985.43 − 1.19T	(15)
FeCr ₂ O ₄ + 2Na ₂ SO ₄ + O ₂ → 2Na ₂ CrO ₄ + 1/2Fe ₂ O ₃ + 2SO ₂	ΔG(T) = 936.43 − 0.59T	(16)
2MgCr ₂ O ₄ + 4Na ₂ SO ₄ + O ₂ → 4Na ₂ CrO ₄ + 2MgO + 4SO ₂	ΔG(T) = 1195.64 − 0.78T	(17)
Sodium chloride (NaCl)		
4/5FeV ₂ O ₄ + 8/5NaCl + 4/5H ₂ O + O ₂ → 8/5NaVO ₃ + 2/5Fe ₂ O ₃ + 8/5HCl	ΔG(T) = −245.36 + 0.04T	(18)
4/9FeV ₂ O ₄ + 16/9NaCl + 4/9H ₂ O + O ₂ → 4/9Na ₄ V ₂ O ₇ + 2/9Fe ₂ O ₃ + 8/9HCl	ΔG(T) = −113.65 − 0.05T	(19)
4/7FeCr ₂ O ₄ + 16/7NaCl + 8/7H ₂ O + O ₂ → 8/7Na ₂ CrO ₄ + 8/7Fe ₂ O ₃ + 16/7HCl	ΔG(T) = 79.07 − 0.01T	(20)
2/3MgCr ₂ O ₄ + 8/3NaCl + 4/3H ₂ O + O ₂ → 4/3Na ₂ CrO ₄ + 4/3MgO + 8/3HCl	ΔG(T) = 148.14 − 0.12T	(21)
4/7FeV ₂ O ₄ + 8/7NaCl + O ₂ → 8/7NaVO ₃ + 2/7Fe ₂ O ₃ + 4/7Cl ₂	ΔG(T) = −186.26 + 0.09T	(22)
4/9FeV ₂ O ₄ + 16/9NaCl + O ₂ → 4/9Na ₄ V ₂ O ₇ + 2/9Fe ₂ O ₃ + 8/9Cl ₂	ΔG(T) = −80.26 + 0.06T	(23)
4/7FeCr ₂ O ₄ + 16/7NaCl + O ₂ → 8/7Na ₂ CrO ₄ + 2/7Fe ₂ O ₃ + 8/7Cl ₂	ΔG(T) = 55.83 + 0.02T	(24)
2/5MgCr ₂ O ₄ + 8/5NaCl + O ₂ → 4/5Na ₂ CrO ₄ + 2/5MgO + 4/5Cl ₂	ΔG(T) = 36.74 + 0.005T	(25)
Sodium carbonate (Na ₂ CO ₃)		
4/5FeV ₂ O ₄ + 4/5Na ₂ CO ₃ + O ₂ → 8/5NaVO ₃ + 2/5Fe ₂ O ₃ + 4/5CO ₂	ΔG(T) = −345.3 + 0.04T	(26)
4/5FeV ₂ O ₄ + 8/5Na ₂ CO ₃ + O ₂ → 4/5Na ₄ V ₂ O ₇ + 2/5Fe ₂ O ₃ + 8/5CO ₂	ΔG(T) = −306.70 + 0.07T	(27)
4/7FeCr ₂ O ₄ + 8/7Na ₂ CO ₃ + O ₂ → 8/7Na ₂ CrO ₄ + 2/7Fe ₂ O ₃ + 8/7CO ₂	ΔG(T) = −94.64 − 0.04T	(28)
2/3MgCr ₂ O ₄ + 4/3Na ₂ CO ₃ + O ₂ → 4/3Na ₂ CrO ₄ + 2/3MgO + 4/3CO ₂	ΔG(T) = −92.39 + 0.14T	(29)
Sodium hydroxide (NaOH)		
4/5FeV ₂ O ₄ + 8/5NaOH + O ₂ → 8/5NaVO ₃ + 2/5Fe ₂ O ₃ + 4/5H ₂ O	ΔG(T) = −458.66 + 0.11T	(30)
4/5FeV ₂ O ₄ + 16/5NaOH + O ₂ → 4/5Na ₄ V ₂ O ₇ + 2/5Fe ₂ O ₃ + 8/5H ₂ O	ΔG(T) = −533.41 + 0.08T	(31)
4FeCr ₂ O ₄ + 8NaOH → 4Na ₂ CrO ₄ + 2Fe ₂ O ₃ + 4H ₂ O	ΔG(T) = −273.10 − 0.02T	(32)
2/3MgCr ₂ O ₄ + 8/3NaOH + O ₂ → 4/3Na ₂ CrO ₄ + 2/3MgO + 4/3H ₂ O	ΔG(T) = −210.17 + 0.01T	(33)
Water leaching of sodium roasted product		
NaVO ₃ + H ₂ O → H ₂ VO(− ₄) + Na ⁺		(34)
Na ₄ V ₂ O ₇ + H ₂ O → 2HVO(− ₄) + Na ⁺		(35)
Acid-leaching of sodium roasted product		
2NaVO ₃ + 2H ₂ SO ₄ → (VO ₂) ₂ SO ₄ + Na ₂ SO ₄ + 2H ₂ O		(36)
Na ₄ V ₂ O ₇ + 3H ₂ SO ₄ → (VO ₂) ₂ SO ₄ + 2Na ₂ SO ₄ + 3H ₂ O		(37)
Na ₂ CrO ₄ + H ₂ SO ₄ → H ₂ CrO ₄ + Na ₂ SO ₄		(38)
Alkaline-leaching of sodium roasted product		
Na ₂ O.V ₂ O ₅ + 4NaOH → 2Na ₃ VO ₄ + 2H ₂ O		(39)
2NaVO ₃ + (NH ₄) ₂ CO ₃ → 2NH ₄ VO ₃ + Na ₂ CO ₃		(40)
Na ₄ V ₂ O ₇ + 2(NH ₄) ₂ CO ₃ → (NH ₄) ₄ V ₂ O ₇ + 2Na ₂ CO ₃		(41)
Na ₂ CrO ₄ + 2(NH ₄) ₂ CO ₃ → (NH ₄) ₄ V ₂ O ₇ + 2Na ₂ CO ₃		(42)

Anyway, the water-leaching process mostly applies to products undergoing sodium roasting, which takes place through Equations (34) and (35). Metal sulfates are formed by dissolving sodium vanadate compounds by H₂SO₄, according to Equations (36)–(38), and ammonium carbonate leaching is accomplished through Equations (39)–(42). However, the leaching effectiveness depends on the degree of metal converted during roasting, where sodium vanadate can be leached out. With regard to this case, there are certain common features for the processes that are used in the commercial plants of vanadium production from industrial wastes, such as the sodium salt roasting-water leaching-ammonia precipitation process utilized at Highveld Steel and Vanadium Corp. (*South Africa*), Chengde Iron and Steel Group (*China*), Nizhniy Tagil Iron and Steel Works (*NTMK, Russia*), etc. [127]. Li [43] reported that only 87.9% of V and 6.3% of Cr were recovered from calcined waste at Na/V molar ratio of 3.3 at 800 °C using water leaching, as shown in Figure 15. When the leaching residue was subjected to second sodium calcination at (Na/(V, Cr) molar ratio of 2.86 and 950 °C), about 90.7% of vanadium and 96.4% of chromium were leached, giving an overall recovery of vanadium and chromium of 98.9% and 96.4%, respectively.

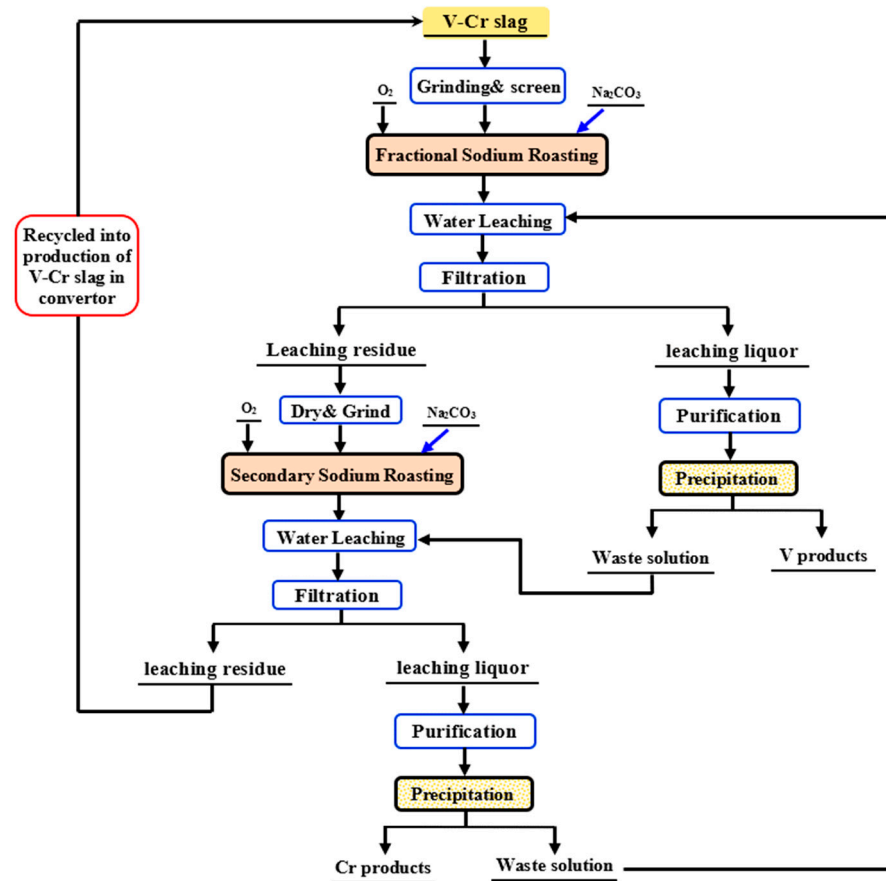


Figure 15. Novel process based on salt-roasting to extract vanadium and chromium from the V-Cr slag [43].

Wen [161] evaluated the leaching of the vanadium and chromium using sodium salts roasting (Na_2CO_3) and then leaching them with $(\text{NH}_4)_2\text{SO}_4$, showing that 94.6% vanadium and 96.5% chromium were leached. According to Zhao [162], vanadium can be leached from stone coal with the addition of 6 wt.% sodium chloride and 10 wt.% sodium sulfates during the roasting process. It was noted that the vanadium-bearing muscovite with quartz was converted to feldspar group minerals (albite, orthoclase, and anorthite). These results could produce some potential methods for vanadium recovery from stone coal. Puhong [129] roasted red cake obtained from multi-processing of stone coal with 22.5 g NaOH /25 g red cake at 170°C for 1 h, then used water leaching at 98°C for 60 min. with a solid/liquid ratio of 1:3.3 g/mL. It was noted that the V leaching efficiency was up to 97% after purification and calcination as V_2O_5 , with a purity of 99.3%.

A three-step process was performed on HOA containing 85 wt.% unburned C and 2.2 wt.% V, beginning with carbon burning, followed by salt roasting and water leaching. It was noted that the 4 h. calcining step at 650°C removes most of the carbon and thus increases the V content to 19 wt.%. Then, the burned enriched-V ash was roasted with sodium carbonate Na_2CO_3 at 650°C for 4 h to convert V oxides into sodium metavanadate (NaVO_3), which is a water-soluble compound [163]. The calcined ash was leached with water for 4 h at 60°C with an S/L ratio of 1:50 g/mL. Water leaching leads to the selective dissolving of V with about 92% recovery, leaving Fe and Ni compounds undissolved in the residue of the ash. By adding $(\text{NH}_4)_2\text{SO}_4$, V is precipitated as NH_4VO_3 from the leaching solution to separate V from the solution [101].

In the same context, Ibrahim et al. [59] discussed a recent technique for converting V compounds into water-soluble vanadates (NaVO_3) through roasting with NaCl , as shown in Figure 16. They found that over 95.5% of the vanadium leached out after the HOA was

roasted with 20% NaCl for 2.5 h. Then, the vanadium was leached using distilled water with an L/S ratio of 10 mL.g⁻¹. The purity of the obtained NH₄VO₃ powder was estimated to be about 92% using direct precipitation from vanadium-pregnant solution by NH₄Cl addition, and the precipitation efficiency of NH₄VO₃ powder was estimated to be around 91.5%, and the total recovery rate of vanadium reached up to 87.60%. Then, the ammonium meta-vanadate was calcined at 550 °C for 3 h to produce V₂O₅ powder with an estimated 83% purity (Figure 17).

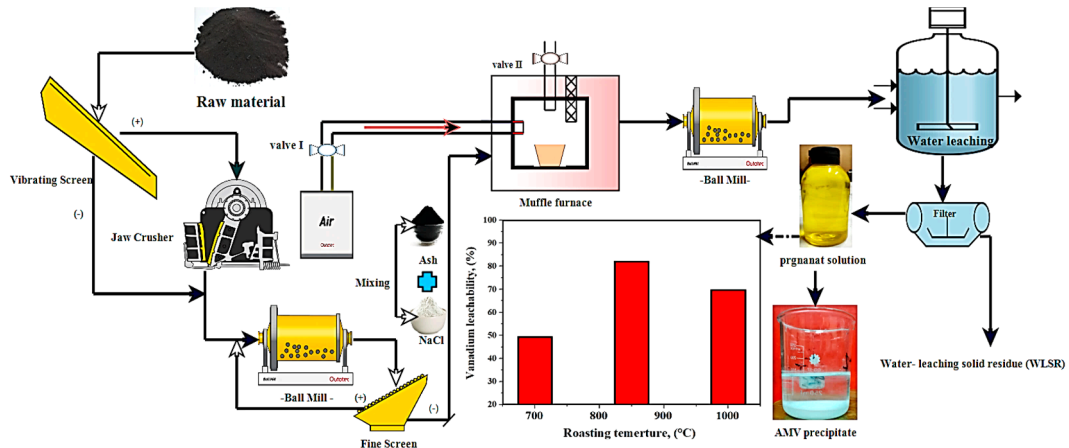


Figure 16. Schematic flow of salt-roasting and water-leaching process from boiler ash for vanadium extraction [59].

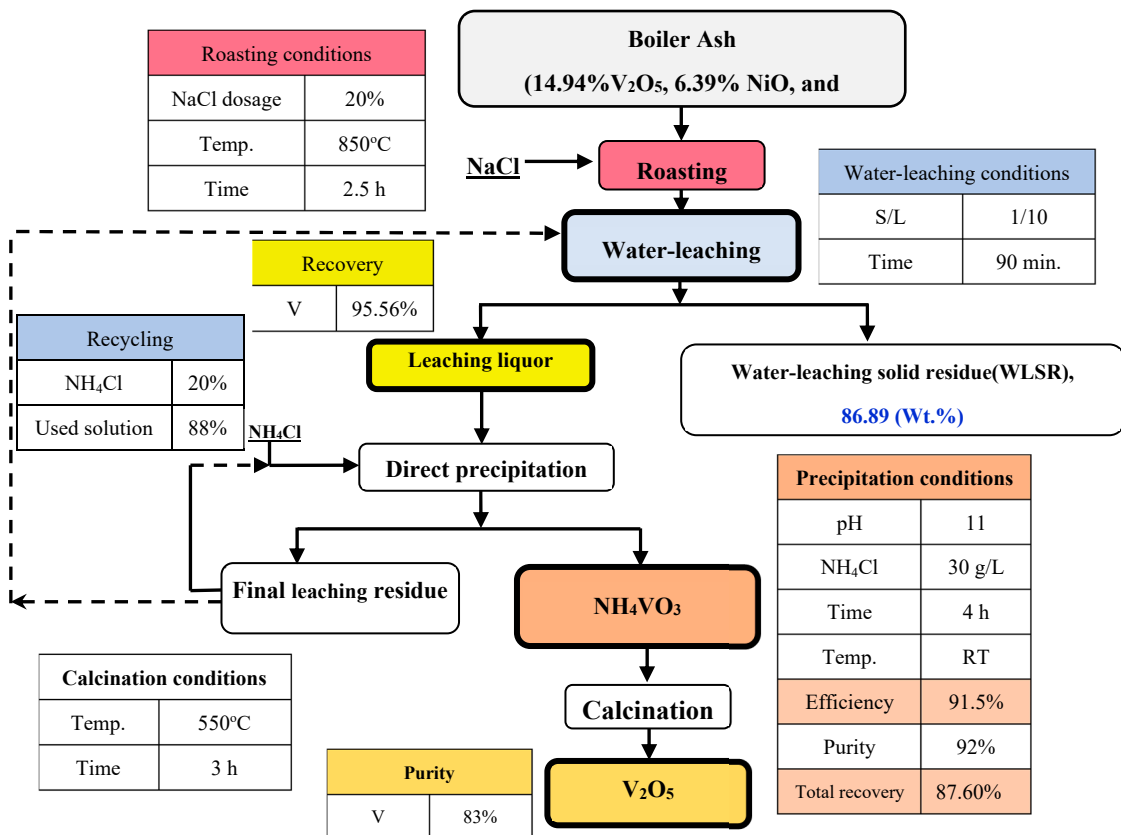


Figure 17. The quantitative flowsheet for V recovery from Egyptian boiler ash using sodium salt-roasting and water-leaching process [59].

The authors [59] comprehensively investigated the solid-state and phase transformation mechanisms that govern the selective extraction of vanadium from HOA. The

SEM images are displayed in Figure 18 for the roasted sample produced at 700 °C, and the corresponding EDS analysis for different points on the burnt ash is listed in Table 10. The results (Figure 18a) showed that the roasted particles are presented in an irregular shape with different sizes, and a few areas of spinel surface structure have been destroyed. According to the elemental mapping analyses shown in points S₁ and S₄, the decomposition of the spinel started to release the vanadium molecules, which indicates that sodium and vanadium are partially compatible (Figure 18b). The main information shown in this figure includes the following: (1) the particles are loose and dispersed, indicating that the interaction between particles is not significant under this temperature; (2) the distribution of sodium is relatively extensive and uniform, indicating that NaCl has not entirely reacted and formed a new sodium phase; and (3) the relative enrichment of vanadium appeared in some particles with high sodium content, indicating that some phases containing sodium and vanadium were formed.

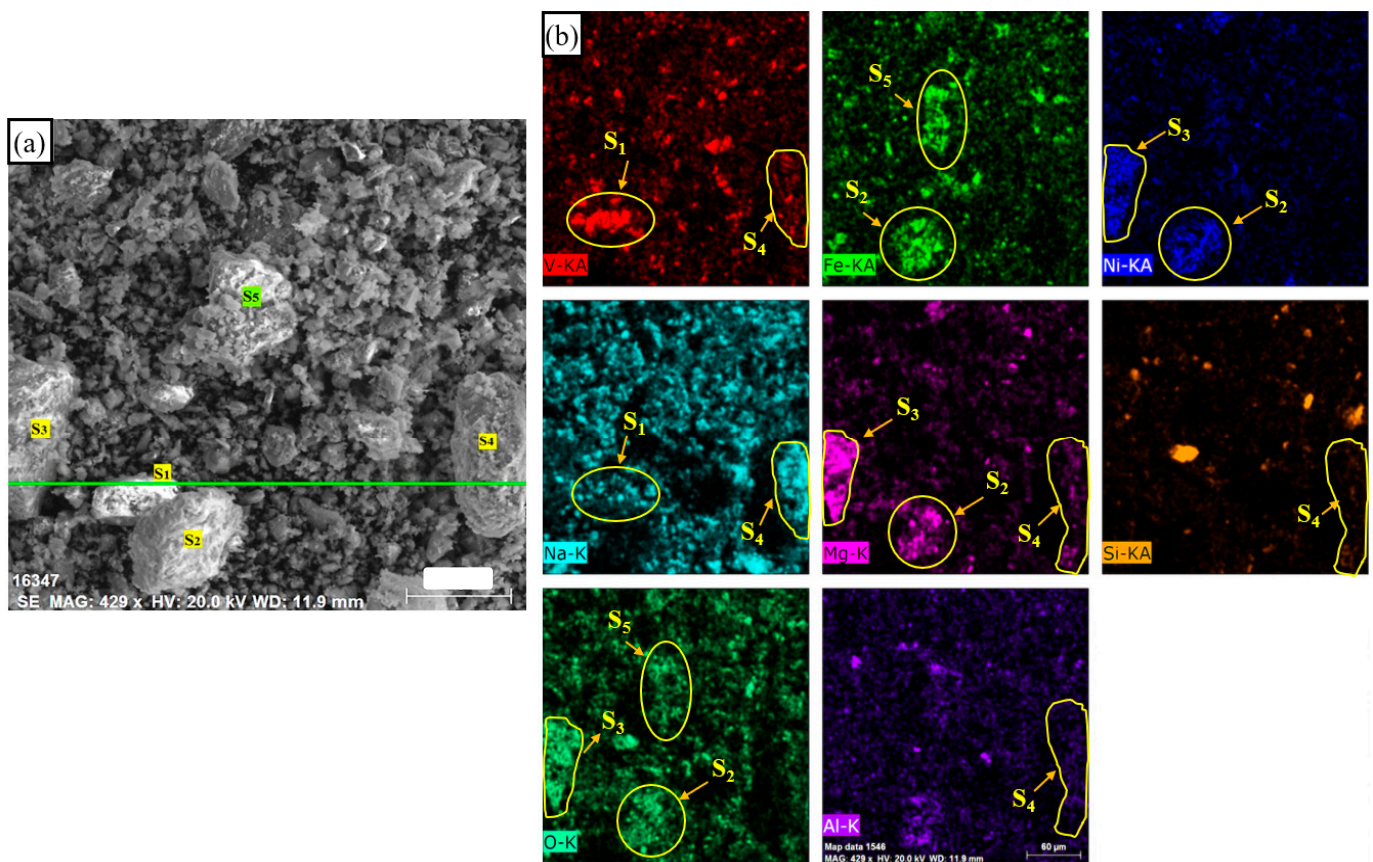


Figure 18. SEM images of roasted boiler ash sample: (a) at 700 °C for 2 h, and (b) elemental mapping images of burned surface.

Table 10. Spots EDS analysis of roasted boiler ash at 700 °C for 2 h and 20 wt.% of NaCl.

Spots	Composition (wt., %)							
	V	Ni	Fe	O	Na	Mg	Al	Si
S ₁	18.57	2.93	5.88	28.07	25.39	15.12	3.03	1.01
S ₂	2.24	7.72	4.47	26.34	23.21	31.59	3.15	1.28
S ₃	1.2	10.39	17.58	20.56	18.05	22.88	5.61	3.73
S ₄	10.08	4.61	6.01	30.5	28.24	13.5	6.02	1.04
S ₅	3.94	3.14	25.2	24.6	19.83	11.42	9.34	2.53

Based on the EDS analysis (Table 10) of the specific locations (S_1 and S_4), it was clear that the chemical composition showed a moderate correlation between the levels of vanadium and sodium due to the limited reaction range of O_2 with vanadium spinel to release their oxides. So, not all quadruple vanadium (V^{4+}) was oxidized to the highest V^{5+} valency [64,164]. As a result, the reaction temperature at $700\text{ }^\circ\text{C}$ was not sufficient to convert more of the V found in the vanadium compound into water-soluble sodium vanadates because almost all of V still exists inside the spinel, with less outer distribution than the central region and not enough opportunity to react with NaCl, resulting in decreasing the vanadium leachability [111]. To further explore, a line scan analysis was performed, as shown in Figure 19. Clearly, it was noted that the V and Na lines are aligned to some extent, suggesting an inconsiderable liberation of the vanadium element from the spinel surface. Furthermore, a large amount of free sodium remains along the line, meaning it did not enter into the chemical reaction.

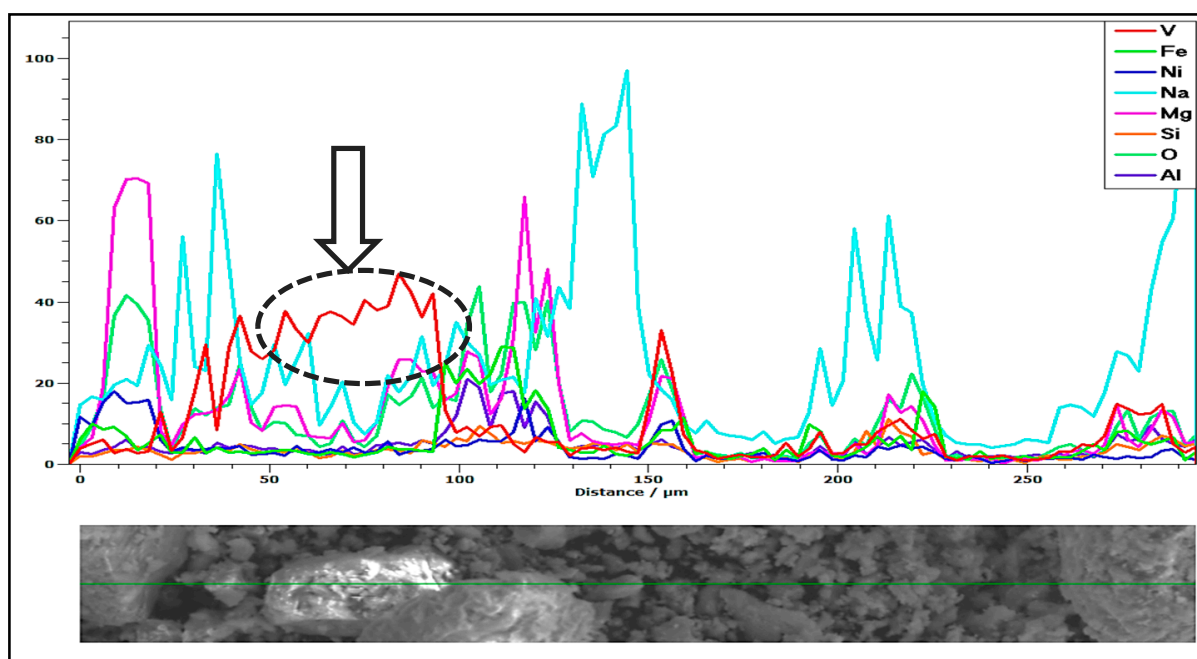


Figure 19. Line scan and distribution elements of the roasted boiler ash at $700\text{ }^\circ\text{C}$.

Their findings indicate that a roasting temperature of $850\text{ }^\circ\text{C}$ (Figure 20) appears optimal for facilitating the O_2 reaction with vanadium-bearing minerals. This temperature provides an excellent opportunity for vanadium molecules to react with sodium chloride, forming the sodium metavanadate phase ($NaVO_3$). However, this phase can be easily extracted through a water-leaching process, resulting in the liberation of vanadium molecules, as shown in. Elemental scan lines demonstrated that the Na and V lines align, indicating that a considerable amount of the V element has been released from the spinel surface.

Elemental scan lines demonstrated the distribution of elements in the roasted ash at $850\text{ }^\circ\text{C}$ is shown in Figure 21. Also, it was noted that there is an abroad alignment of the Na and V lines, suggesting that there is a significant liberation of the V element from the spinel surface. Also, along the line, there are no remains of free sodium, which means that all of it was entirely consumed in the process of forming a water-soluble sodium vanadate compound. This result confirms the hypothesis explained in the TGA data of the same study, which has been attributable to the complete thermal decomposition of vanadium spinel (FeV_2O_4) and vanadyl sulfates at $850\text{ }^\circ\text{C}$.

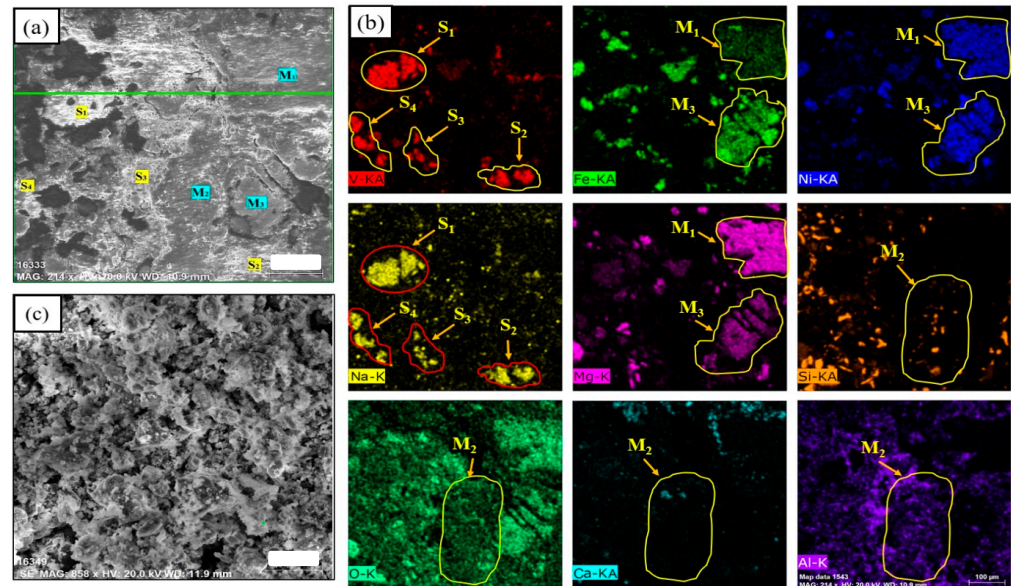


Figure 20. SEM images of roasted boiler ash sample: (a) at 850 °C for 2 h, (b) elemental mapping images of the surface, and (c) back-scattered morphology image [59].

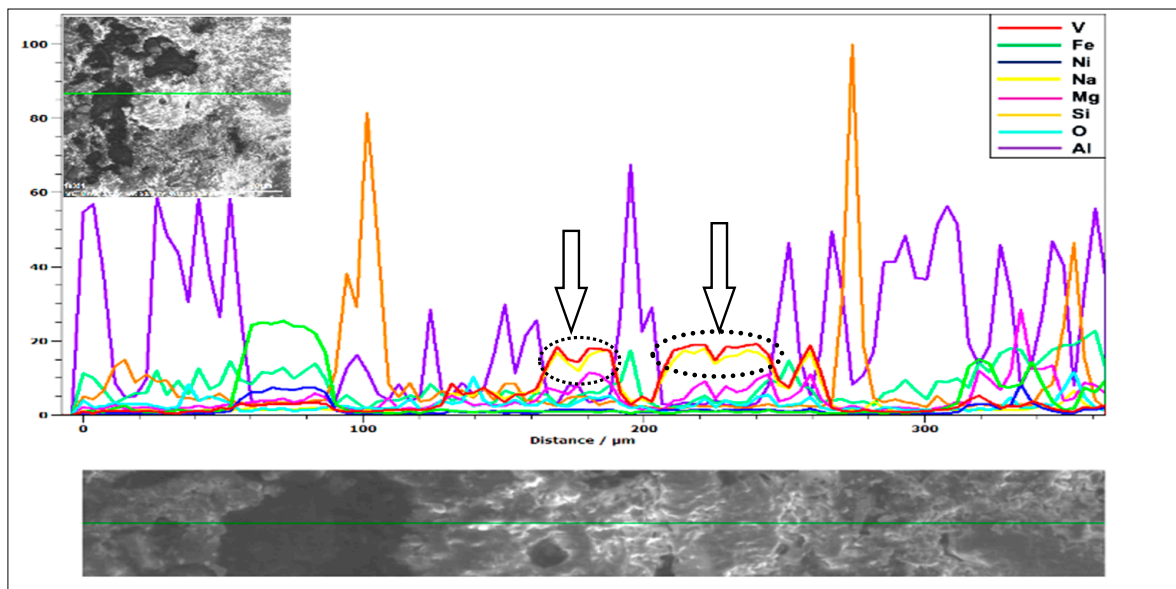


Figure 21. Line scan and distribution elements of the roasted boiler ash at 850 °C.

Furthermore, there are no signs of unbound sodium present in the mixture, suggesting that it was entirely consumed in the process of forming a water-soluble sodium vanadate compound. The results of the point-scan analysis of three different surface products are listed in Table 11. Meanwhile, the excessive roasting temperature of up to 1000 °C (Figure 22) would allow for the formation of refractory compounds (i.e., sintered from V, Ni, Fe). In addition, the formation of the aluminum silicate ($\text{NaAlSi}_2\text{O}_6$) phase increases due to the melting of NaCl salt, which leads to the formation of agglomerate that could hinder oxygen transfer during the roasting process and hence decrease the vanadium percent recovery.

Generally, the direct leaching process is poorly selective and has varying leaching efficiencies among different vanadium-containing phases. Consequently, subsequent separation and purification processes for vanadium and other metals in the leaching solution are more complex, with a wide range of reagent types and high consumption rates. On

the other hand, the roasting-leaching process enables control over the occurrence form of vanadium through roasting, thereby ensuring efficient vanadium leaching. Specifically, the sodium salt roasting process can be employed to selectively separate vanadium using the water leaching method, which offers advantages such as high leaching efficiency, excellent selectivity, reduced consumption of leaching reagents, and suitability for treating materials with complex forms of vanadium occurrence. Based on the characteristics of V-bearing waste of high vanadium content and complex vanadium occurrence forms, NaCl has been used, a low-cost and abundantly available salt compared to other salts in the roasting-water leaching process, to study the extraction process of vanadium and focus on the transition law and mechanism of the vanadium-containing phase during sodium salt roasting so as to provide the theoretical basis for efficient extraction of vanadium. A summary of the comprehensive research carried out on various vanadium resources using sodium-salt roasting and leaching processes is presented in Table 12.

Table 11. Spots EDS analysis of roasted boiler ash at 850 °C and 1000 °C for 2 h and 20 wt.% of NaCl.

	Spots	Composition (wt., %)								
		V	Ni	Fe	O	Na	Mg	Ca	Al	Si
850 °C	S ₁	17.86	1.45	5.29	38.23	20.45	7.19	1.02	3.96	4.55
	S ₂	12.62	1.74	4.83	35.01	25.11	7.05	0.98	7.58	5.08
	S ₃	10.06	1.41	3.27	37.54	27.04	6.89	1.08	7.26	5.45
	S ₄	14.08	1.97	2.46	33.93	25.06	8.87	1.5	5.97	6.16
	M ₁	0.92	22.11	38.77	27.87	1.15	5.45	1.01	1.63	1.09
	M ₂	0.81	4.28	7.24	35.3	15.42	3.95	1.92	14.57	16.51
	M ₃	1.07	19.95	36.81	25.76	2.08	9.03	1.02	1.45	2.83
1000 °C	S ₁	19.35	16.76	23.21	25.61	1.03	9.5	2.02	1.51	1.01
	S ₂	18.87	15.98	21.28	27.84	1.31	10.46	1.98	1.36	0.92
	S ₃	19.06	19.19	20.14	26.75	1.56	9.69	1.04	1.47	1.1
	M	-	-	-	47.18	3.14	32.21	1.5	-	15.97
	N ₁	-	-	-	30.65	46.04	-	3.51	9.7	10.1
	N ₂	-	-	-	28.71	39.45	-	2.08	19.84	9.92

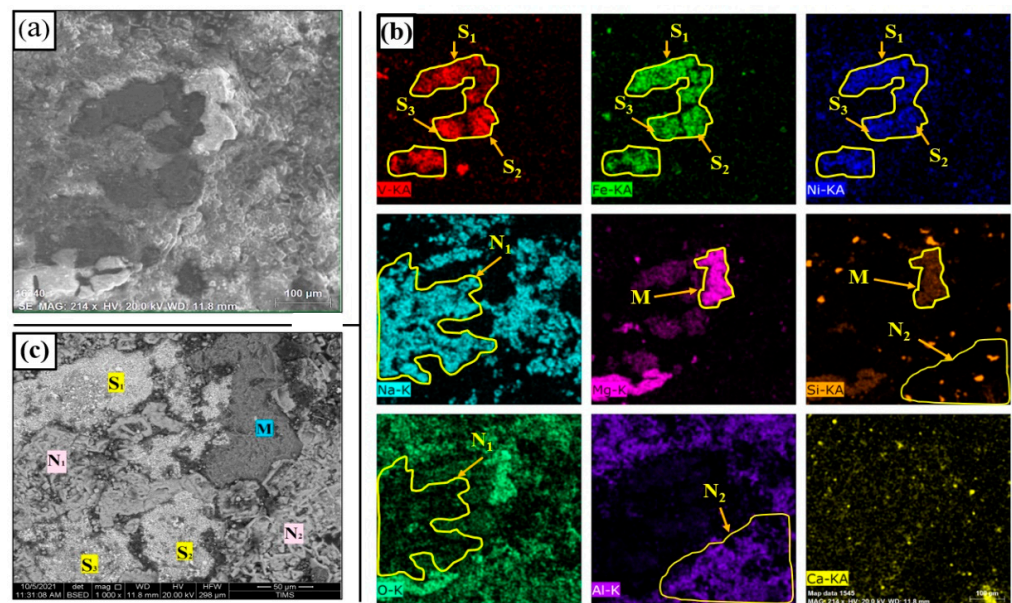


Figure 22. SEM images of roasted boiler ash sample: (a) at 1000 °C for 2 h, (b) elemental mapping images of the polished surface, and (c) back-scattered morphology image.

Table 12. Results of different studies on vanadium’s sodium-salt roasting and leaching from various V sources.

Ref.	Sodium-Salt Roasting	Roasting Conditions	Lixiviant	Leaching Conditions	Results
[59,165]	NaCl	1st stage Roasting at 850 °C for 150 min. 2nd stage Water leaching solid residue (WLSR)	Water H ₂ SO ₄	10 (mL/g) L/S ratio at 25 °C for 90 min. –63 µm, 8% H ₂ SO ₄ Conc., in 15 (mL/g) L/S ratio at 85 °C; for 240 min.	1st stage: <ul style="list-style-type: none">• V = 95.5% 2nd stage: <ul style="list-style-type: none">• Ni = 95.02%• Zn = 90.13%
[43]	Na ₂ CO ₃ + O ₂	1st stage (V-roasting) 3.3 Na/V molar ratio at 800 °C for 120 min. 2nd stage (Cr-roasting) 2.86 Na/(V,Cr) molar ratio at 950 °C for 120 min.	Water	1st stage: 3 (mL/g) L/S ratio at 25 °C; for 20 min. 2nd stage: 3 (mL/g) L/S ratio at 25 °C; for 20 min.	1st stage: <ul style="list-style-type: none">• V = 87.9%• Cr = 6.3% 2nd stage: <ul style="list-style-type: none">• Cr = 96.4%• V = 90.7%
[166]	Na ₂ CO ₃	41/9 Na ₂ CO ₃ /solid ratio at 700 °C for 150 min.	Water	5 (mL/g) L/S ratio at 90 °C for 30 min.	<ul style="list-style-type: none">• V = 90%
[167]	Na ₂ CO ₃	0.1 Na ₂ CO ₃ /solid ratio at 0.2 1000 °C for 45 min.	Na ₂ CO ₃ + NaOH	45 + 10 (g/L) of Na ₂ CO ₃ + NaOH Conc., in 20 L/S at 80 °C for 60 min.	<ul style="list-style-type: none">• V = 80%
[41]	Na ₂ CO ₃	1.0 Na ₂ CO ₃ /solid ratio, at 2.0 1000 °C for 120 min.	H ₂ SO ₄	3.0 M H ₂ SO ₄ Conc., in 15 (mL/g) L/S ratio at 70 °C; for 150 min.	<ul style="list-style-type: none">• V = 95%
[161]	Na ₂ CO ₃	2.5 Na ₂ CO ₃ /solid ratio at 850 °C for 60 min.	(NH ₄) ₂ SO ₄	30.0 (g/L) (NH ₄) ₂ SO ₄ Conc., in 3 (mL/g) L/S ratio at 20 °C for 60 min.	<ul style="list-style-type: none">• V = 94.6%• Cr = 96.5%
[153]	NaOH + O ₂	7.67 Na/V molar ratio at 700 °C for 120 min.	Water	70 (mL/g) L/S ratio at 25 °C for 60 min.	<ul style="list-style-type: none">• V = 99%
[168]	NaOH	0.3 NaOH/solid ratio at 800 °C for 180 min.	Water	10 (mL/g) L/S ratio at 30 °C for 60 min.	<ul style="list-style-type: none">• V = 94.9%• Cr = 80.5%
[169]	Na ₂ CO ₃ + NaCl	3:2:5 Na ₂ CO ₃ /NaCl/solid ratio at 700 °C for 120 min.	Water	4 (mL/g) L/S ratio at 95 °C for 180 min.	<ul style="list-style-type: none">• V = 96%• Cr = 91%
[170]	NaOH	0.3 NaOH/solid ratio at 850 °C for 120 min.	NaOH pressure leaching	5 (mL/g) L/S ratio; 0–5 MPa O ₂ partial pressure at 210 °C for 120 min.	<ul style="list-style-type: none">• V = 98%

Likewise, Ibrahim [165] studied the cost-effective extraction of precious metals, such as Ni and Zn, by hydro-metallurgical processing of the water-leaching solid residue (as shown in Figure 23) after vanadium extraction from salt-roasting Egyptian boiler ash [59]. Under the most favorable leaching conditions of 8% (vol%) H₂SO₄ concentration, 85 °C leaching temperature, and 1/15 S/L ratio, a maximum extraction of 95.02% Ni and 90.13% Zn was achieved after 240 min of leaching, while the iron impurity was removed by Fe₂O₃ as a nucleating agent and the magnesium impurity was effectively removed by oxalic acid precipitant. After the removal of Fe and Mg, Ni and Zn in the purified solution were precipitated at a pH of 10 as Ni-Zn hydroxide (Ni(OH)₂ and Zn(OH)₂), which was subsequently transformed into NiO-ZnO by its calcining at 450 °C for 2 h. The precipitation efficiency of Ni and Zn was 95.25% and 89.51%, respectively, and the final calcined product was composed mainly of 37% Ni and 23% Zn. Based on a kinetic analysis, it was discovered that the process of leaching nickel is primarily controlled by diffusion through the solid product layer and chemical reactions. The diffusion process through the solid product layer is the main contributor, with an activation energy of 20.26 kJ/mol. The kinetic of zinc dissolving is governed by the diffusion that occurs through a layer of a solid product, and this diffusion has an activation energy of 11.67 kJ/mol.

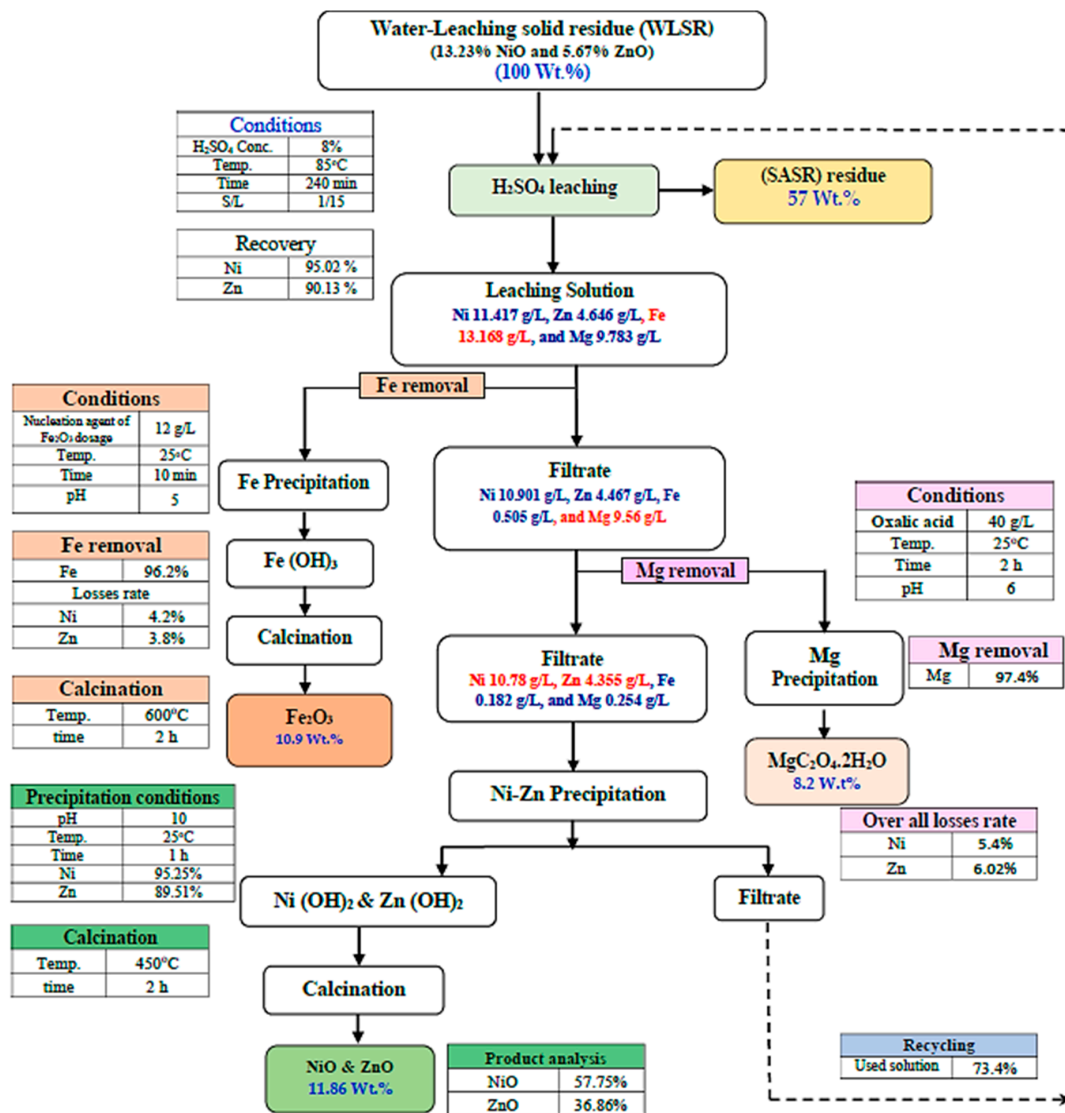


Figure 23. The quantitative scheme for the recovery of Ni, Zn, and other by-products from water leaching solid residue obtained from the salt roasting of Egyptian boiler ash.

3.2.4. Promising Modification Methods

Continuous efforts have been made to develop alternative processes, including sub-molten salts and supercritical fluid for recovering vanadium from various sources. Sub-molten salt and novel leaching methods can extract vanadium from various sources (vanadium-bearing slag, stone coal, spent catalysts, etc.) and should be discussed in this review. The method of sub-molten salts ($\text{NaOH}/\text{KOH}/\text{NaOH}\text{-}\text{NaNO}_3 = 75\%$ (w/w) at high pressure) can decrease the cost of energy due to the lower reaction temperature [171,172]. According to a report by Liu [171], a new study has discovered a unique approach to breaking down vanadium slag using KOH as a sub-molten salt under regular pressure. When the reaction conditions are optimal, including a temperature of 180 °C, an initial ratio of 4:1 potassium hydroxide to ore mass, a stirring speed of 700 rpm, a gas flow rate of 1 L/min, and a reaction time of 300 min, the extraction rates of vanadium and chromium can attain up to 95% and 90%, respectively. Still, the requirement of reactors with high corrosion resistance, the large consumption of alkaline, and the high dissolution rate of silica phases limit its wide application. The problems of inefficient vanadium separation and serious environmental pollution greatly hinder the application of these V extraction processes [158,159]. Recently, novel leaching methods have been reported for vanadium recovery using urea, specific chelating agents, or supercritical fluid, resulting in low environmental impact [173–176].

A leaching method has also been reported by adjusting the vanadium particles' surface wettability to intensify the solid–liquid contact using certain surfactants [177]. Though tested in a few cases, as shown in Table 13, such conditions have resulted in considerably lower vanadium recovery yields (60~70%); however, they can still be considered a “green option” to the traditional processes. Accordingly, the broadly available theoretical underpinnings and technological background of such approaches make them worth investigating in the future. Once proven promising, they may eventually be considered for exploitation and optimization.

Table 13. Details of some novel leaching methods for vanadium recovery from various sources.

Source	Method	Conditions	Results	Principle	Highlight	Ref.
Vanadium spent catalyst	Urea leaching	Time, 1 h; temperature, 20 °C; urea conc., 20%; pH = 14	V = 80%	<ul style="list-style-type: none"> Considering the mutual solubility effect of urea to vanadium solubility in water 	<ul style="list-style-type: none"> High kinetic leaching of vanadium even at low temperatures is an advantage 	[175]
Vanadium-bearing shale, vanadium-bearing coal	Chelating leaching	Time, 4 h; temperature, 95 °C; chelator conc., 6.0 M; additive (CaF ₂), 5% (wt.)	87% V	<ul style="list-style-type: none"> The principle is similar to that of bioleaching, which is to obtain a product of a complex metal-chelator. Chelators used are citric acid, oxalic acid, and ethylenediaminetetraacetic acid (EDTA). 	<ul style="list-style-type: none"> The process offers the advantage of an eco-friendly approach compared to conventional leaching using mineral acids. Even so, slower kinetic leaching becomes the main problem of this approach, being the limitation for its wider application. 	[3,173]
Vanadium-bearing slag	Surface wettability control	Leaching conditions: not specified Surfactant added: 0.25–1.0% (wt.)	69% V (with surfactant), 51% V (without surfactant)	<ul style="list-style-type: none"> To intensify the interaction between the solid particle and leaching solution by adding surfactants like polydimethylsiloxane/PDMS and sodium dodecyl sulfate/SDS. The surfactants play roles in reducing the surface tension of the solution and changing the surface properties of the solid particles 	<ul style="list-style-type: none"> The pioneered study showed the capacity of this approach to enhance vanadium extraction. Further studies in this area are worth encouraging while assessing the economic and environmental impact of the added surfactants. 	[177]
Vanadium spent catalyst	Supercritical leaching	Fluid, acetylacetone; temperature, 190 °C; time, 7 h	V = 60%	<ul style="list-style-type: none"> Characterized by the use of fluids where they are in their critical point; for instance, CO₂ (critical pressure/P_c, 7.38 MPa; critical temperature/T_c, 31.1 °C), ethanol (P_c, 6.3 MPa; T_c, 241 °C), methanol (P_c, 7.85 MPa; T_c, 240 °C), acetylacetone (P_c, 4.05 MPa; T_c, 339 °C) and other alcohol groups. 	<ul style="list-style-type: none"> Research on this area is still green. The advantages in the environment, energy, and chemical aspects are worth considering while preliminary studies show an unsatisfactory result. The development of novel supercritical solvents and co-solvents is believed to be the main factor attributing to the greater interest in applying this technology in the extractive metallurgy field, including extracting vanadium. 	[178]

4. Utilizing By-Products for Industrial Applications

The world is dealing with water scarcity issues due to the discharge of partially treated or untreated wastewater from industries and groundwater pollution. The demand for clean water has increased to meet the needs of a sustainable society. The need for cost-effective and efficient water treatment methods has become a growing concern as we look towards the future. This has led to an increased focus on recycling industrial waste to produce low-cost adsorbents and reduce environmental pollution [179]. Thus, developing an affordable, accessible, and highly effective adsorbent for removing hazardous metal ions presented in wastewater has become necessary. The utilization of solid industrial wastes by reusing them in the manufacturing of useful materials used for environmental purposes has been the subject of several recent studies, and it is one of the most crucial issues for maintaining sustainable development [180,181].

The solid wastes containing silica (SiO_2) and alumina (Al_2O_3), including industrial waste forms, i.e., fly ash, steel slag, waste perlite, waste porcelain, lithium slag, waste metallic residues, paper sludge, cupola slag, kaolin waste, windshield waste, asbestos wastes, etc., could be converted into ecological zeolite-based adsorbents [182–191]. To date, several physicochemical and solvothermal techniques, including the hydrothermal approach [192–194], alkali-fusion processes [195–197], sol–gel processes [198–200], microwave processes [201–204], and alkali-leaching method [205–208] have been adopted and developed to produce synthetic adsorbents. Figure 24 shows the major preparation processes and methods for synthesizing zeolite from industrial solid waste. So, in this review, we focused on the synthesis of low-cost adsorbent from industrial waste.

However, many researchers have studied the synthesis of zeolites from solid wastes to be used as an adsorbent for removing heavy metal ions from wastewater. Zeolites are crystal formations built on stiff anionic aluminosilicate structures with distinct pores or channels that link at cavities or cages [209]. These materials are favorable for adsorption processes due to their high cation exchange capacity (CEC), large surface area, good thermal stability, porosity, surface active functional groups, and nontoxicity [210–212]. New zeolite materials have been processed from fly ash, successfully eliminating heavy metal ions from aqueous solutions [213]. Chen [214] synthesized zeolite X by an alkaline fusion-hydrothermal reaction using industrial lithium slag containing $\text{SiO}_2:\text{Al}_2\text{O}_3$ in a weight ratio of 71.73:25.16 (wt. %). The results highlight the performance similarity between Zeolite NaX-1 and commercial Zeolite X.

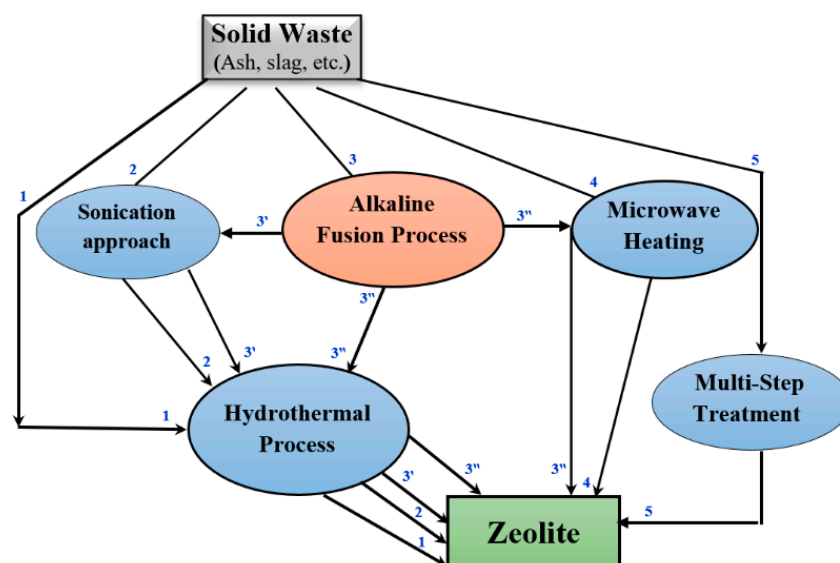


Figure 24. Diagram of the different procedures for synthesizing zeolite from fly ash [215].

R. Anuwattana [216] has reported successfully synthesizing Na-A type zeolite using industrial waste materials such as the solid by-product of cupola slag, which contains $\text{SiO}_2/\text{Al}_2\text{O}_3$ in a weight ratio of 47:12 (wt.%), and aluminum sludge from an aluminum plating plant. In their investigation, two preparation methods were carried out using the same starting material compositions. To begin the process, alkaline fusion was utilized, and then the material was subjected to hydrothermal treatment to produce sodium aluminosilicate. This substance was subsequently crystallized in a NaOH solution at a temperature of 90°C for 1–9 h with varying $\text{H}_2\text{O}/\text{SiO}_2$ ratios. The results indicated that a more excellent ratio of $\text{H}_2\text{O}/\text{SiO}_2$ resulted in an increased crystallization rate. The highest level of crystallization was observed for Na-A after 3 h. The second method involved alkaline hydrothermal treatment without fusion, using the same conditions as the first procedure. However, this approach did not yield any Na-A zeolite. It is worth considering blast furnace slag (BFS) as a possible source of raw materials for zeolite synthesis. This material primarily comprises CaO , SiO_2 , Al_2O_3 , and MgO , with minor Fe, Ti, and Mn quantities. Several groups have reported that zeolite can be made from industrial waste.

However, prior attempts to use BFS as a chemical source of zeolite were unsuccessful due to its complex composition, specifically its high Ca content [192]. Hence, further study is needed to produce a variety of zeolites for possible uses. In the same context, Kuwahara [217,218] discovered a new way to synthesize a hydroxyapatite-zeolite micro composite from BFS in a recent study. The process involves using affordable chemical reagents such as H_3PO_4 and NaOH and suitable preparation techniques. This innovative approach provides practical solutions for waste management. Furthermore, using the alkali fusion process, Takaaki Wajima [197] demonstrated how to create zeolite-A, zeolite-X, and hydroxysodalite from the BFS. A more recent approach (Figure 25) for synthesizing a high-crystalline and affordable zeolite from a combination of SASR-kaolin as a readily accessible and low-cost raw material using an alkaline fusion hydrothermal process [219]. The weight ratio of the SASR-kaolin mixture of 1:1.5 gives the best composition and properties of the synthesized zeolite. The optimal conditions for the synthesized zeolite are a fusion temperature of 600°C , a 1:3 wt. ratio (SASR-kaolin)-NaOH, a 1:4 solid–liquid ratio, an 80°C crystallization temperature, and a 24 h crystallization time.

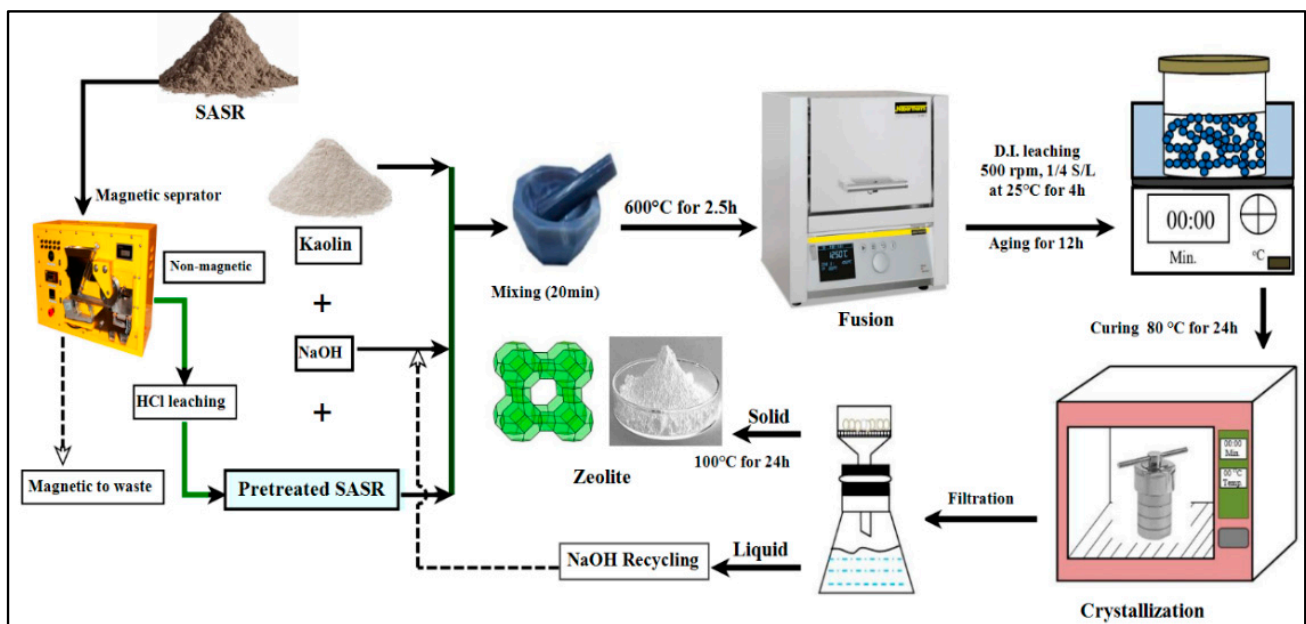


Figure 25. Schematic procedures of synthesized zeolite based on Egyptian boiler ash residues [219].

Figure 26 illustrates the mineralogical structure of the produced synthesized zeolite by mixing pretreated SASR and kaolin mixtures at different weight ratios in the presence of NaOH (Mixture-NaOH mass ratio of 1:1.3). As shown in Figure 26A, the Faujasite zeolite ($\text{Na}_2\text{Al}_2\text{Si}_3.8\text{O}_{11.63}\cdot 8\text{H}_2\text{O}$) has been formed as the major mineral phase from SASR-Kaolin weight ratios of 1:0, 1:2, 1:1.5, 1:1, and 2:1.

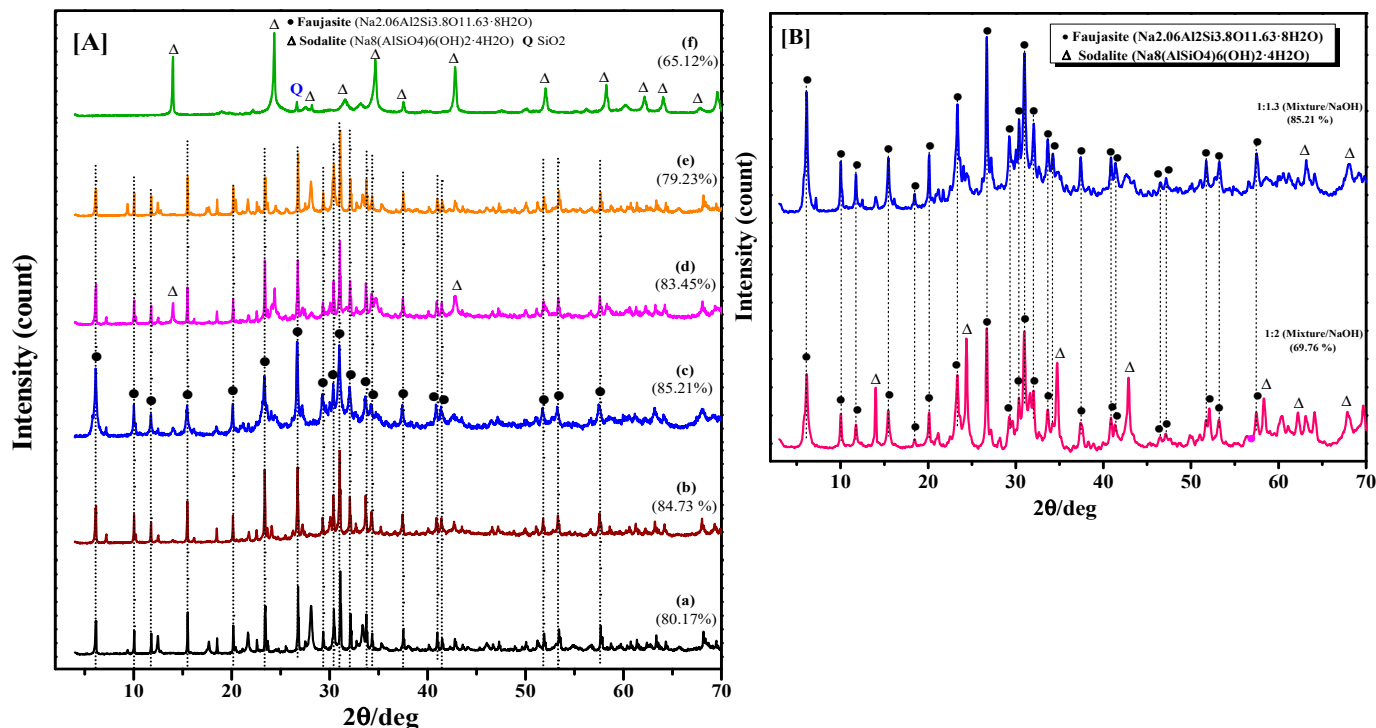


Figure 26. XRD Patterns of synthesized zeolite produced from mixture of SASR-Kaolin at weight ratios of (a) 1:0, (b) 1:2, (c) 1:1.5, (d) 1:1, (e) 2:1, and (f) 0:1. (A) XRD Patterns of synthesized products with different mass ratio of mixture-NaOH of 1:1.3 and 1:2. (B) where ●: Faujasite, and Δ: Sodalite zeolite [219].

However, the intensity of its peaks increased with increases in the mass of kaolin, and a high rate of crystallinity (85.21%) can be obtained when the ratio of SASR to kaolin is 1:1.5, due to the stability of the zeolite composition. A percentage of sodalite zeolite ($\text{Na}_8(\text{AlSiO}_4)_6(\text{OH})_2\cdot 4\text{H}_2\text{O}$) groups have also existed at an SASR-Kaolin weight ratio of 0:1. Figure 26B shows that the crystallinity of the synthesized zeolite decreased from 85.21% to 69.76% at 1:2 mixture-NaOH weight ratio. However, when the system's alkalinity is too high, a decline in crystalline is caused. This can be attributed to one of the following two reasons: either the created zeolite spontaneously transforms into hydroxyl sodalite, which has more excellent thermodynamic stability [220], or the zeolite will dissolve in the hot alkali solution because of its metastable state and exposure to disturbances [180,221]. Table 14 illustrates how various industrial wastes can be used to create synthetic zeolites, each with its own advantages and disadvantages.

Additionally, in the same context of research [219], synthesized zeolite was an effective adsorbent for removing Zn^{2+} , Pb^{2+} , Cu^{2+} , and Cd^{2+} heavy metal ions from industrial wastewater based on readily accessible and low-cost raw materials. It was noted that the adsorption process was exothermic, pH-dependent, and spontaneous in nature. Significant adsorption occurs when the pH is 7.0 for Zn and Cd ions and 6.0 for Pb and Cu ions. The adsorption process was found to follow the pseudo second-order kinetic model and Langmuir isotherm model.

Table 14. Synthetic zeolites from different industrial wastes and their advantages and limitations.

Raw Material	Chemical Composition %	Advantages	Limitations	Synthesis Route	Zeolite Type	Ref.
BFS	CaO (40.1), SiO ₂ (34.58), Al ₂ O ₃ (14.78), MgO (5.29)	Availability, low cost, convenient preparation steps.	<ul style="list-style-type: none"> Higher CaO content. 	Hydrothermal	A	[217,218]
Natural obsidian	80.04% SiO ₂ , 12.27% Al ₂ O ₃ , 0.16% TiO ₂ , 0.84% FeO, 0.18% MgO, 1.10% CaO, 3.14% Na ₂ O and 3.04% K ₂ O	Higher silica content, availability.	<ul style="list-style-type: none"> Still, limited studies did not mention any specific application. Due to the wide range of behavior changes concerning synthetic conditions. 	Hydrothermal	Organic template-free EMT-type, natrolite, Za-gmelinite	[222,223]
RHA (Residue is rich in amorphous silica)	80% silica, Al ₂ O ₃ , iron oxide, CaO, MgO, sodium and potassium oxides, and others	Low cost, ultrafine size, highly porous, and chemically reactive.	<ul style="list-style-type: none"> Pre-treatment of RHA and waste glasses increase the cost. 	Hydrothermal	ZSM5, T, Na-Y	[224,225]
Waste glass materials	SiO ₂ (63%), Al ₂ O ₃ (18%), B ₂ O ₃ (10%), and alkaline earth oxides	Excellent mechanical and thermal properties, free of harmful elements.	<ul style="list-style-type: none"> Problem in handling, need a substrate or base material for commercial use. 	Hydrothermal	A	[198,199,226]
SASR	SiO ₂ 26.57%, Al ₂ O ₃ 5.81%, Fe ₂ O ₃ 18.93%, TiO ₂ 0.13%, MgO 0.04%, K ₂ O 0.13%, Na ₂ O 0.18%, P ₂ O ₅ 3.61%, LOI 17.88%	Availability, low cost, ultrafine size, convenient preparation steps.	<ul style="list-style-type: none"> Pre-treatment (Physical and Chemical) needs to be a source of Al. 	Hydrothermal, Alkali fusion	Faujasite	[219]
Paper sludge ash	SiO ₂ 35.9%, Al ₂ O ₃ 22.8%, CaO 33.2%, Na ₂ O 0.6%, MgO 4.5%, Fe ₂ O ₃ 0.9%, TiO ₂ 2.2%	Amorphous and crystalline phases formed by incineration; low temperature required.	<ul style="list-style-type: none"> Low abundance of Si and significant Ca content. 	Hydrothermal	Na-P1	[227,228]
Waste stone cake	SiO ₂ 38.9%, Al ₂ O ₃ 12.2%, CaO 6.9%, Na ₂ O 1.4%, K ₂ O 1.8%, MgO 2.7%, Fe ₂ O ₃ 3.1%, CO ₂ 32.6%, SO ₃ 0.1%, P ₂ O ₅ 0.1%	Specific pore sizes and large surface areas, high silica content.	<ul style="list-style-type: none"> Most SiO₂ and Al₂O₃ are in crystalline phases; it is difficult to dissolve into an alkali solution, contains impurities. 	Hydrothermal, Alkali fusion	zeolite-A, P, X and ZSM-5	[195]
Clay materials (kaolin, smectite)	SiO ₂ 46.5%, Al ₂ O ₃ 41.18%, Fe ₂ O ₃ 0.19%, TiO ₂ 0.13%, MgO 0.04%, K ₂ O 0.13%, Na ₂ O 0.18%, ZrO ₂ 0.01%, SO ₃ 0.15%, P ₂ O ₅ 0.03%, LOI 16.25%	Availability, convenient source for producing low silica zeolites like Y, and use of kaolin waste for zeolite synthesis reduces the cost of reagents.	<ul style="list-style-type: none"> High energy consumption processes like grinding, calcination, and fusion are required. Raw materials mining destroys the natural landscape. 	Hydrothermal, Alkali fusion	NaA, mordenite, Faujasite, and, NaP	[229]

Table 14. Cont.

Raw Material	Chemical Composition %	Advantages	Limitations	Synthesis Route	Zeolite Type	Ref.
Coal fly ash	SiO ₂ 38.3%, Al ₂ O ₃ 34.8%, CaO 11.0%, Fe ₂ O ₃ 8.1%, Others 7.8%	The main constituents are silica and alumina, which offer the potential to convert it to zeolite, producing low-price zeolite with high purity; and no harmful effect.	<ul style="list-style-type: none"> Effect of the impeller type and agitation during the hydrothermal treatment stage of the process. 	Hydrothermal, microwave-assisted hydrothermal method, and fusion methods.	X, Na-P1, A, Y	[183,206,230]
Lithium slag	SiO ₂ 70.67%, Al ₂ O ₃ 27.24%, Fe ₂ O ₃ 0.52%, SO ₃ 0.45%, CaO 0.29%, K ₂ O 0.22%, MgO 0.16%, Na ₂ O 0.13%, P ₂ O ₅ 0.12%, Others < 0.1%	High silicon aluminum ratio.	<ul style="list-style-type: none"> Very few experiments have been conducted in this field. 	Hydrothermal	X, FAU/LTA	[214,231]
Waste of iron mine tailings/iron ore tailing	SiO ₂ 67.58%, Al ₂ O ₃ 8.70%, Fe ₂ O ₃ 7.42%, CaO 5.78%, MgO 4.37%, K ₂ O 2.32%, Na ₂ O 2.15%, Cl 0.69%, TiO ₂ 0.33%, P ₂ O ₅ 0.26%, SO ₃ 0.23%, MnO 0.10%, SrO 0.06%	Have economic and environmental aspects.	<ul style="list-style-type: none"> Very few experiments have been conducted in this field, which contains hazardous impurities that decrease the quality of zeolites. 	Hydrothermal	A, ZSM-5	[232]

The maximum monolayer adsorption capacities of Zn²⁺, Pb²⁺, Cu²⁺, and Cd²⁺ ions onto zeolite at 20 °C were 12.025, 15.96, 12.247, and 16.17 mg.g⁻¹, respectively, showing a significantly greater removal efficiency, which agrees with the previously obtained results. Ion exchange was the principal mechanism controlling the removal of Zn²⁺ and Cd²⁺ from aqueous solution by synthesized zeolite. In contrast, the main mechanism controlling the process of the removal of Pb²⁺ and Cu²⁺ ions is proposed to be either surface adsorption or precipitation. The proposed adsorption mechanism in Figure 27 shows that the adsorption of Zn²⁺, Pb²⁺, Cu²⁺, and Cd²⁺ on zeolite likely can be divided into three major phenomena: precipitation, ion exchange, and surface adsorption [233,234]. The cations exchange is the crucial mechanism for absorbing Zn²⁺ and Cd²⁺ from an aqueous solution. The following equation can represent this process:

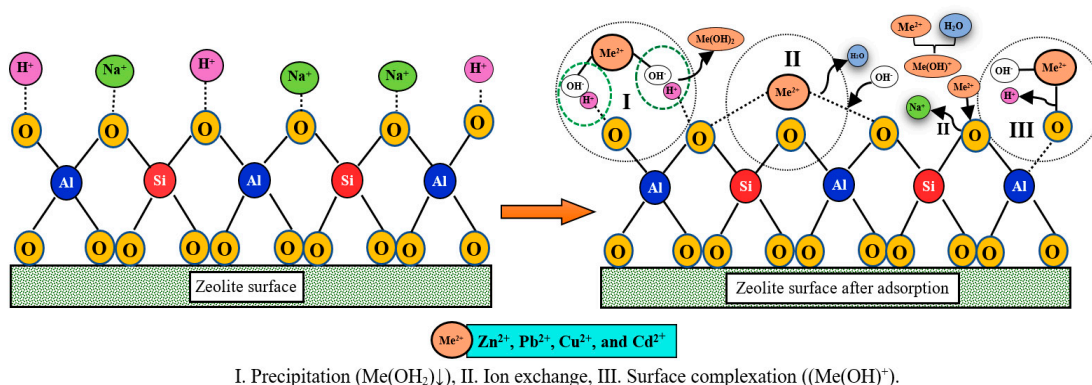


Figure 27. The proposed adsorption mechanism of heavy metal ions on synthesized zeolite.

As a result of industrially applying a synthetic zeolite derived from the SASR by-product, it was demonstrated that the synthesized zeolite effectively removed heavy metal ions from the wastewater sample collected from the Egyptian General Petroleum Corporation (EGPC) (Eastern Desert, Egypt). The targeted levels of heavy metal ion concentrations before and during adsorption using synthesized zeolite are shown in Table 15. However, in the fourth adsorption cycle, the residual heavy metal ion concentrations follow WHO guidelines for wastewater disposal in the marine environment with high removal efficiency [235]. When the number of circulations increases (5th and 6th cycles), the amount of heavy metal ions in the effluent also goes up. As a result, when the pollutants are enriched to a specific level, the adsorbent needs to be cleaned to achieve closed recycling. Finally, the synthesized zeolite can be utilized to safeguard industrial wastewater drainage systems.

Table 15. Applying the synthetic zeolites based on SASR-kaolin mixture for removing heavy metal ions from EGPC industrial wastewater sample.

Metals	Cd	Cr	Cu	Mn	Pb	Fe	Ni	Zn	V
C ₀ (mg.L ⁻¹)	6.127	7.016	10.294	8.152	11.493	8.219	0.002	17.051	0.01
MLD _{WHO}	0.01	0.01	1	0.1	0.01	1.5	0.1	1	0.002
Number of Cycles	1	U. D	U. D	U. D	2.1	U. D	3.1	U. D	U. D
	2	U. D	U. D	U. D	0.6	U. D	1.1	U. D	U. D
	3	U. D	U. D	U. D	0.05	U. D	U. D	U. D	U. D
	4	U. D	U. D	U. D	U. D	U. D	U. D	U. D	U. D
	5	0.08	0.05	1.3	2.12	0.51	2.5	0.054	1.66
	6	0.45	2.01	1.7	7.12	1.07	4.5	0.098	3.87

U. D: Under detection limit; MLD_{WHO}: Maximum limits for wastewater disposal according to WHO.

It was noted that zeolites synthesized based on oil shale ash by an alkaline hydrothermal process were effectively used to extract Pb^{2+} and Cd^{2+} metal ions [236]. Synthesized Na-A zeolite from class F fly ash (FA) and modified oil shale ash (MOSA) by alkaline fusion followed by refluxing was used as an adsorbent for lead, zinc, and chrome [237]. Fly ash hydrothermally modified with NaOH solution was utilized to synthesize zeolites for Cd^{2+} adsorption, which showed effective removal of Cd^{2+} from the wastewater source [238]. Applying a low-temperature roasting process, the novel adsorbent was prepared from fly ash and solid alkali (NaOH). This adsorbent was manufactured under the following conditions: the pristine fly ash and NaOH mass ratio was 5:8, the calcination temperature was from 300 to 350 °C, and the reaction time was 3 h. The obtained results showed a better adsorption capacity of Cd^{2+} on modified fly ash (MFA) [239]. A zeolitic material that was prepared from coal fly ash (CFA) through NaOH fusion treatment, followed by hydrothermal processing, was applied to remove heavy metal ions such as Ni^{2+} , Cu^{2+} , Cd^{2+} , and Pb^{2+} from the wastewater source [240]. The adsorption capacity of the synthesized Na-A zeolite based on the fusion and hydrothermal treatment of oil shale was evaluated by measuring the maximum removal efficiency of Cu^{2+} , Ni^{2+} , Pb^{2+} , and Cd^{2+} from aqueous solutions [241]. A new composite material was formulated based on fly ash (FA), meta-kaolin (MK), and TiO_2 to form a micro-porous zeolitic material with enhanced photocatalytic properties for the adsorption of methylene blue (MB) dye [242]. A modified geopolymer based on fly ash was used to study the effectiveness of adsorbing Cd^{2+} ions from aqueous solutions, as previously described by Javadian [243]. The alkaline fusion-hydrothermal process was used to synthesize zeolites from Brazil oil shale ash. It was noted that the synthesized zeolites are composed of likewise mixed phases (Na-A zeolite, Na-X zeolite, hydroxy sodalite, and quartz) [244].

Yu [245] investigated the efficiency of zeolite-based fly ash to adsorb and remove Ni^{2+} ions from aqueous solutions. This study examined the adsorption capacities of synthetic and commercial zeolite (4A), indicating that zeolite 4A had a lower adsorption capacity than fly ash-based zeolite (75.6 mg/g). Chen [246] developed four different fly ash-based zeolites to adsorb Ni^{2+} ions from aqueous solutions and achieved removal efficiencies ranging from 92.5% to 96.2%. A specific kind of geopolymer made from fly ash showed a significant effect in removing Pb^{2+} ions from aqueous solutions. The maximum removal efficiency of 90.66% has been achieved at 5 pH and a contact time of 2 h [247]. In order to remove Pb^{2+} ions from aqueous solutions, fly ash was employed to create the hydroxysodalite zeolite. The maximum adsorption efficiency of synthetic zeolite was 98.1%, demonstrating the adsorbent's excellent efficiency [181].

Multi-cation wastewater containing Pb^{2+} , Zn^{2+} , and Cd^{2+} was treated using a type of zeolite synthesized from fly ash. Pb^{2+} and Zn^{2+} ions were efficiently and selectively removed with 100% and 70% adsorption efficiencies, respectively, compared to Cd^{2+} ions with a 60% adsorption efficiency [248]. Shyam [249] used fly ash adsorbent modified with CaCO_3 to minimize the concentration of Pb^{2+} , Ni^{2+} , and Cr^{6+} ions from aqueous solutions. This study found that 1:10 CaCO_3 /FA eliminated Pb^{2+} up to 90%, Ni^{2+} 50%, and Cr^{6+} 30% under ideal conditions. In the same way, the adsorption of several heavy metal ions from aqueous solutions was also studied using FA coated with chitosan. It was noted that within 3 h, the produced adsorbent exhibited satisfactory performance. The adsorption capacities of different metal ions have been reported as follows: 36.22, 28.65, 55.52, and 19.10 mg/g for Cr^{3+} , Cu^{2+} , Zn^{2+} , and As^{5+} ions, respectively [250]. The highest Cd^{2+} ions removal efficiency of 84% was obtained under the best-recommended conditions. The isotherm and kinetic studies indicated that the Langmuir and pseudo second-order models were in good agreement with the adsorption data. Also, they employed FA to synthesize zeolite through the fusion process and showed effective adsorbent to remove Cr^{6+} ions from aqueous

solutions. More than 80% of the Cr⁶⁺ ions were eliminated, and both the Freundlich and Langmuir isotherm models provided an excellent fit to the equilibrium data. The thermodynamic studies revealed that the process was spontaneous and endothermic, and the adsorption kinetics exhibited pseudo second-order behavior [251]. In conclusion, fly ash has been converted into various ceramic products, zeolite materials, and geopolymers, which in turn are used for wastewater treatment [252]. Table 16 summarizes the adsorbents synthesized and their metal ion removal efficiency using various preparation methods.

Table 16. Adsorption conditions of various heavy metals by zeolite-based adsorbents [252].

Heavy Metals and Nutrients	Adsorbent	Removal Efficiency	Ref.
Cd ²⁺	ZFA-600	84%	[243]
	Zeolite X	100%	[253]
	TiO ₂ /FA)	80%	[254]
	FA-Z	60%	[248]
	MG-Z and MT-Z	~98% and 75%	[255]
Co ²⁺	MCM-41	~90%	[256]
Cr ³⁺		~90%	
Cr ⁶⁺	ZFA	>80%	[257]
	CFA-FeOOH	84.9%	[258]
	MSFA/PPy		[259]
	ZFA-Na-A		[260]
	Zeolite X		[261]
	Chitosan/CFA		[262]
Cu ²⁺	FA-MS	98%	[263]
	FA-IOT-Geo	98.3%	[264]
	CFA-Geo	93.9%	[265]
	MPF		[266]
	TiO ₂ /FA	90%	[254]
	MG-Z and MT-Z	100%	[255]
Fe ³⁺	Ag-Fe ₃ O ₄ /FA		[267]
	Zeolite NaeP1	100%	[268]
Hg ²⁺	Zeolite LTA	94%	[269]
	ZFA	91.27%	[270]
	HMAS zeolite	~95%	[271]
Mn ²⁺	CFA Zeolite	100%	[272]
	Zeolite	100%	[273]
	Zeolite		[245]
Ni ²⁺	FA-Na-P/TEA	96.2%	[246]
	FA-Na-X	95.5%	
	FA-Na-P/Na-Br	95%	
	FA-Na-P	92.5%	
	Zeolite X	95%	[253]
	MG-Z and MT-Z	~50% and 52%	[255]
Pb ²⁺	PB/FA—SA-FA	100%	[274]
		98.1%	[181]
	ZCFA	90.66%	[247]
	Geopolymer		
	FA-Z	100%	[248]
	1:10 FA	>90%	[249]
	MG-Z and MT-Z		
	PB/FA—SA-FA	100%	[255]
	100%	[274]	

Table 16. Cont.

Heavy Metals and Nutrients	Adsorbent	Removal Efficiency	Ref.
Zn ²⁺	FA-Z	70%	[248]
	FAICS		[250]
	FA		[275]
	FA		[276]
NH ₄ ⁺	PB/FA—SA-FA	100%	[274]
	Zeolite NaeP1	~61%	[277]
	Z-P1	65.2%	[278]
PO ₄ ³⁺	ZHLO	60%	[279]
	ZFA	91%	[280]
	Z-P1	92.3%	[278]

5. Future Recommendations

The synthesizing and application of zeolite from useless by-product waste need further investigation.

To enhance the sustainability and efficiency of salt-roasting processes, alternative methods must be explored for recycling released gasses and barren solutions, along with extracting valuable metals from a secondary vanadium source. Additionally, producing chemical compounds for further use in the relevant process needs further studies.

Other synthetic pathways for producing zeolite materials with high surface area, adjustable molecular dimensions, and adsorption capacities are needed for industrial by-product application. Further research is needed to identify low-cost raw materials for the synthesis of zeolites.

In addition, to reduce the production costs, it is necessary to develop accessible synthetic routes. Kinetic studies and energy calculations are needed to investigate how nucleation occurs during zeolite synthesis. Further studies on the regeneration of synthetic zeolite are required to increase the cost-effectiveness of the process.

6. Conclusions

The shortage of vanadium primary resources from high-grade ores makes it necessary to find a suitable alternative that covers this shortage. Also, the world vision concerning the solution to climate change and environmental pollution problems is based on decreasing or completely getting rid of the amounts of the produced waste. One of these promising alternatives is the utilization of different wastes containing vanadium to decrease their environmental adverse effects and, at the same time, enhance their economic value by converting them into valuable products.

The current study aims to present and analyze the worldwide available alternative vanadium-bearing waste resources, proprieties, reserves, and processing technologies. The heavy oil fly ash “HOFA” and vanadium slag showed a promising alternative for the production of vanadium metal due to their high content of vanadium and the cost-effectiveness of their processing to extract vanadium metal compared to processing their corresponding low-grade ores.

Vanadium can be extracted from these wastes using pyro- or hydro-metallurgical methods or a combination. The hydro-metallurgical extraction can be carried out using one of the vital mineral acids such as HCl, H₂SO₄, or HNO₃, and previous studies reported that HCl and H₂SO₄ have comparable leaching efficiencies. H₂SO₄ is preferred due to its significantly lower cost and its wide application in the leaching of many metals. In addition to V and Ni, H₂SO₄ effectively dissolves almost all metals in HOFA and other

vanadium-bearing wastes, such as Mo, Mg, Mn, and others. In addition to acidic leaching reagents, alkaline leaching reagents like NaOH, Na₂CO₃, and NH₄OH can be used for leaching vanadium from their containing wastes. The previous study showed that NaOH has the highest selectivity and leaching efficiency for V compared to other alkaline leaching reagents.

Two-stage leaching can be used for more selectivity and productivity of vanadium from their containing wastes. The first stage includes the alkaline leaching of high-contented and alkaline leachable vanadium using NaOH, followed by the second acidic leaching of acidic leachable elements using H₂SO₄. A combination of pyro- and hydro-metallurgical processes is carried out for more effective extraction of vanadium from their containing wastes. Firstly, pyro-metallurgical processes like roasting are carried out to convert low-leachable vanadium to high-leachable phase. Alkaline salt roasting using NaCl and Na₂CO₃ converts contained vanadium into water-leachable phase NaVO₃. Previous studies showed that the roasting temperature is the main controlling parameter on the efficiency of vanadium extraction. The hydro-metallurgical processes include leaching the modified (roasted) wastes using water or a very low-concentration acidic leaching process. Recent studies confirm the cost-effectiveness of the salt roasting process followed by the water leaching process for treating vanadium-bearing wastes, which showed high percent recovery and purity of the extracted vanadium. After leaching, V can recover from the leaching solution by chemical precipitation, solvent extraction, or ion exchange processes.

Complex processing of vanadium-bearing wastes, including firstly the extraction of valuable metals followed by the complete utilization of the resulting residue in the production of adsorbent, i.e., zeolite with different composition and properties to be used in wastewater treatment, is very promising and applied alternative for complex processing of these wastes.

Author Contributions: Conceptualization, X.L. and A.H.I.; methodology, A.H.I., X.L., H.E.S. and A.B.E.; software, A.H.I., H.E.S. and A.B.E.; validation, X.L. and A.B.E.; formal analysis, A.H.I., H.E.S. and A.B.E.; investigation, A.H.I. and A.B.E.; data curation, A.H.I. and A.B.E.; writing—original draft preparation, A.H.I.; writing—review and editing, X.L., H.E.S. and A.B.E.; visualization, A.H.I.; supervision, X.L.; project administration, X.L.; funding acquisition, X.L. All authors have read and agreed to the published version of the manuscript.

Funding: This work was supported by Qingdao West Coast New Area 2020 Annual Science and Technology Project (3-2-2020), the National Natural Science Foundation of China (No. 51674161), and the Natural Science Foundation of Shandong Province (No. ZR2017ZC0735).

Institutional Review Board Statement: Not applicable.

Informed Consent Statement: Not applicable.

Data Availability Statement: No new data were created or analyzed in this study. Data sharing is not applicable to this article.

Acknowledgments: All the authors would like to express their sincere gratitude and appreciation to Shandong University of Science and Technology, Qingdao, China for providing the required funding.

Conflicts of Interest: The authors declare no conflicts of interest.

References

1. Perles, T. *Vanadium Market Analysis*; TTP Squared Inc.: Upper St. Clair, PA, USA, 2021; pp. 23–38.
2. Simandl, G.J.; Paradis, S. Vanadium as a Critical Material: Economic Geology with Emphasis on Market and the Main Deposit Types. *Appl. Earth Sci. Trans. Inst. Min. Metall.* **2022**, *131*, 218–236. [[CrossRef](#)]
3. Hu, P.; Zhang, Y.; Huang, J.; Liu, T.; Yuan, Y.; Xue, N. Eco-Friendly Leaching and Separation of Vanadium over Iron Impurity from Vanadium-Bearing Shale Using Oxalic Acid as a Leachant. *ACS Sustain. Chem. Eng.* **2018**, *6*, 1900–1908. [[CrossRef](#)]

4. Hu, P.; Zhang, Y.; Liu, T.; Yuan, Y.; Xue, N. Source Separation of Vanadium over Iron from Roasted Vanadium-Bearing Shale during Acid Leaching via Ferric Fluoride Surface Coating. *J. Clean. Prod.* **2018**, *181*, 399–407. [[CrossRef](#)]
5. Yan, B.; Wang, D.; Wu, L.; Dong, Y. A Novel Approach for Pre-Concentrating Vanadium from Stone Coal Ore. *Miner. Eng.* **2018**, *125*, 231–238. [[CrossRef](#)]
6. Wenk, H.; Bulakh, A. *Minerals, Their Constitution and Origin*; Cambridge University Press: Cambridge, UK, 2004.
7. Schindler, M.; Hawthorne, F.C.; Baur, W.H. A Crystal-Chemical Approach to the Composition and Occurrence of Vanadium Minerals. *Can. Mineral.* **2000**, *38*, 1443–1456. [[CrossRef](#)]
8. Boni, M.; Bouabdellah, M.; Boukirou, W.; Putzolu, F.; Mondillo, N. Vanadium Ore Resources of the African Continent: State of the Art. *Ore Geol. Rev.* **2023**, *157*, 105423. [[CrossRef](#)]
9. Judd, J.C.; Sandberg, R.G.; Huiatt, J.L. *Recovery of Vanadium, Uranium and Phosphate From Idaho Phosphorite Ores*; Bureau of Mines, Report of Investigations 9025; United States Department of the Interior: Washington, DC, USA, 1986.
10. U.S. Geological Survey. *Mineral Commodity Summaries 2023*; U.S. Geological Survey: Reston, NA, USA, 2023; ISBN 9781411345041.
11. Reznitsky, L.Z.; Sklyarov, E.V.; Suvorova, L.F.; Karmanov, N.S.; Ushchapovskaya, Z.F. The Chromite–Coulsonite–Magnetite Solid Solution: The First Find of a Rare Variety of Spinel in Terrestrial Rocks. *Dokl. Earth Sci.* **2005**, *404*, 1121–1125.
12. Xu, C.; Zhang, Y.; Liu, T.; Huang, J. Characterization and Pre-Concentration of Low-Grade Vanadium-Titanium Magnetite Ore. *Minerals* **2017**, *7*, 137. [[CrossRef](#)]
13. Lauf, R.J. *Mineralogy of Uranium and Thorium*; Schiffer Publishing: Atglen, PA, USA, 2016; ISBN 0764351133.
14. Merritt, R.C. *Extractive Metallurgy of Uranium*; Colorado School of Mines Research Institute: Golden, CO, USA, 1971.
15. Henning Stonehenge Metals Corporate Presentation. In Proceedings of the Australian-Uranium-Rare-Earths-Conference, Fremantle, Australia, 16–17 July 2013.
16. Liu, S.; Jaireth, S. Exploring for Calcrete–Hosted Uranium Deposits in the Paterson Region, Western Australia. *Ausgeo News*, 2011; pp. 1–5.
17. Wang, M.; Xian, P.; Wang, X.; Li, B. Extraction of Vanadium from Stone Coal by Microwave Assisted Sulfation Roasting. *JOM* **2015**, *67*, 369–374. [[CrossRef](#)]
18. Lewis, S.E.; Henderson, R.A.; Dickens, G.R.; Shields, G.A.; Coxhell, S. The Geochemistry of Primary and Weathered Oil Shale and Coquina across the Julia Creek Vanadium Deposit (Queensland, Australia). *Miner. Depos.* **2010**, *45*, 599–620. [[CrossRef](#)]
19. Dechaine, G.P.; Gray, M.R. Chemistry and Association of Vanadium Compounds in Heavy Oil and Bitumen, and Implications for Their Selective Removal. *Energy Fuels* **2010**, *24*, 2795–2808. [[CrossRef](#)]
20. Martínez-Palou, R.; Cerón-Camacho, R.; Chávez, B.; Vallejo, A.A.; Villanueva-Negrete, D.; Castellanos, J.; Karamath, J.; Reyes, J.; Aburto, J. Demulsification of Heavy Crude Oil-in-Water Emulsions: A Comparative Study between Microwave and Thermal Heating. *Fuel* **2013**, *113*, 407–414. [[CrossRef](#)]
21. Mofarragh, A.; Husain, T. Evaluation of Environmental Pollution and Possible Management Options of Heavy Oil Fly Ash. *J. Mater. Cycles Waste Manag.* **2013**, *15*, 73–81. [[CrossRef](#)]
22. Mohammed, H.; Sadeek, S.; Mahmoud, A.R.; Zaky, D. Comparison of AAS, EDXRF, ICP-MS and INAA Performance for Determination of Selected Heavy Metals in HFO Ashes. *Microchem. J.* **2016**, *128*, 1–6. [[CrossRef](#)]
23. Gupta, C.K.; Krishnamurthy, N. *Extractive Metallurgy of Vanadium*; Elsevier Science Publishing: Amsterdam, The Netherlands, 1992.
24. Brough, C.; Bowell, R.J.; Larkin, J. The Geology of Vanadium Deposits. In *An Introduction to Vanadium*; Nova Science Publishers, Inc.: New York, NY, USA, 2019; pp. 87–117.
25. Abd El-Hamid, A.A.M.; Abu Khoziem, H.A. Physical and Chemical Characterization of El Kriymat Boiler Ash to Optimize the Leachability of Some Valuable Elements. *J. Environ. Chem. Eng.* **2019**, *7*, 103362. [[CrossRef](#)]
26. Vitolo, S.; Seggiani, M.; Filippi, S.; Brocchini, C. Recovery of Vanadium from Heavy Oil and Orimulsion Fly Ashes. *Hydrometallurgy* **2000**, *57*, 141–149. [[CrossRef](#)]
27. Holloway, P.C.; Etsell, T.H. Salt Roasting of Suncor Oil Sands Fly Ash. *Can. Metall. Q.* **2004**, *43*, 535–544. [[CrossRef](#)]
28. White, D.; Levy, L. Vanadium: Environmental Hazard or Environmental Opportunity? A Perspective on Some Key Research Needs. *Environ. Sci. Process. Impacts* **2021**, *23*, 527–534. [[CrossRef](#)]
29. International Energy Agency. *Electricity Market Report*; IEA: Paris, France, 2020.
30. Egypt Electricity Holding Company (EEHC). *Egypt Electricity Holding Company Annual Report*; EEHC: Cairo, Egypt, 2021.
31. Mowafa taib. The Mineral Industry of Egypt. In *U.S. Geological Survey Minerals Yearbook*; United States Geological Survey: Reston, VA, USA, 2018; pp. 1–17.
32. Survey of Energy Resources. *World Energy Resources*; World Energy Council Registered in England and Wales: London, UK, 2013; pp. 1–56.
33. Statistical Review of World Energy. *Country Analysis Executive Summary: China*; U.S. Energy Information Administration (EIA): Washington, DC, USA, 2022.

34. Statistical Review of World Energy. *Country Analysis Executive Summary: Egypt*; U.S. Energy Information Administration (EIA): Washington, DC, USA, 2022.
35. Bakkar, A.; Seleman, M.M.E.; Ahmed, M.M.Z.; Harb, S.; Goren, S.; Howsawi, E. Recovery of Vanadium and Nickel from Heavy Oil Fly Ash (HOFA): A Critical Review. *RSC Adv.* **2023**, *13*, 6327–6345. [[CrossRef](#)]
36. Li, X.; Xie, B. Extraction of Vanadium from High Calcium Vanadium Slag Using Direct Roasting and Soda Leaching. *Int. J. Miner. Metall. Mater.* **2012**, *19*, 595–601. [[CrossRef](#)]
37. Song, W.C.; Li, K.; Zheng, Q.; Li, H. A Novel Process of Vanadium Extraction from Molten Vanadium Bearing Slag. *Waste Biomass Valorization* **2014**, *5*, 327–332. [[CrossRef](#)]
38. Xiao, Q.; Chen, Y.; Gao, Y.; Xu, H.; Zhang, Y. Leaching of Silica from Vanadium-Bearing Steel Slag in Sodium Hydroxide Solution. *Hydrometallurgy* **2010**, *104*, 216–221. [[CrossRef](#)]
39. Wu, K.; Wang, Y.; Wang, X.; Wang, S.; Liu, B.; Zhang, Y.; Du, H. Co-Extraction of Vanadium and Chromium from High Chromium Containing Vanadium Slag by Low-Pressure Liquid Phase Oxidation Method. *J. Clean. Prod.* **2018**, *203*, 873–884. [[CrossRef](#)]
40. Li, X.; Yu, H.; Xue, X. Extraction of Iron from Vanadium Slag Using Pressure Acid Leaching. *Procedia Environ. Sci.* **2016**, *31*, 582–588. [[CrossRef](#)]
41. Aarabi-Karasgani, M.; Rashchi, F.; Mostoufi, N.; Vahidi, E. Leaching of Vanadium from LD Converter Slag Using Sulfuric Acid. *Hydrometallurgy* **2010**, *102*, 14–21. [[CrossRef](#)]
42. Zhang, J.; Zhang, W.; Zhang, L.; Gu, S. Mechanism of Vanadium Slag Roasting with Calcium Oxide. *Int. J. Miner. Process.* **2015**, *138*, 20–29. [[CrossRef](#)]
43. Li, H.Y.; Fang, H.X.; Wang, K.; Zhou, W.; Yang, Z.; Yan, X.M.; Ge, W.S.; Li, Q.W.; Xie, B. Asynchronous Extraction of Vanadium and Chromium from Vanadium Slag by Stepwise Sodium Roasting-Water Leaching. *Hydrometallurgy* **2015**, *156*, 124–135. [[CrossRef](#)]
44. Zhang, X.; Fang, D.; Song, S.; Cheng, G.; Xue, X. Selective Leaching of Vanadium over Iron from Vanadium Slag. *J. Hazard. Mater.* **2019**, *368*, 300–307. [[CrossRef](#)]
45. Hobson, A.J.; Stewart, D.I.; Mortimer, R.J.G.; Mayes, W.M.; Rogerson, M.; Burke, I.T. Leaching Behaviour of Co-Disposed Steel Making Wastes: Effects of Aeration on Leachate Chemistry and Vanadium Mobilisation. *Waste Manag.* **2018**, *81*, 1–10. [[CrossRef](#)]
46. Speight, J.G. *The Chemistry and Technology of Coal*, 3rd ed.; CRC Press: Boca Raton, FL, USA, 2013; ISBN 9781439836484.
47. Hsieh, Y.-M.; Tsai, M.-S. An Investigation of the Characteristics of Unburned Carbon in Oil Fly Ash. In *Environmental Challenges and Greenhouse Gas Control for Fossil Fuel Utilization in the 21st Century*; Springer: Boston, MA, USA, 2002; Volume 21, pp. 387–401, ISBN 9789896540821.
48. Tsygankova, M.V.; Bukin, V.I.; Lysakova, E.I.; Smirnova, A.G.; Reznik, A.M. The Recovery of Vanadium from Ash Obtained during the Combustion of Fuel Oil at Thermal Power Stations. *Russ. J. Non-Ferrous Met.* **2011**, *52*, 19–23. [[CrossRef](#)]
49. Kim, J.Y.; Mukherjee, S.; Ngo, L.; Christiani, D.C. Urinary 8-Hydroxy-2'-Deoxyguanosine as a Biomarker of Oxidative DNA Damage in Workers Exposed to Fine Particulates. *Environ. Health Perspect.* **2004**, *112*, 666–671. [[CrossRef](#)] [[PubMed](#)]
50. Di Pietro, A.; Visalli, G.; Munaò, F.; Baluce, B.; La Maestra, S.; Primerano, P.; Corigliano, F.; De Flora, S. Oxidative Damage in Human Epithelial Alveolar Cells Exposed in Vitro to Oil Fly Ash Transition Metals. *Int. J. Hyg. Environ. Health* **2009**, *212*, 196–208. [[CrossRef](#)] [[PubMed](#)]
51. Pattanaik, S.; Huggins, F.E.; Huffman, G.P.; Linak, W.P.; Miller, C.A. XAFS Studies of Nickel and Sulfur Speciation in Residual Oil Fly-Ash Particulate Matters. *Environ. Sci. Technol.* **2007**, *41*, 1104–1110. [[CrossRef](#)] [[PubMed](#)]
52. Gomez-Bueno, C.O.; Spink, D.R.; Rempel, G.L. Extraction of Vanadium and Nickel From Athabasca Oil Sands Fly Ash. *Metall. Trans.* **1984**, *12*, 341–352. [[CrossRef](#)]
53. Al-Malack, M.H.; Bukhari, A.A.; Al-Amoudi, O.S.; Al-Muhanna, H.H.; Zaidi, T.H. Characteristics of Fly Ash Produced at Power and Water Desalination Plants Firing Fuel Oil. *Int. J. Environ. Res.* **2013**, *7*, 455–466.
54. Mofarrah, A.; Husain, T. Use of Heavy Oil Fly Ash as a Color Ingredient in Cement Mortar. *Int. J. Concr. Struct. Mater.* **2013**, *7*, 111–117. [[CrossRef](#)]
55. Stas, J.; Dahdouh, A.; Al-chayah, O. Recovery of Vanadium, Nickel and Molybdenum from Fly Ash of Heavy Oil-Fired Electrical Power Station. *Period. Polytech. Chem. Eng.* **2007**, *51*, 67–70. [[CrossRef](#)]
56. Vitolo, S.; Seggiani, M.; Falaschi, F. Recovery of Vanadium from a Previously Burned Heavy Oil Fly Ash. *Hydrometallurgy* **2001**, *62*, 145–150. [[CrossRef](#)]
57. Aslam, Z.; Hussein, I.A.; Shawabkeh, R.A.; Parvez, M.A.; Ahmad, W. Ihsanullah Adsorption Kinetics and Modeling of H₂S by Treated Waste Oil Fly Ash. *J. Air Waste Manag. Assoc.* **2019**, *69*, 246–257. [[CrossRef](#)]
58. Tokuyama, H.; Nii, S.; Kawaizumi, F.; Takahashi, K. Process Development for Recovery of Vanadium and Nickel from Heavy Oil Fly Ash by Leaching and Ion Exchange. *Sep. Sci. Technol.* **2003**, *38*, 1329–1344. [[CrossRef](#)]
59. Ibrahim, A.H.; Lyu, X.; Atia, B.M.; Gado, M.A.; ElDeeb, A.B. Phase Transformation Mechanism of Boiler Ash Roasted with Sodium Salt for Vanadium Extraction. *J. Mater. Cycles Waste Manag.* **2022**, *25*, 86–102. [[CrossRef](#)]
60. Yildirim, I.Z.; Prezzi, M. Chemical, Mineralogical, and Morphological Properties of Steel Slag. *Adv. Civ. Eng.* **2011**, *2011*, 463638. [[CrossRef](#)]

61. Li, W.; Zhang, Y.; Liu, T.; Huang, J.; Wang, Y. Comparison of Ion Exchange and Solvent Extraction in Recovering Vanadium from Sulfuric Acid Leach Solutions of Stone Coal. *Hydrometallurgy* **2013**, *131–132*, 1–7. [[CrossRef](#)]
62. Zhang, X.; Xie, B.; Diao, J.; Li, X.J. Nucleation and Growth Kinetics of Spinel Crystals in Vanadium Slag. *Ironmak. Steelmak.* **2012**, *39*, 147–154. [[CrossRef](#)]
63. Dabbagh, A.; Heidary Moghadam, A.; Naderi, S.; Hamdi, M. Erratum: A Study on the Effect of Coke Particle Size on the Thermal Profile of the Sinters Produced in Esfahan Steel Company (ESCO) (SAIMM Journal 113:12 (941–945)). *J. South. Afr. Inst. Min. Metall.* **2014**, *114*, 418.
64. Dondi, M.; Ercolani, G.; Guarini, G.; Raimondo, M. Orimulsion Fly Ash in Clay Bricks—Part 1: Composition and Thermal Behaviour of Ash. *J. Eur. Ceram. Soc.* **2002**, *22*, 1729–1735. [[CrossRef](#)]
65. Miller, C.A.; Srivastava, R.K. Combustion of Orimulsion and Its Generation of Air Pollutants. *Prog. Energy Combust. Sci.* **2000**, *26*, 131–160. [[CrossRef](#)]
66. Xiao, Y.; Mambote, C.R.; Jalkanen, H.; Yang, Y.; Boom, R. Vanadium Recovery as FeV from Petroleum Fly Ash. In Proceedings of the 12th International Ferrous Congress Sustainable Future, Helsinki, Finland, 6–9 June 2010; pp. 179–188.
67. Li, J.; Chen, Z.; Shen, B.; Xu, Z.; Zhang, Y. The Extraction of Valuable Metals and Phase Transformation and Formation Mechanism in Roasting-Water Leaching Process of Laterite with Ammonium Sulfate. *J. Clean. Prod.* **2017**, *140*, 1148–1155. [[CrossRef](#)]
68. Mu, W.; Huang, Z.; Xin, H.; Luo, S.; Zhai, Y.; Xu, Q. Extraction of Copper and Nickel from Low-Grade Nickel Sulfide Ore by Low-Temperature Roasting, Selective Decomposition and Water-Leaching Process. *JOM* **2019**, *71*, 4647–4658. [[CrossRef](#)]
69. Li, J.; Li, D.; Xu, Z.; Liao, C.; Liu, Y.; Zhong, B. Selective Leaching of Valuable Metals from Laterite Nickel Ore with Ammonium Chloride-Hydrochloric Acid Solution. *J. Clean. Prod.* **2018**, *179*, 24–30. [[CrossRef](#)]
70. Huaiwei, Z.; Xin, H. An Overview for the Utilization of Wastes from Stainless Steel Industries. *Resour. Conserv. Recycl.* **2011**, *55*, 745–754. [[CrossRef](#)]
71. Alex, P.; Mishra, P.; Suri, A.K. Studies on Processing of an Alnico Scrap. *Miner. Process. Extr. Metall. Rev.* **2001**, *22*, 547–565. [[CrossRef](#)]
72. Shen, Y.; Xue, W.; Niu, W. Recovery of Co(II) and Ni(II) from Hydrochloric Acid Solution of Alloy Scrap. *Trans. Nonferrous Met. Soc. China* **2008**, *18*, 1262–1268. [[CrossRef](#)]
73. Goel, S.; Pant, K.K.; Nigam, K.D.P. Extraction of Nickel from Spent Catalyst Using Fresh and Recovered EDTA. *J. Hazard. Mater.* **2009**, *171*, 253–261. [[CrossRef](#)]
74. Vuyyuru, K.R.; Pant, K.K.; Krishnan, V.V.; Nigam, K.D.P. Recovery of Nickel from Spent Industrial Catalysts Using Chelating Agents. *Ind. Eng. Chem. Res.* **2010**, *49*, 2014–2024. [[CrossRef](#)]
75. Sahu, K.K.; Agarwal, A.; Pandey, B.D. Nickel Recovery from Spent Nickel Catalyst. *Waste Manag. Res. J. A Sustain. Circ. Econ.* **2005**, *23*, 148–154. [[CrossRef](#)]
76. Idris, J.; Musa, M.; Yin, C.-Y.; Hamid, K.H.K. Recovery of Nickel from Spent Catalyst from Palm Oil Hydrogenation Process Using Acidic Solutions. *J. Ind. Eng. Chem.* **2010**, *16*, 251–255. [[CrossRef](#)]
77. Marafi, M.; Stanislaus, A. Waste Catalyst Utilization: Extraction of Valuable Metals from Spent Hydroprocessing Catalysts by Ultrasonic-Assisted Leaching with Acids. *Ind. Eng. Chem. Res.* **2011**, *50*, 9495–9501. [[CrossRef](#)]
78. Oza, R.; Shah, N.; Patel, S. Recovery of Nickel from Spent Catalysts Using Ultrasonication-Assisted Leaching. *J. Chem. Technol. Biotechnol.* **2011**, *86*, 1276–1281. [[CrossRef](#)]
79. Ognyanova, A.; Ozturk, A.T.; De Michelis, I.; Ferella, F.; Taglieri, G.; Akcil, A.; Vegliò, F. Metal Extraction from Spent Sulfuric Acid Catalyst through Alkaline and Acidic Leaching. *Hydrometallurgy* **2009**, *100*, 20–28. [[CrossRef](#)]
80. Ferella, F.; Ognyanova, A.; De Michelis, I.; Taglieri, G.; Vegliò, F. Extraction of Metals from Spent Hydrotreating Catalysts: Physico-Mechanical Pre-Treatments and Leaching Stage. *J. Hazard. Mater.* **2011**, *192*, 176–185. [[CrossRef](#)] [[PubMed](#)]
81. Yang, Q.Z.; Ng, R.S.; Qi, G.J.; Low, H.C.; Zhang, Y.P. Economic Viability of Nickel Recovery from Waste Catalyst. *Key Eng. Mater.* **2010**, *447–448*, 765–769. [[CrossRef](#)]
82. Yang, Q.Z.; Qi, G.J.; Low, H.C.; Song, B. Sustainable Recovery of Nickel from Spent Hydrogenation Catalyst: Economics, Emissions and Wastes Assessment. *J. Clean. Prod.* **2011**, *19*, 365–375. [[CrossRef](#)]
83. Abd El-Hamid, A.M.; Zahran, M.A.; Khalid, F.M.; Mahmoud, A.H. Leaching of Hafnium, Zirconium, Uranium and Other Nuclear Economic Elements from Petroleum Ash. *RSC Adv.* **2014**, *4*, 12506. [[CrossRef](#)]
84. Deng, Z.G.; Wei, C.; Fan, G.; Li, M.T.; Li, C.X.; Li, X. Bin Extracting Vanadium from Stone-Coal by Oxygen Pressure Acid Leaching and Solvent Extraction. *Trans. Nonferrous Met. Soc. China (Engl. Ed.)* **2010**, *20*, s118–s122. [[CrossRef](#)]
85. Barik, S.P.; Park, K.H.; Nam, C.W. Process Development for Recovery of Vanadium and Nickel from an Industrial Solid Waste by a Leaching-Solvent Extraction Technique. *J. Environ. Manag.* **2014**, *146*, 22–28. [[CrossRef](#)]
86. Akcil, A.; Vegliò, F.; Ferella, F.; Okudan, M.D.; Tuncuk, A. A Review of Metal Recovery from Spent Petroleum Catalysts and Ash. *Waste Manag.* **2015**, *45*, 420–433. [[CrossRef](#)]
87. Nazari, E.; Rashchi, F.; Saba, M.; Mirazimi, S.M.J. Simultaneous Recovery of Vanadium and Nickel from Power Plant Fly-Ash: Optimization of Parameters Using Response Surface Methodology. *Waste Manag.* **2014**, *34*, 2687–2696. [[CrossRef](#)]

88. Navarro, R.; Guzman, J.; Saucedo, I.; Revilla, J.; Guibal, E. Vanadium Recovery from Oil Fly Ash by Leaching, Precipitation and Solvent Extraction Processes. *Waste Manag.* **2007**, *27*, 425–438. [[CrossRef](#)]
89. Aburizaiza, A. Sequential Leaching of Vanadium from Heavy Fuel Oil Fly Ash Generated from Saudi Arabia Thermal Power Plants. *Curr. J. Appl. Sci. Technol.* **2019**, *32*, 1–17. [[CrossRef](#)]
90. Khalafalla, M.S.; Abdellah, W.M.; Khoziem, H.A.A.; Abd El-Hamid, A.A.M. Ecological Treatment of El Kriymat Boiler Ash for Recovering Vanadium, Nickel and Zinc from Sulfate Leach Liquor. *J. Mater. Cycles Waste Manag.* **2023**, *25*, 441–455. [[CrossRef](#)]
91. Weshahy, A.R.; Gouda, A.A.; Atia, B.M.; Sakr, A.K.; Al-Otaibi, J.S.; Almuqrin, A.; Hanfi, M.Y.; Sayyed, M.I.; El Sheikh, R.; Radwan, H.A.; et al. Efficient Recovery of Rare Earth Elements and Zinc from Spent Ni–Metal Hydride Batteries: Statistical Studies. *Nanomaterials* **2022**, *12*, 2305. [[CrossRef](#)] [[PubMed](#)]
92. Rahimi, G.; Rastegar, S.O.; Rahmani Chianeh, F.; Gu, T. Ultrasound-Assisted Leaching of Vanadium from Fly Ash Using Lemon Juice Organic Acids. *RSC Adv.* **2020**, *10*, 1685–1696. [[CrossRef](#)] [[PubMed](#)]
93. Mu, W.; Zhang, T.; Dou, Z.; Lü, G.; Hu, L.; Yu, B.; Liu, Y. Oxygen Pressure Acid Leaching of Vanadium Slag. *Appl. Mech. Mater.* **2011**, *79*, 242–247. [[CrossRef](#)]
94. Zhang, G.; Zhang, T.; Lü, G.; Zhang, Y.; Liu, Y.; Liu, Z. Extraction of Vanadium from Vanadium Slag by High Pressure Oxidative Acid Leaching. *Int. J. Miner. Metall. Mater.* **2015**, *22*, 21–26. [[CrossRef](#)]
95. Guoquan, Z.; Ting'an, Z.; Guozhi, L.; Ying, Z.; Yan, L.; Gang, X. Extraction of Vanadium from LD Converter Slag by Pressure Leaching Process with Titanium White Waste Acid. *Rare Met. Mater. Eng.* **2015**, *44*, 1894–1898. [[CrossRef](#)]
96. Zhang, G.-Q.; Zhang, T.-A.; Zhang, Y.; Lv, G.-Z.; Liu, Y.; Liu, Z.-L. Pressure Leaching of Converter Vanadium Slag with Waste Titanium Dioxide. *Rare Met.* **2016**, *35*, 576–580. [[CrossRef](#)]
97. Zhou, X.; Wei, C.; Xia, W.; Li, M.; Li, C.; Deng, Z.; Xu, H. Dissolution Kinetics and Thermodynamic Analysis of Vanadium Trioxide during Pressure Oxidation. *Rare Met.* **2012**, *31*, 296–302. [[CrossRef](#)]
98. Amer, A.M. Processing of Egyptian Boiler-Ash for Extraction of Vanadium and Nickel. *Waste Manag.* **2002**, *22*, 515–520. [[CrossRef](#)]
99. Tsai, S.-L.; Tsai, M.-S. A Study of the Extraction of Vanadium and Nickel in Oil-Fired Fly Ash. *Resour. Conserv. Recycl.* **1998**, *22*, 163–176. [[CrossRef](#)]
100. Al-Zuhairi, M.A.H. Vanadium Extraction from Residual of Fired Crude Oil in Power Plants. *Iraqi J. Mech. Mater. Eng.* **2014**, *14*, 423–431.
101. Hakimi, M.; Kiani, P.; Alikhani, M.; Feizi, N.; Bajestani, A.M.; Alimard, P. Reducing Environmental Pollution of Fuel Fly Ash by Extraction and Removal Vanadium Pentoxide. *Solid Fuel Chem.* **2020**, *54*, 337–342. [[CrossRef](#)]
102. Akita, S.; Maeda, T.; Takeuchi, H. Recovery of Vanadium and Nickel in Fly Ash from Heavy Oil. *J. Chem. Technol. Biotechnol.* **1995**, *62*, 345–350. [[CrossRef](#)]
103. Al-Ghouti, M.A.; Al-Degs, Y.S.; Ghrair, A.; Khoury, H.; Ziedan, M. Extraction and Separation of Vanadium and Nickel from Fly Ash Produced in Heavy Fuel Power Plants. *Chem. Eng. J.* **2011**, *173*, 191–197. [[CrossRef](#)]
104. Shahnazi, A.; Rashchi, F.; Vahidi, E. A Kinetics Study on the Hydrometallurgical Recovery of Vanadium from LD Converter Slag in Alkaline Media. In Proceedings of the TMS 2012 Annual Meeting, Orlando, FL, USA, 11–15 March 2012; pp. 425–433. [[CrossRef](#)]
105. Qiu, S.; Wei, C.; Li, M.; Zhou, X.; Li, C.; Deng, Z. Dissolution Kinetics of Vanadium Trioxide at High Pressure in Sodium Hydroxide-Oxygen Systems. *Hydrometallurgy* **2011**, *105*, 350–354. [[CrossRef](#)]
106. Liu, B.; Du, H.; Wang, S.N.; Zhang, Y.; Zheng, S.L.; Li, L.J.; Chen, D.H. A Novel Method to Extract Vanadium and Chromium from Vanadium Slag Using Molten NaOH–NaNO₃ Binary System. *AIChE J.* **2013**, *59*, 541–552. [[CrossRef](#)]
107. Mirazimi, S.M.J.; Rashchi, F.; Saba, M. A New Approach for Direct Leaching of Vanadium from LD Converter Slag. *Chem. Eng. Res. Des.* **2015**, *94*, 131–140. [[CrossRef](#)]
108. Zhang, G.; Chen, D.; Zhao, W.; Zhao, H.; Wang, L.; Li, D.; Qi, T. A Novel Synergistic Extraction Method for Recovering Vanadium (V) from High-Acidity Chloride Leaching Liquor. *Sep. Purif. Technol.* **2016**, *165*, 166–172. [[CrossRef](#)]
109. Li, M.; Zheng, S.; Liu, B.; Wang, S.; Dreisinger, D.B.; Zhang, Y.; Du, H.; Zhang, Y. A Clean and Efficient Method for Recovery of Vanadium from Vanadium Slag: Nonsalt Roasting and Ammonium Carbonate Leaching Processes. *Miner. Process. Extr. Metall. Rev.* **2017**, *38*, 228–237. [[CrossRef](#)]
110. Wang, Z.; Chen, L.; Aldahrib, T.; Li, C.; Liu, W.; Zhang, G.; Yang, Y.; Luo, D. Direct Recovery of Low Valence Vanadium from Vanadium Slag—Effect of Roasting on Vanadium Leaching. *Hydrometallurgy* **2020**, *191*, 105156. [[CrossRef](#)]
111. Li, D.-Q.; Yang, Y.; Li, H.-Y.; Xie, B. Study on Vanadium Phase Evolution Law in Vanadium Slag During the Interface Reaction Process of Sodium Roasting. In *Rare Metal Technology 2020*; Minerals, Metals and Materials Series; Springer International Publishing: New York, NY, USA, 2020; pp. 253–264, ISBN 9783030367572.
112. Zhang, G.; Zhang, Y.; Bao, S.; Yuan, Y.; Jian, X.; Li, R. Selective Vanadium Extraction from Vanadium Bearing Ferro-Phosphorus via Roasting and Pressure Hydrogen Reduction. *Sep. Purif. Technol.* **2019**, *220*, 293–299. [[CrossRef](#)]
113. Ettlér, V.; Kvapil, J.; Šebek, O.; Johan, Z.; Mihaljevič, M.; Ratié, G.; Garnier, J.; Quantin, C. Leaching Behaviour of Slag and Fly Ash from Laterite Nickel Ore Smelting (Niquelândia, Brazil). *Appl. Geochem.* **2016**, *64*, 118–127. [[CrossRef](#)]

114. Hu, P.; Zhang, Y.; Liu, T.; Huang, J.; Yuan, Y.; Zheng, Q. Highly Selective Separation of Vanadium over Iron from Stone Coal by Oxalic Acid Leaching. *J. Ind. Eng. Chem.* **2017**, *45*, 241–247. [[CrossRef](#)]
115. Liu, Z.; Huang, J.; Zhang, Y.; Liu, T.; Hu, P.; Liu, H.; Zheng, Q. Separation and Recovery of Iron Impurities from a Complex Oxalic Acid Solution Containing Vanadium by $K_3Fe(C_2O_4)_3 \cdot 3H_2O$ Crystallization. *Sep. Purif. Technol.* **2020**, *232*, 115970. [[CrossRef](#)]
116. Mirazimi, S.M.J.; Rashchi, F. Optimization of Bioleaching of a Vanadium Containing Slag Using RSM. In Proceedings of the 7th International Chemical Engineering Congress & Exhibition, Kish, Iran, 21–24 November 2011.
117. Mirazimi, S.M.J.; Abbasalipour, Z.; Rashchi, F. Vanadium Removal from LD Converter Slag Using Bacteria and Fungi. *J. Environ. Manag.* **2015**, *153*, 144–151. [[CrossRef](#)]
118. Ntita, J.; Nheta, W. Investigation on the Mechanisms of Bio-Processing Vanadium Slags. In Proceedings of the 5th International Slag Volatilisation Symposium, Leuven, Belgium, 3–5 April 2017; pp. 173–176.
119. Ntita, J.; Nheta, W.; Staden, P.V. Selective Leaching of Vanadium from Vanadium Slag Using Organic Acids. In Proceedings of the 9th International Conference on Advances in Science, Engineering, Technology & Waste Management (ASETWM-17), Parys, South Africa, 27–28 November 2017.
120. Thallner, S.; Hemmelmaier, C.; Martinek, S.; Schnitzhofer, W. Bioleaching for Removal of Chromium and Associated Metals from LD Slag. *Solid State Phenom.* **2017**, *262*, 79–83. [[CrossRef](#)]
121. Lee, J.C.; Pandey, B.D. Bio-Processing of Solid Wastes and Secondary Resources for Metal Extraction—A Review. *Waste Manag.* **2012**, *32*, 3–18. [[CrossRef](#)]
122. Zeng, L.; Cheng, C.Y. A Literature Review of the Recovery of Molybdenum and Vanadium from Spent Hydrodesulphurisation Catalysts. Part I: Metallurgical Processes. *Hydrometallurgy* **2009**, *98*, 1–9. [[CrossRef](#)]
123. Gomes, H.I.; Funari, V.; Mayes, W.M.; Rogerson, M.; Prior, T.J. Recovery of Al, Cr and V from Steel Slag by Bioleaching: Batch and Column Experiments. *J. Environ. Manag.* **2018**, *222*, 30–36. [[CrossRef](#)]
124. Liu, Z.; Nueraihemaiti, A.; Chen, M.; Du, J.; Fan, X.; Tao, C. Hydrometallurgical Leaching Process Intensified by an Electric Field for Converter Vanadium Slag. *Hydrometallurgy* **2015**, *155*, 56–60. [[CrossRef](#)]
125. Peng, H.; Liu, Z.; Tao, C. Selective Leaching of Vanadium from Chromium Residue Intensified by Electric Field. *J. Environ. Chem. Eng.* **2015**, *3*, 1252–1257. [[CrossRef](#)]
126. Liu, Z.; Li, Y.; Chen, M.; Nueraihemaiti, A.; Du, J.; Fan, X.; Tao, C.Y. Enhanced Leaching of Vanadium Slag in Acidic Solution by Electro-Oxidation. *Hydrometallurgy* **2016**, *159*, 1–5. [[CrossRef](#)]
127. Lee, J.; Kurniawan, Kim, E.; Chung, K.W.; Kim, R.; Jeon, H.-S. A Review on the Metallurgical Recycling of Vanadium from Slags: Towards a Sustainable Vanadium Production. *J. Mater. Res. Technol.* **2021**, *12*, 343–364. [[CrossRef](#)]
128. Peng, H. A Literature Review on Leaching and Recovery of Vanadium. *J. Environ. Chem. Eng.* **2019**, *7*, 103313. [[CrossRef](#)]
129. Ye, P.; Wang, X.; Wang, M.; Fan, Y.; Xiang, X. Recovery of Vanadium from Stone Coal Acid Leaching Solution by Coprecipitation, Alkaline Roasting and Water Leaching. *Hydrometallurgy* **2012**, *117–118*, 108–115. [[CrossRef](#)]
130. Gao, H.; Jiang, T.; Zhou, M.; Wen, J.; Li, X.; Wang, Y.; Xue, X. Effect of Microwave Irradiation and Conventional Calcification Roasting with Calcium Hydroxide on the Extraction of Vanadium and Chromium from High-Chromium Vanadium Slag. *Miner. Eng.* **2020**, *145*, 106056. [[CrossRef](#)]
131. Chen, L.; Wang, Z.; Qin, Z.; Zhang, G.; Yue, H.; Liang, B.; Luo, D. Investigation of the Selective Oxidation Roasting of Vanadium-iron Spinel. *Powder Technol.* **2021**, *387*, 434–443. [[CrossRef](#)]
132. Zeng, L.; Yong Cheng, C. A Literature Review of the Recovery of Molybdenum and Vanadium from Spent Hydrodesulphurisation Catalysts. Part II: Separation and Purification. *Hydrometallurgy* **2009**, *98*, 10–20. [[CrossRef](#)]
133. Li, M.; Du, H.; Zheng, S.; Wang, S.; Zhang, Y.; Liu, B.; Dreisinger, D.B.; Zhang, Y. Extraction of Vanadium from Vanadium Slag Via Non-Salt Roasting and Ammonium Oxalate Leaching. *JOM* **2017**, *69*, 1970–1975. [[CrossRef](#)]
134. Li, M.; Liu, B.; Zheng, S.; Wang, S.; Du, H.; Dreisinger, D.B.; Zhang, Y. A Cleaner Vanadium Extraction Method Featuring Non-Salt Roasting and Ammonium Bicarbonate Leaching. *J. Clean. Prod.* **2017**, *149*, 206–217. [[CrossRef](#)]
135. Zhang, X.; Liu, F.; Xue, X.; Jiang, T. Effects of Microwave and Conventional Blank Roasting on Oxidation Behavior, Microstructure and Surface Morphology of Vanadium Slag with High Chromium Content. *J. Alloys Compd.* **2016**, *686*, 356–365. [[CrossRef](#)]
136. Wang, M.; Xiang, X.; Zhang, L.; Xiao, L. Effect of Vanadium Occurrence State on the Choice of Extracting Vanadium Technology from Stone Coal. *Rare Met.* **2008**, *27*, 112–115. [[CrossRef](#)]
137. Zhang, Y.; Zhang, T.A.; Dreisinger, D.; Lv, C.; Lv, G.; Zhang, W. Recovery of Vanadium from Calcification Roasted-Acid Leaching Tailing by Enhanced Acid Leaching. *J. Hazard. Mater.* **2019**, *369*, 632–641. [[CrossRef](#)]
138. Zhang, J.; Zhang, W.; Xue, Z. Oxidation Kinetics of Vanadium Slag Roasting in the Presence of Calcium Oxide. *Miner. Process. Extr. Metall. Rev.* **2017**, *38*, 265–273. [[CrossRef](#)]
139. Wen, J.; Jiang, T.; Zheng, X.; Wang, J.; Cao, J.; Zhou, M. Efficient Separation of Chromium and Vanadium by Calcification Roasting–Sodium Carbonate Leaching from High Chromium Vanadium Slag and V_2O_5 Preparation. *Sep. Purif. Technol.* **2020**, *230*, 115881. [[CrossRef](#)]

140. Zhang, J.; Zhang, W.; Xue, Z. An Environment-Friendly Process Featuring Calcified Roasting and Precipitation Purification to Prepare Vanadium Pentoxide from the Converter Vanadium Slag. *Metals* **2019**, *9*, 21. [\[CrossRef\]](#)
141. Peng, H.; Guo, J.; Zheng, X.; Liu, Z.; Tao, C. Leaching Kinetics of Vanadium from Calcification Roasting Converter Vanadium Slag in Acidic Medium. *J. Environ. Chem. Eng.* **2018**, *6*, 5119–5124. [\[CrossRef\]](#)
142. Xiang, J.; Huang, Q.; Lv, X.; Bai, C. Extraction of Vanadium from Converter Slag by Two-Step Sulfuric Acid Leaching Process. *J. Clean. Prod.* **2018**, *170*, 1089–1101. [\[CrossRef\]](#)
143. Li, H.-Y.; Wang, K.; Hua, W.-H.; Yang, Z.; Zhou, W.; Xie, B. Selective Leaching of Vanadium in Calcification-Roasted Vanadium Slag by Ammonium Carbonate. *Hydrometallurgy* **2016**, *160*, 18–25. [\[CrossRef\]](#)
144. Xu, Y.; Cai, Y.; Lu, X.; Ma, P. Study on Recovery of Vanadium from Low-Vanadium Slag by Calcified Roasting Methods. *Adv. Mater. Res.* **2011**, *284–286*, 2127–2130. [\[CrossRef\]](#)
145. Wen, J.; Jiang, T.; Zhou, M.; Gao, H.Y.; Liu, J.Y.; Xue, X.X. Roasting and Leaching Behaviors of Vanadium and Chromium in Calcification Roasting–Acid Leaching of High-Chromium Vanadium Slag. *Int. J. Miner. Metall. Mater.* **2018**, *25*, 515–526. [\[CrossRef\]](#)
146. Xiang, J.; Huang, Q.; Lv, X.; Bai, C. Effect of Mechanical Activation Treatment on the Recovery of Vanadium from Converter Slag. *Metall. Mater. Trans. B Process Metall. Mater. Process. Sci.* **2017**, *48*, 2759–2767. [\[CrossRef\]](#)
147. Yang, Z.; Li, H.-Y.; Yin, X.-C.; Yan, Z.-M.; Yan, X.-M.; Xie, B. Leaching Kinetics of Calcification Roasted Vanadium Slag with High CaO Content by Sulfuric Acid. *Int. J. Miner. Process.* **2014**, *133*, 105–111. [\[CrossRef\]](#)
148. Wang, G.; Lin, M.M.; Diao, J.; Li, H.Y.; Xie, B.; Li, G. A Novel Strategy for Green Comprehensive Utilization of Vanadium Slag with High-Content Chromium. *ACS Sustain. Chem. Eng.* **2019**, *7*, 18133–18141. [\[CrossRef\]](#)
149. Wen, J.; Jiang, T.; Zhou, W.; Gao, H.; Xue, X. A Cleaner and Efficient Process for Extraction of Vanadium from High Chromium Vanadium Slag: Leaching in $(\text{NH}_4)_2\text{SO}_4\text{-H}_2\text{SO}_4$ Synergistic System and NH_4^+ Recycle. *Sep. Purif. Technol.* **2019**, *216*, 126–135. [\[CrossRef\]](#)
150. Xiang, J.; Pei, G.; Huang, Q.; Lv, W.; Yang, M.; Hu, K.; Lv, X. *A Multi-Step Process for the Cleaner Utilization of Vanadium-Bearing Converter Slag*; Springer International Publishing: New York, NY, USA, 2019; ISBN 9783030057398.
151. Wen, J.; Jiang, T.; Xu, Y.; Liu, J.; Xue, X. Efficient Separation and Extraction of Vanadium and Chromium in High Chromium Vanadium Slag by Selective Two-Stage Roasting–Leaching. *Metall. Mater. Trans. B Process Metall. Mater. Process. Sci.* **2018**, *49*, 1471–1481. [\[CrossRef\]](#)
152. Cai, Z.; Zhang, Y. Phase Transformations of Vanadium Recovery from Refractory Stone Coal by Novel NaOH Molten Roasting and Water Leaching Technology. *RSC Adv.* **2017**, *7*, 36917–36922. [\[CrossRef\]](#)
153. Ji, Y.; Shen, S.; Liu, J.; Xue, Y. Cleaner and Effective Process for Extracting Vanadium from Vanadium Slag by Using an Innovative Three-Phase Roasting Reaction. *J. Clean. Prod.* **2017**, *149*, 1068–1078. [\[CrossRef\]](#)
154. Nkosi, S.; Dire, P.; Nyambeni, N.; Goso, X.C. A Comparative Study of Vanadium Recovery from Titaniferous Magnetite Using Salt, Sulphate, and Soda Ash Roast-Leach Processes. In Proceedings of the 3rd Young Professionals Conference, Pretoria, South Africa, 9–10 March 2017; pp. 191–200.
155. Geng, C.; Sun, T.; Yang, H.; Ma, Y.; Gao, E.; Xu, C. Effect of Na_2SO_4 on the Embedding Direct Reduction of Beach Titanomagnetite and the Separation of Titanium and Iron by Magnetic Separation. *ISIJ Int.* **2015**, *55*, 2543–2549. [\[CrossRef\]](#)
156. Nugraha, A.; Priyono, B.; Maksun, A.; Juna, H.; Soedarsono, J.W. The Effect of Sodium Sulfate (Na_2SO_4) and Sodium Carbonate (Na_2CO_3) Addition on the Reduction-Roasting Process of Titania Iron Sand. *E3S Web Conf.* **2018**, *67*, 2–7. [\[CrossRef\]](#)
157. Sui, Y.L.; Guo, Y.F.; Travyanov, A.Y.; Jiang, T.; Chen, F.; Qiu, G.Z. Reduction Roasting–Magnetic Separation of Vanadium Tailings in Presence of Sodium Sulfate and Its Mechanisms. *Rare Met.* **2016**, *35*, 954–960. [\[CrossRef\]](#)
158. Ju, Z.-J.; Wang, C.-Y.; Yin, F. Dissolution Kinetics of Vanadium from Black Shale by Activated Sulfuric Acid Leaching in Atmosphere Pressure. *Int. J. Miner. Process.* **2015**, *138*, 1–5. [\[CrossRef\]](#)
159. Huang, K.; Inoue, K.; Harada, H.; Kawakita, H.; Ohto, K. Leaching of Heavy Metals by Citric Acid from Fly Ash Generated in Municipal Waste Incineration Plants. *J. Mater. Cycles Waste Manag.* **2011**, *13*, 118–126. [\[CrossRef\]](#)
160. Pan, B.; Jin, W.; Liu, B.; Zheng, S.; Wang, S.; Du, H.; Zhang, Y. Cleaner Production of Vanadium Oxides by Cation-Exchange Membrane-Assisted Electrolysis of Sodium Vanadate Solution. *Hydrometallurgy* **2017**, *169*, 440–446. [\[CrossRef\]](#)
161. Wen, J.; Jiang, T.; Xu, Y.; Cao, J.; Xue, X. Efficient Extraction and Separation of Vanadium and Chromium in High Chromium Vanadium Slag by Sodium Salt Roasting- $(\text{NH}_4)_2\text{SO}_4$ Leaching. *J. Ind. Eng. Chem.* **2019**, *71*, 327–335. [\[CrossRef\]](#)
162. Zhao, Y.; Wang, W.; Zhang, Y.; Song, S.; Bao, S. In-Situ Investigation on Mineral Phase Transition during Roasting of Vanadium-Bearing Stone Coal. *Adv. Powder Technol.* **2017**, *28*, 1103–1107. [\[CrossRef\]](#)
163. Jung, M.; Mishra, B. Vanadium Recovery from Oil Fly Ash by Carbon Removal and Roast-Leach Process. *JOM* **2018**, *70*, 168–172. [\[CrossRef\]](#)
164. Yuan, J.; Cao, Y.; Fan, G.; Du, H.; Dreisinger, D.; Han, G.; Li, M. Study on the Mechanisms for Vanadium Phases' Transformation of Vanadium Slag Non-Salt Roasting Process. In *Rare Metal Technology 2020*; Azimi, G., Forsberg, K., Ouchi, T., Kim, H., Alam, S., Baba, A.A., Eds.; Springer International Publishing: Cham, Switzerland, 2020; pp. 235–242, ISBN 978-3-030-36757-2.

165. Ibrahim, A.H.; Lyu, X.; Atia, B.M.; Gado, M.A.; ElDeeb, A.B. Cost-Effective and High Purity Valuable Metals Extraction from Water Leaching Solid Residues Obtained as a By-Product from Processing the Egyptian Boiler Ash. *Minerals* **2022**, *12*, 1084. [[CrossRef](#)]
166. Li, X.; Xie, B.; Wang, G.; Li, X. Oxidation Process of Low-Grade Vanadium Slag in Presence of Na_2CO_3 . *Trans. Nonferrous Met. Soc. China* **2011**, *21*, 1860–1867. [[CrossRef](#)]
167. Mahdavian, A.; Shafyei, A.; Alamdariand, E.K.; Haghshenas, D.F. Recovery of Vanadium from Esfahan Steel Company Steel Slag; Optimizing of Roasting and Leaching Parameters. *Int. J. ISSI* **2006**, *3*, 17–21.
168. Li, H.Y.; Wang, C.; Lin, M.; Guo, Y.; Xie, B. Green One-Step Roasting Method for Efficient Extraction of Vanadium and Chromium from Vanadium-Chromium Slag. *Powder Technol.* **2020**, *360*, 503–508. [[CrossRef](#)]
169. Wang, M.; Chen, B.; Huang, S.; Wang, X.; Liu, B.; Ge, Q.; Xie, S. A Novel Technology for Vanadium and Chromium Recovery from V-Cr-Bearing Reducing Slag. *Hydrometallurgy* **2017**, *171*, 116–122. [[CrossRef](#)]
170. Liu, S.; Wang, L.; Chou, K. A Novel Process for Simultaneous Extraction of Iron, Vanadium, Manganese, Chromium, and Titanium from Vanadium Slag by Molten Salt Electrolysis. *Ind. Eng. Chem. Res.* **2016**, *55*, 12962–12969. [[CrossRef](#)]
171. Liu, H.; Du, H.; Wang, D.W.; Wang, S.N.; Zheng, S.L.; Zhang, Y. Kinetics Analysis of Decomposition of Vanadium Slag by KOH Sub-Molten Salt Method. *Trans. Nonferrous Met. Soc. China (Engl. Ed.)* **2013**, *23*, 1489–1500. [[CrossRef](#)]
172. Wang, Z.; Zheng, S.; Wang, S.; Qin, Y.; Du, H.; Zhang, Y. Electrochemical Decomposition of Vanadium Slag in Concentrated NaOH Solution. *Hydrometallurgy* **2015**, *151*, 51–55. [[CrossRef](#)]
173. Hu, P.; Zhang, Y.; Liu, T.; Huang, J.; Yuan, Y.; Yang, Y. Separation and Recovery of Iron Impurity from a Vanadium-Bearing Stone Coal via an Oxalic Acid Leaching-Reduction Precipitation Process. *Sep. Purif. Technol.* **2017**, *180*, 99–106. [[CrossRef](#)]
174. Mazurek, K. Recovery of Vanadium, Potassium and Iron from a Spent Vanadium Catalyst by Oxalic Acid Solution Leaching, Precipitation and Ion Exchange Processes. *Hydrometallurgy* **2013**, *134–135*, 26–31. [[CrossRef](#)]
175. Mazurek, K.; Białowicz, K.; Trypuć, M. Recovery of Vanadium, Potassium and Iron from a Spent Catalyst Using Urea Solution. *Hydrometallurgy* **2010**, *103*, 19–24. [[CrossRef](#)]
176. Sánchez-Camargo, A.P.; Mendiola, J.A.; Ibáñez, E.; Herrero, M. Supercritical Fluid Extraction. In *Reference Module in Chemistry, Molecular Sciences and Chemical Engineering*; Elsevier: Amsterdam, The Netherlands, 2014; ISBN 978-0-12-409547-2.
177. Yang, Q.W.; Xie, Z.M.; Peng, H.; Liu, Z.H.; Tao, C.Y. Leaching of Vanadium and Chromium from Converter Vanadium Slag Intensified with Surface Wettability. *J. Cent. South Univ.* **2018**, *25*, 1317–1325. [[CrossRef](#)]
178. Olehile, O.D.; van Dyk, L. Gas Phase Extraction of Vanadium from Spent Vanadium Catalyst and from Tantalum Oxide. 2017.
179. Aljerf, L. High-Efficiency Extraction of Bromocresol Purple Dye and Heavy Metals as Chromium from Industrial Effluent by Adsorption onto a Modified Surface of Zeolite: Kinetics and Equilibrium Study. *J. Environ. Manag.* **2018**, *225*, 120–132. [[CrossRef](#)] [[PubMed](#)]
180. Ojha, K.; Pradhan, N.C.; Samanta, A.N. Zeolite from Fly Ash: Synthesis and Characterization. *Bull. Mater. Sci.* **2004**, *27*, 555–564. [[CrossRef](#)]
181. Golbad, S.; Khoshnoud, P.; Abu-Zahra, N. Hydrothermal Synthesis of Hydroxy Sodalite from Fly Ash for the Removal of Lead Ions from Water. *Int. J. Environ. Sci. Technol.* **2017**, *14*, 135–142. [[CrossRef](#)]
182. Kang, Y.; Swain, B.; Im, B.; Yoon, J.H.; Park, K.H.; Lee, C.G.; Kim, D.G. Synthesis of Zeolite Using Aluminum Dross and Waste LCD Glass Powder: A Waste to Waste Integration Valorization Process. *Metals* **2019**, *9*, 1240. [[CrossRef](#)]
183. Liu, Y.; Yan, C.; Zhao, J.; Zhang, Z.; Wang, H.; Zhou, S.; Wu, L. Synthesis of Zeolite P1 from Fly Ash under Solvent-Free Conditions for Ammonium Removal from Water. *J. Clean. Prod.* **2018**, *202*, 11–22. [[CrossRef](#)]
184. Mallapur, V.P.; Oubagaranadin, J.U.K. A Brief Review on the Synthesis of Zeolites from Hazardous Wastes. *Trans. Indian Ceram. Soc.* **2017**, *76*, 1–13. [[CrossRef](#)]
185. Vigil de la Villa Mencía, R.; Goiti, E.; Ocejó, M.; Giménez, R.G. Synthesis of Zeolite Type Analcime from Industrial Wastes. *Microporous Mesoporous Mater.* **2020**, *293*, 109817. [[CrossRef](#)]
186. Grela, A.; Łach, M.; Bajda, T.; Mikula, J.; Hebda, M. Characterization of the Products Obtained from Alkaline Conversion of Tuff and Metakaolin. *J. Therm. Anal. Calorim.* **2018**, *133*, 217–226. [[CrossRef](#)]
187. Li, X.Y.; Jiang, Y.; Liu, X.Q.; Shi, L.Y.; Zhang, D.Y.; Sun, L.B. Direct Synthesis of Zeolites from a Natural Clay, Attapulgitite. *ACS Sustain. Chem. Eng.* **2017**, *5*, 6124–6130. [[CrossRef](#)]
188. Pereira, P.M.; Ferreira, B.F.; Oliveira, N.P.; Nassar, E.J.; Ciuffi, K.J.; Vicente, M.A.; Trujillano, R.; Rives, V.; Gil, A.; Korili, S.; et al. Synthesis of Zeolite A from Metakaolin and Its Application in the Adsorption of Cationic Dyes. *Appl. Sci.* **2018**, *8*, 608. [[CrossRef](#)]
189. Aytas, S.; Yurtlu, M.; Donat, R. Adsorption Characteristic of U(VI) Ion onto Thermally Activated Bentonite. *J. Hazard. Mater.* **2009**, *172*, 667–674. [[CrossRef](#)] [[PubMed](#)]
190. Wang, G.; Wang, X.; Chai, X.; Liu, J.; Deng, N. Adsorption of Uranium (VI) from Aqueous Solution on Calcined and Acid-Activated Kaolin. *Appl. Clay Sci.* **2010**, *47*, 448–451. [[CrossRef](#)]

191. Khaleque, A.; Alam, M.M.; Hoque, M.; Mondal, S.; Haider, J.B.; Xu, B.; Johir, M.A.H.; Karmakar, A.K.; Zhou, J.L.; Ahmed, M.B.; et al. Zeolite Synthesis from Low-Cost Materials and Environmental Applications: A Review. *Environ. Adv.* **2020**, *2*, 100019. [[CrossRef](#)]
192. Sugano, Y.; Sahara, R.; Murakami, T.; Narushima, T.; Iguchi, Y.; Ouchi, C. Hydrothermal Synthesis of Zeolite a Using Blast Furnace Slag. *ISIJ Int.* **2005**, *45*, 937–945. [[CrossRef](#)]
193. Johnson, E.B.G.; Arshad, S.E. Hydrothermally Synthesized Zeolites Based on Kaolinite: A Review. *Appl. Clay Sci.* **2014**, *97–98*, 215–221. [[CrossRef](#)]
194. Yao, G.; Lei, J.; Zhang, X.; Sun, Z.; Zheng, S. One-Step Hydrothermal Synthesis of Zeolite X Powder from Natural Low-Grade Diatomite. *Materials* **2018**, *11*, 906. [[CrossRef](#)]
195. Wajima, T.; Yoshizuka, K.; Hirai, T.; Ikegami, Y. Synthesis of Zeolite X from Waste Sandstone Cake Using Alkali Fusion Method. *Mater. Trans.* **2008**, *49*, 612–618. [[CrossRef](#)]
196. Ayele, L.; Pérez-Pariente, J.; Chebude, Y.; Díaz, I. Conventional versus Alkali Fusion Synthesis of Zeolite A from Low Grade Kaolin. *Appl. Clay Sci.* **2016**, *132–133*, 485–490. [[CrossRef](#)]
197. Wajima, T. Synthesis of Zeolite from Blast Furnace Slag Using Alkali Fusion with Addition of EDTA. *Adv. Mater. Res.* **2014**, *1044–1045*, 124–127. [[CrossRef](#)]
198. Tsujiguchi, M.; Kobashi, T.; Oki, M.; Utsumi, Y.; Kakimori, N.; Nakahira, A. Synthesis and Characterization of Zeolite A from Crushed Particles of Aluminoborosilicate Glass Used in LCD Panels. *J. Asian Ceram. Soc.* **2014**, *2*, 27–32. [[CrossRef](#)]
199. Tsujiguchi, M.; Kobashi, T.; Utsumi, Y.; Kakimori, N.; Nakahira, A. Synthesis of Zeolite a from Aluminoborosilicate Glass Used in Glass Substrates of Liquid Crystal Display Panels and Evaluation of Its Cation Exchange Capacity. *J. Am. Ceram. Soc.* **2014**, *97*, 114–119. [[CrossRef](#)]
200. Wu, Y.; Ren, X.; Wang, J. Facile Synthesis and Morphology Control of Zeolite MCM-22 via a Two-Step Sol-Gel Route with Tetraethyl Orthosilicate as Silica Source. *Mater. Chem. Phys.* **2009**, *113*, 773–779. [[CrossRef](#)]
201. Le, T.; Wang, Q.; Pan, B.; Ravindra, A.V.; Ju, S.; Peng, J. Process Regulation of Microwave Intensified Synthesis of Y-Type Zeolite. *Microporous Mesoporous Mater.* **2019**, *284*, 476–485. [[CrossRef](#)]
202. Ou, X.; Xu, S.; Warnett, J.M.; Holmes, S.M.; Zaheer, A.; Garforth, A.A.; Williams, M.A.; Jiao, Y.; Fan, X. Creating Hierarchies Promptly: Microwave-Accelerated Synthesis of ZSM-5 Zeolites on Macrocellular Silicon Carbide (SiC) Foams. *Chem. Eng. J.* **2017**, *312*, 1–9. [[CrossRef](#)]
203. Meng, X.; Xiao, F.S. Green Routes for Synthesis of Zeolites. *Chem. Rev.* **2014**, *114*, 1521–1543. [[CrossRef](#)]
204. Khalil, U.; Muraza, O. Microwave-Assisted Hydrothermal Synthesis of Mordenite Zeolite: Optimization of Synthesis Parameters. *Microporous Mesoporous Mater.* **2016**, *232*, 211–217. [[CrossRef](#)]
205. Shoppert, A.A.; Loginova, I.V.; Chaikin, L.I.; Rogozhnikov, D.A. Alkali Fusion-Leaching Method For Comprehensive Processing Of Fly Ash. *KnE Mater. Sci.* **2017**, *2*, 89. [[CrossRef](#)]
206. Yoldi, M.; Fuentes-Ordoñez, E.G.; Korili, S.A.; Gil, A. Zeolite Synthesis from Industrial Wastes. *Microporous Mesoporous Mater.* **2019**, *287*, 183–191. [[CrossRef](#)]
207. Wang, M.; Yang, J.; Ma, H.; Shen, J.; Li, J.; Guo, F. Extraction of Aluminum Hydroxide from Coal Fly Ash by Pre-Desilication and Calcination Methods. *Adv. Mater. Res.* **2012**, *396–398*, 706–710. [[CrossRef](#)]
208. Yang, J.; Sun, H.; Peng, T.; Zeng, L.; Chao, L. Separation of Alumina from Aluminum-Rich Coal Fly Ash Using NaOH Molten Salt Calcination and Hydrochemical Process. *Clean Technol. Environ. Policy* **2022**, *24*, 1507–1519. [[CrossRef](#)]
209. Ghasemi, Z.; Sourinejad, I.; Kazemian, H.; Hadavifar, M.; Rohani, S.; Younesi, H. Kinetics and Thermodynamic Studies of Cr(VI) Adsorption Using Environmental Friendly Multifunctional Zeolites Synthesized from Coal Fly Ash under Mild Conditions. *Chem. Eng. Commun.* **2020**, *207*, 808–825. [[CrossRef](#)]
210. Hammed, A.K.; Dewayanto, N.; Du, D.; Ab Rahim, M.H.; Nordin, M.R. Novel Modified ZSM-5 as an Efficient Adsorbent for Methylene Blue Removal. *J. Environ. Chem. Eng.* **2016**, *4*, 2607–2616. [[CrossRef](#)]
211. Ji, Y.; Xu, F.; Wei, W.; Gao, H.; Zhang, K.; Zhang, G.; Xu, Y.; Zhang, P. Efficient and Fast Adsorption of Methylene Blue Dye onto a Nanosheet MFI Zeolite. *J. Solid State Chem.* **2021**, *295*, 121917. [[CrossRef](#)]
212. Yuan, W.; Yuan, P.; Liu, D.; Yu, W.; Laipan, M.; Deng, L.; Chen, F. In Situ Hydrothermal Synthesis of a Novel Hierarchically Porous TS-1/Modified-Diatomite Composite for Methylene Blue (MB) Removal by the Synergistic Effect of Adsorption and Photocatalysis. *J. Colloid Interface Sci.* **2016**, *462*, 191–199. [[CrossRef](#)]
213. Visa, M. Synthesis and Characterization of New Zeolite Materials Obtained from Fly Ash for Heavy Metals Removal in Advanced Wastewater Treatment. *Powder Technol.* **2016**, *294*, 338–347. [[CrossRef](#)]
214. Chen, D.; Hu, X.; Shi, L.; Cui, Q.; Wang, H.; Yao, H. Synthesis and Characterization of Zeolite X from Lithium Slag. *Appl. Clay Sci.* **2012**, *59–60*, 148–151. [[CrossRef](#)]
215. Belviso, C. State-of-the-Art Applications of Fly Ash from Coal and Biomass: A Focus on Zeolite Synthesis Processes and Issues. *Prog. Energy Combust. Sci.* **2018**, *65*, 109–135. [[CrossRef](#)]

216. Anuwattana, R.; Khummongkol, P. Conventional Hydrothermal Synthesis of Na-A Zeolite from Cupola Slag and Aluminum Sludge. *J. Hazard. Mater.* **2009**, *166*, 227–232. [[CrossRef](#)]
217. Kuwahara, Y.; Ohmichi, T.; Kamegawa, T.; Mori, K.; Yamashita, H. A Novel Synthetic Route to Hydroxyapatite-Zeolite Composite Material from Steel Slag: Investigation of Synthesis Mechanism and Evaluation of Physicochemical Properties. *J. Mater. Chem.* **2009**, *19*, 7263–7272. [[CrossRef](#)]
218. Kuwahara, Y.; Ohmichi, T.; Kamegawa, T.; Mori, K.; Yamashita, H. A Novel Conversion Process for Waste Slag: Synthesis of a Hydrotalcite-like Compound and Zeolite from Blast Furnace Slag and Evaluation of Adsorption Capacities. *J. Mater. Chem.* **2010**, *20*, 5052–5062. [[CrossRef](#)]
219. Ibrahim, A.H.; Lyu, X.; ElDeeb, A.B. Synthesized Zeolite Based on Egyptian Boiler Ash Residue and Kaolin for the Effective Removal of Heavy Metal Ions from Industrial Wastewater. *Nanomaterials* **2023**, *13*, 1091. [[CrossRef](#)] [[PubMed](#)]
220. Wang, P.; Cao, J.; Zhang, Y.; Sun, Q. Controllable Preparation of Cubic Zeolite A and Application of Langmuir Model in Carbon Dioxide Adsorption. *Nanomaterials* **2021**, *11*, 3375. [[CrossRef](#)] [[PubMed](#)]
221. Bai, S.X.; Zhou, L.M.; Chang, Z.B.; Zhang, C.; Chu, M. Synthesis of Na-X Zeolite from Longkou Oil Shale Ash by Alkaline Fusion Hydrothermal Method. *Carbon Resour. Convers.* **2018**, *1*, 245–250. [[CrossRef](#)]
222. Mamedova, G.A. Hydrothermal Synthesis of Natrolite-Type Zeolite in the Natural Halloysite-Obsidian System. *Glas. Phys. Chem.* **2014**, *40*, 380–383. [[CrossRef](#)]
223. Mamedova, G.A.; Kamseu, E.; Beleuk à Moungam, L.M.; Cannio, M.; Billong, N.; Chaysuwan, D.; Melo, U.C.; Leonelli, C. Synthesis of Zeolite with a Gmelinite Structure in the Dolomite-Halloysite-Obsidian System. *J. Clean. Prod.* **2016**, *42*, 518–521. [[CrossRef](#)]
224. Kamseu, E.; Beleuk à Moungam, L.M.; Cannio, M.; Billong, N.; Chaysuwan, D.; Melo, U.C.; Leonelli, C. Substitution of Sodium Silicate with Rice Husk Ash-NaOH Solution in Metakaolin Based Geopolymer Cement Concerning Reduction in Global Warming. *J. Clean. Prod.* **2017**, *142*, 3050–3060. [[CrossRef](#)]
225. Alam, M.M.; Hossain, M.A.; Hossain, M.D.; Johir, M.A.H.; Hossen, J.; Rahman, M.S.; Zhou, J.L.; Hasan, A.T.M.K.; Karmakar, A.K.; Ahmed, M.B. The Potentiality of Rice Husk-Derived Activated Carbon: From Synthesis to Application. *Processes* **2020**, *8*, 203. [[CrossRef](#)]
226. Taylor, J.H.; Elmes, V.K.; Hurt, A.P.; Coleman, N.J. Synthesis of Feldspathoids and Zeolite K-F from Waste Amber Container Glass. *Mater. Chem. Phys.* **2020**, *246*, 122805. [[CrossRef](#)]
227. Mun, S.P.; Ahn, B.J. Chemical Conversion of Paper Sludge Incineration Ash into Synthetic Zeolite. *J. Ind. Eng. Chem.* **2001**, *7*, 292–298.
228. Wajima, T.; Ikegami, Y. Zeolite Synthesis from Paper Sludge Ash via Acid Leaching. *Chem. Eng. Commun.* **2008**, *195*, 305–315. [[CrossRef](#)]
229. Tavasoli, M.; Kazemian, H.; Sadjadi, S.; Tamizifar, M. Synthesis and Characterization of Zeolite Nay Using Kaolin with Different Synthesis Methods. *Clays Clay Miner.* **2014**, *62*, 508–518. [[CrossRef](#)]
230. Amoni, B.d.C.; de Freitas, A.D.L.; Loiola, A.R.; Soares, J.B.; Soares, S.d.A. A Method for NaA Zeolite Synthesis from Coal Fly Ash and Its Application in Warm Mix Asphalt. *Road Mater. Pavement Des.* **2019**, *20*, S558–S567. [[CrossRef](#)]
231. Lin, G.; Zhuang, Q.; Cui, Q.; Wang, H.; Yao, H. Synthesis and Adsorption Property of Zeolite FAU/LTA from Lithium Slag with Utilization of Mother Liquid. *Chin. J. Chem. Eng.* **2015**, *23*, 1768–1773. [[CrossRef](#)]
232. Zhang, C.; Li, S. Utilization of Iron Ore Tailing for the Synthesis of Zeolite A by Hydrothermal Method. *J. Mater. Cycles Waste Manag.* **2018**, *20*, 1605–1614. [[CrossRef](#)]
233. Poudel, M.B.; Awasthi, G.P.; Kim, H.J. Novel Insight into the Adsorption of Cr(VI) and Pb(II) Ions by MOF Derived Co-Al Layered Double Hydroxide @hematite Nanorods on 3D Porous Carbon Nanofiber Network. *Chem. Eng. J.* **2021**, *417*, 129312. [[CrossRef](#)]
234. Kandel, D.R.; Kim, H.J.; Lim, J.M.; Poudel, M.B.; Cho, M.; Kim, H.W.; Oh, B.T.; Nah, C.; Lee, S.H.; Dahal, B.; et al. Cold Plasma-Assisted Regeneration of Biochar for Dye Adsorption. *Chemosphere* **2022**, *309*, 136638. [[CrossRef](#)]
235. WHO (World Health Organization). Guidelines for the Safe Use of Wastewater, Excreta and Greywater. In *Wastewater Use in Agriculture*; World Health Organization: Geneva, Switzerland, 2006; Volume 2.
236. Shawabkeh, R.; Al-Harabsheh, A.; Hami, M.; Khlaifat, A. Conversion of Oil Shale Ash into Zeolite for Cadmium and Lead Removal from Wastewater. *Fuel* **2004**, *83*, 981–985. [[CrossRef](#)]
237. Hamadi, A.; Nabih, K. Synthesis of Zeolites Materials Using Fly Ash and Oil Shale Ash and Their Applications in Removing Heavy Metals from Aqueous Solutions. *J. Chem.* **2018**, *2018*, 6207910. [[CrossRef](#)]
238. Qiu, R.; Cheng, F.; Huang, H. Removal of Cd²⁺ from Aqueous Solution Using Hydrothermally Modified Circulating Fluidized Bed Fly Ash Resulting from Coal Gangue Power Plant. *J. Clean. Prod.* **2018**, *172*, 1918–1927. [[CrossRef](#)]
239. Huang, X.; Zhao, H.; Hu, X.; Liu, F.; Wang, L.; Zhao, X.; Gao, P.; Ji, P. Optimization of Preparation Technology for Modified Coal Fly Ash and Its Adsorption Properties for Cd²⁺. *J. Hazard. Mater.* **2020**, *392*, 122461. [[CrossRef](#)] [[PubMed](#)]
240. Jha, V.K.; Nagae, M.; Matsuda, M.; Miyake, M. Zeolite Formation from Coal Fly Ash and Heavy Metal Ion Removal Characteristics of Thus-Obtained Zeolite X in Multi-Metal Systems. *J. Environ. Manag.* **2009**, *90*, 2507–2514. [[CrossRef](#)] [[PubMed](#)]

241. Bao, W.; Zou, H.; Gan, S.; Xu, X.; Ji, G.; Zheng, K. Adsorption of Heavy Metal Ions from Aqueous Solutions by Zeolite Based on Oil Shale Ash: Kinetic and Equilibrium Studies. *Chem. Res. Chin. Univ.* **2013**, *29*, 126–131. [[CrossRef](#)]
242. Setthaya, N.; Pimraksa, K.; Damrongwiriyanupap, N.; Panias, D.; Mekrattanachai, P.; Chindawong, C. Modified Zeolite from Metakaolin and Fly Ash as Efficient Adsorbent for Cationic Methylene Blue Dye Removal. *Chem. Eng. Commun.* **2022**, *210*, 1178–1194. [[CrossRef](#)]
243. Javadian, H.; Ghorbani, F.; Tayebi, H.A.; Asl, S.H. Study of the Adsorption of Cd (II) from Aqueous Solution Using Zeolite-Based Geopolymer, Synthesized from Coal Fly Ash; Kinetic, Isotherm and Thermodynamic Studies. *Arab. J. Chem.* **2015**, *8*, 837–849. [[CrossRef](#)]
244. Fernandes Machado, N.R.C.; Miotto, D.M.M. Synthesis of Na-A and -X Zeolites from Oil Shale Ash. *Fuel* **2005**, *84*, 2289–2294. [[CrossRef](#)]
245. Yu, J.; Yang, Y.; Chen, W.; Xu, D.; Guo, H.; Li, K.; Liu, H. The Synthesis and Application of Zeolitic Material from Fly Ash by One-Pot Method at Low Temperature. *Green Energy Environ.* **2016**, *1*, 166–171. [[CrossRef](#)]
246. Chen, Y.; Xu, T.; Xie, C.; Han, H.; Zhao, F.; Zhang, J.; Song, H.; Wang, B. Pure Zeolite Na-P and Na-X Prepared from Coal Fly Ash under the Effect of Steric Hindrance. *J. Chem. Technol. Biotechnol.* **2016**, *91*, 2018–2025. [[CrossRef](#)]
247. Al-Zboon, K.; Al-Harashsheh, M.S.; Hani, F.B. Fly Ash-Based Geopolymer for Pb Removal from Aqueous Solution. *J. Hazard. Mater.* **2011**, *188*, 414–421. [[CrossRef](#)]
248. Visa, M.; Isac, L.; Duta, A. Fly Ash Adsorbents for Multi-Cation Wastewater Treatment. *Appl. Surf. Sci.* **2012**, *258*, 6345–6352. [[CrossRef](#)]
249. Shyam, R.; Puri, J.K.; Kaur, H.; Amutha, R.; Kapila, A. Single and Binary Adsorption of Heavy Metals on Fly Ash Samples from Aqueous Solution. *J. Mol. Liq.* **2013**, *178*, 31–36. [[CrossRef](#)]
250. Adamczuk, A.; Kołodyńska, D. Equilibrium, Thermodynamic and Kinetic Studies on Removal of Chromium, Copper, Zinc and Arsenic from Aqueous Solutions onto Fly Ash Coated by Chitosan. *Chem. Eng. J.* **2015**, *274*, 200–212. [[CrossRef](#)]
251. Mostafa Hosseini Asl, S.; Ghadi, A.; Sharifzadeh Baei, M.; Javadian, H.; Maghsudi, M.; Kazemian, H. Porous Catalysts Fabricated from Coal Fly Ash as Cost-Effective Alternatives for Industrial Applications: A Review. *Fuel* **2018**, *217*, 320–342. [[CrossRef](#)]
252. Asl, S.M.H.; Javadian, H.; Khavarpour, M.; Belviso, C.; Taghavi, M.; Maghsudi, M. Porous Adsorbents Derived from Coal Fly Ash as Cost-Effective and Environmentally-Friendly Sources of Aluminosilicate for Sequestration of Aqueous and Gaseous Pollutants: A Review. *J. Clean. Prod.* **2019**, *208*, 1131–1147. [[CrossRef](#)]
253. Wang, H.; Wang, X.; Xu, Z.; Zhang, M. Synthetic Zeolite from Coal Bottom Ash and Its Application in Cadmium and Nickel Removal from Acidic Wastewater. *Desalin. Water Treat.* **2016**, *57*, 26089–26100. [[CrossRef](#)]
254. Visa, M.; Duta, A. TiO₂/Fly Ash Novel Substrate for Simultaneous Removal of Heavy Metals and Surfactants. *Chem. Eng. J.* **2013**, *223*, 860–868. [[CrossRef](#)]
255. Itskos, G.; Koutsianos, A.; Koukouzas, N.; Vasilatos, C. Zeolite Development from Fly Ash and Utilization in Lignite Mine-Water Treatment. *Int. J. Miner. Process.* **2015**, *139*, 43–50. [[CrossRef](#)]
256. Hui, K.S.; Hui, K.N.; Lee, S.K. A Novel and Green Approach to Produce Nano- Porous Materials Zeolite A and MCM-41 from Coal Fly Ash and Their Applications in Environmental Protection. *Int. J. Chem. Biol. Eng.* **2009**, *3*, 165–175.
257. Asl, S.H.; Ahmadi, M.; Ghiasvand, M.; Tardast, A.; Katal, R. Artificial Neural Network (ANN) Approach for Modeling of Cr(VI) Adsorption from Aqueous Solution by Zeolite Prepared from Raw Fly Ash (ZFA). *J. Ind. Eng. Chem.* **2013**, *19*, 1044–1055. [[CrossRef](#)]
258. Asl, S.M.H.; Masomi, M.; Hosseini, M.; Javadian, H.; Ruiz, M.; Sastre, A.M. Synthesis of Hydrous Iron Oxide/Aluminum Hydroxide Composite Loaded on Coal Fly Ash as an Effective Mesoporous and Low-Cost Sorbent for Cr(VI) Sorption: Fuzzy Logic Modeling. *Process Saf. Environ. Prot.* **2017**, *107*, 153–167. [[CrossRef](#)]
259. Zhou, Q.; Yan, C.; Luo, W. Polypyrrole Coated Secondary Fly Ash-Iron Composites: Novel Floatable Magnetic Adsorbents for the Removal of Chromium (VI) from Wastewater. *Mater. Des.* **2016**, *92*, 701–709. [[CrossRef](#)]
260. Xiao, M.; Hu, X.; Gong, Y.; Gao, D.; Zhang, P.; Liu, Q.; Liu, Y.; Wang, M. Solid Transformation Synthesis of Zeolites from Fly Ash. *RSC Adv.* **2015**, *5*, 100743–100749. [[CrossRef](#)]
261. Wang, W.X.; Qiao, Y.; Li, T.; Liu, S.; Zhou, J.; Yao, H.; Yang, H.; Xu, M. Improved Removal of Cr(VI) from Aqueous Solution Using Zeolite Synthesized from Coal Fly Ash via Mechano-Chemical Treatment. *Asia-Pac. J. Chem. Eng.* **2017**, *12*, 259–267. [[CrossRef](#)]
262. Wen, Y.; Tang, Z.; Chen, Y.; Gu, Y. Adsorption of Cr(VI) from Aqueous Solutions Using Chitosan-Coated Fly Ash Composite as Biosorbent. *Chem. Eng. J.* **2011**, *175*, 110–116. [[CrossRef](#)]
263. Pizarro, J.; Castillo, X.; Jara, S.; Ortiz, C.; Navarro, P.; Cid, H.; Rioseco, H.; Barros, D.; Belzile, N. Adsorption of Cu²⁺ on Coal Fly Ash Modified with Functionalized Mesoporous Silica. *Fuel* **2015**, *156*, 96–102. [[CrossRef](#)]
264. Duan, P.; Yan, C.; Zhou, W.; Ren, D. Development of Fly Ash and Iron Ore Tailing Based Porous Geopolymer for Removal of Cu(II) from Wastewater. *Ceram. Int.* **2016**, *42*, 13507–13518. [[CrossRef](#)]
265. Al-Harashsheh, M.S.; Al Zboon, K.; Al-Makhadmeh, L.; Hararah, M.; Mahasneh, M. Fly Ash Based Geopolymer for Heavy Metal Removal: A Case Study on Copper Removal. *J. Environ. Chem. Eng.* **2015**, *3*, 1669–1677. [[CrossRef](#)]

266. Wu, X.W.; Ma, H.W.; Zhang, L.T.; Wang, F.J. Adsorption Properties and Mechanism of Mesoporous Adsorbents Prepared with Fly Ash for Removal of Cu(II) in Aqueous Solution. *Appl. Surf. Sci.* **2012**, *261*, 902–907. [[CrossRef](#)]
267. Joshi, M.K.; Pant, H.R.; Liao, N.; Kim, J.H.; Kim, H.J.; Park, C.H.; Kim, C.S. In-Situ Deposition of Silver-Iron Oxide Nanoparticles on the Surface of Fly Ash for Water Purification. *J. Colloid Interface Sci.* **2015**, *453*, 159–168. [[CrossRef](#)]
268. Cardoso, A.M.; Paprocki, A.; Ferret, L.S.; Azevedo, C.M.; Pires, M. Synthesis of Zeolite Na-P1 under Mild Conditions Using Brazilian Coal Fly Ash and Its Application in Wastewater Treatment. *Fuel* **2015**, *139*, 59–67. [[CrossRef](#)]
269. Attari, M.; Bukhari, S.S.; Kazemian, H.; Rohani, S. A Low-Cost Adsorbent from Coal Fly Ash for Mercury Removal from Industrial Wastewater. *J. Environ. Chem. Eng.* **2017**, *5*, 391–399. [[CrossRef](#)]
270. Tauanov, Z.; Shah, D.; Itskos, G.; Inglezakis, V. Optimized Production of Coal Fly Ash Derived Synthetic Zeolites for Mercury Removal from Wastewater. *IOP Conf. Ser. Mater. Sci. Eng.* **2017**, *230*, 012044. [[CrossRef](#)]
271. Liu, M.; Hou, L.A.; Xi, B.; Zhao, Y.; Xia, X. Synthesis, Characterization, and Mercury Adsorption Properties of Hybrid Mesoporous Aluminosilicate Sieve Prepared with Fly Ash. *Appl. Surf. Sci.* **2013**, *273*, 706–716. [[CrossRef](#)] [[PubMed](#)]
272. Belviso, C.; Cavalcante, F.; Di Gennaro, S.; Lettino, A.; Palma, A.; Ragone, P.; Fiore, S. Removal of Mn from Aqueous Solution Using Fly Ash and Its Hydrothermal Synthetic Zeolite. *J. Environ. Manag.* **2014**, *137*, 16–22. [[CrossRef](#)]
273. He, K.; Chen, Y.; Tang, Z.; Hu, Y. Removal of Heavy Metal Ions from Aqueous Solution by Zeolite Synthesized from Fly Ash. *Environ. Sci. Pollut. Res.* **2016**, *23*, 2778–2788. [[CrossRef](#)]
274. Koukouzas, N.; Vasilatos, C.; Itskos, G.; Mitsis, I.; Moutsatsou, A. Removal of Heavy Metals from Wastewater Using CFB-Coal Fly Ash Zeolitic Materials. *J. Hazard. Mater.* **2010**, *173*, 581–588. [[CrossRef](#)]
275. Đolić Maja, K.M.; Đorđe, V.; Veličković, Z.R.-O.V.; Vladimir, P.; Marinković, A. The Removal of Zn²⁺, Pb²⁺, and As(V) Ions by Lime Activated Fly Ash and Valorization of the Exhausted Adsorbent. *Waste Manag.* **2018**, *78*, 366–378. [[CrossRef](#)]
276. Visa, M.; Andronic, L.; Enesca, A. Behavior of the New Composites Obtained from Fly Ash and Titanium Dioxide in Removing of the Pollutants from Wastewater. *Appl. Surf. Sci.* **2016**, *388*, 359–369. [[CrossRef](#)]
277. Cardoso, A.M.; Horn, M.B.; Ferret, L.S.; Azevedo, C.M.; Pires, M. Integrated Synthesis of Zeolites 4A and Na-P1 Using Coal Fly Ash for Application in the Formulation of Detergents and Swine Wastewater Treatment. *J. Hazard. Mater.* **2015**, *287*, 69–77. [[CrossRef](#)]
278. He, H.; Xu, S.; Han, R.; Wang, Q. Nutrient Sequestration from Wastewater by Using Zeolite Na-P1 Synthesized from Coal Fly Ash. *Environ. Technol.* **2017**, *38*, 1022–1029. [[CrossRef](#)]
279. Wang, Z.; Fan, Y.; Li, Y.; Qu, F.; Wu, D.; Kong, H. Synthesis of Zeolite/Hydrous Lanthanum Oxide Composite from Coal Fly Ash for Efficient Phosphate Removal from Lake Water. *Microporous Mesoporous Mater.* **2016**, *222*, 226–234. [[CrossRef](#)]
280. Chen, X.Y.; Wendell, K.; Zhu, J.; Li, J.L.; Yu, X.; Zhang, Z. Synthesis of Nano-Zeolite from Coal Fly Ash and Its Potential for Nutrient Sequestration from Anaerobically Digested Swine Wastewater. *Bioresour. Technol.* **2012**, *110*, 79–85. [[CrossRef](#)] [[PubMed](#)]

Disclaimer/Publisher's Note: The statements, opinions and data contained in all publications are solely those of the individual author(s) and contributor(s) and not of MDPI and/or the editor(s). MDPI and/or the editor(s) disclaim responsibility for any injury to people or property resulting from any ideas, methods, instructions or products referred to in the content.